UNIVERSITY OF CALGARY

Vibroseis Deconvolution: Frequency-Domain Methods

By

Katherine Fiona Brittle

A THESIS
SUBMITTED TO THE FACULTY OF GRADUATE STUDIES
IN PARTIAL FULFILMENT OF THE REQUIREMENTS FOR THE
DEGREE OF MASTER OF SCIENCE

DEPARTMENT OF GEOLOGY AND GEOPHYSICS

CALGARY, ALBERTA

JUNE 2001

THE UNIVERSITY OF CALGARY

FACULTY OF GRADUATE STUDIES

The undersigned certify that they have read, and recommended to the Faculty of Graduate Studies for acceptance, a thesis entitled: Vibroseis deconvolution: frequency-domain methods" submitted by Katherine Fiona Brittle in partial fulfillment of the requirements for the degree of Master of Science.

Supervisor, Dr. Laurence R. Lines
Department of Geology and Geophysics

Dr. Gary F. Margrave
Department of Geology and Geophysics

Dr. R. James. Brown
Department of Geology and Geophysics

Dr. Michael Slawinski
Department of Mathematics and Statistics

June 5, 2001

ABSTRACT

A vibroseis sweep is often used as a source signal for seismic exploration. During the process of vibroseis acquisition, reflections of the sweep signal are recorded with geophones. Processing techniques are required to remove the embedded vibroseis sweep from the recorded trace. Traditional vibroseis processing involves cross-correlating the trace with the sweep used in the acquisition, producing an embedded zero-phase Klauder wavelet. However, it is also possible to remove the vibroseis sweep using the method of frequency-domain sweep deconvolution (FDSD). This method utilizes the frequency domain to remove the sweep from the trace. The two sweep-deconvolution methods are compared by using synthetic traces, which include variations in sweep type, random noise and minimum-phase earth-attenuation. A comparison of the vibroseis deconvolution methods with the inclusion of Q values is provided through the use of model data and a vertical seismic profile. Further analysis is also completed with the VSP corridor stacks and with three seismic lines, determining the effects of the sweep deconvolution methods on field data. Results from the study indicate that frequency-domain sweep deconvolution is an excellent method for vibroseis deconvolution, allowing amplitude and phase information to be processed more accurately than with the method of crosscorrelation. The amplitude and phase accuracy for the final result, due to the lack of sweep dependency in FDSD, is important for further amplitude analyses and seismic interpretation techniques.

ACKNOWLEDGEMENTS

I would like to extend my gratitude to the many people that I have worked with and who have helped to make this thesis possible over the last couple of years.

The greatest acknowledgement goes to my supervisor, Dr. Laurence *R*. Lines who encouraged and guided me through all my work at the University of Calgary and greatly enhanced the results presented as part of this thesis. I also thank Dr. Gary Margrave for the Matlab programs and assistance over the last two years. I am grateful to Ayon K. Dey, who helped out as I started at the University and was always available to give advice. I would like to thank Richard Xu for helping with the VSP processing.

All of the CREWES personnel provide excellent support and I would like to extend an extra acknowledgement to Hanxing Lu for processing and ProMAX help, Kevin Hall and Brain Hoffe for loading the field data, Henry Bland and Mark Kirkland for computer assistance and Louise Forges for all the administrative support.

The assistance of CREWES sponsors and the government of Alberta's AOSTRA and COURSE programs, which provided me with financial support during my studies, are gratefully acknowledged. Husky Energy Inc. and Petro-Canada are recognized for the assistance in obtaining uncorrelated and unsummed data for the field data processing.

Finally, I would like to thank all of the students, staff and professors at the University of Calgary for their assistance and friendship.

DEDICATION

To all the people who have been a positive influence in my life.

CONTENTS

LIST OF FIGURES

CHAPTER 1

1 INTRODUCTION AND BACKGROUND

1.0 CHAPTER SUMMARY

This chapter reviews the terminology associated with a vibroseis source and the results of the embedded sweep in the recorded data. An overview of crosscorrelation, used to remove the vibroseis sweep from the trace is completed and the problems associated with minimum-phase earth-attenuation related to earth filtering are examined. Summaries of the minimum-phase deconvolution processes used for the removal of the minimum-phase earth filter are reviewed.

1.1 INTRODUCTION TO THE VIBROSEIS SOURCE

Vibroseis is a seismic method where the energy source is a vibrator that generates a controlled wavetrain for which a sinusoidal vibration with continuously varying frequency is applied (Sheriff, 1990). Vibroseis has enjoyed worldwide popularity in land seismic acquisition ever since its development by Conoco's researchers (Crawford et al., 1960). The vibroseis source is widely used in seismic acquisition as it is a non-destructive method with a controllable frequency range and ideally produces a zero-phase wavelet. With increasing environmental awareness and seismic acquisition close to infrastructure, it is important to use a method that is not destructive. Vibroseis can operate in urban environments where dynamite sources are prohibited. Other advantages of the source include cost savings, such as the reduction in shot hole drilling associated with a dynamite source. The higher the preserved frequencies obtained from a vibroseis source, the better the resolution of the thin beds associated with heavy-oil reservoirs and reservoir geophysics. In vibroseis data, the recorded trace has an embedded sweep. It is necessary to remove the sweep from the trace to resolve the reflectivities of the beds. This is traditionally completed with the use of crosscorrelation, where the sweep is crosscorrelated with the trace. The crosscorrelation of the sweep creates an embedded Klauder wavelet, defined as the autocorrelation of a linear vibroseis sweep (Sheriff, 1990). This definition includes nonlinear sweeps as they can be characterized by numerous linear sweeps. Additional problems for vibroseis data are the mixed-phase wavelets associated with the combination of the zero-phase Klauder wavelet produced by crosscorrelation and minimum-phase effects, such as attenuation and transmission effects that are encountered during acquisition. There are changes in amplitude and phase due to linear and nonlinear filter effects from the vibrator system as well as "earth filtering" effects on the waves as they travel through the earth. This results in the higher frequencies being attenuated more than the low frequencies and the creation of a mixed-phase wavelet. An excellent source of information containing papers related to the vibroseis source is the SEG Geophysics reprint book on Vibroseis (Geyer, 1989). The work in this thesis is also summarized in the papers by Brittle et al. (2001) and Brittle and Lines (2001).

1.2 BACKGROUND

Heavy-oil deposits in Canada are of significant importance in future world petroleum production as conventional oil reserves decline. One of the main characteristics of a heavy-oil deposit is the shallow depth of the reservoir and importance of stratigraphic identification for advanced production methods such as steam-injection. For these reasons it is important to obtain an accurate seismic image. Work is being completed at the University of Calgary in the area of seismic monitoring for enhanced heavy-oil recovery in relation to steam-front identification, inversion and maximizing data resolution. In Canada, the geographical areas with heavy-oil deposits are ideal for the use of a vibroseis source as they are associated with significant production areas. These areas include production pads with both producing and steam-injection wells that are sensitive to dynamite explosions. One other advantage is the repeatability of a vibroseis source for time-lapse seismic acquisition related to steam zone monitoring. For this it is important to resolve the thin beds and steam zones. The higher the preserved frequencies from the vibroseis source, the better the resolution of the thin beds (Widess, 1973).

The P-wave vibroseis source can be considered as a vertical point source at the surface. The propagation of waves is governed by Newton's second law, the stress-strain (Hooke's Law) relationship and impedance contrasts (product of the seismic velocity and density). If the source is indicated as $s(t)$ and the response from the ground is $r(t)$ then the recorded trace by the geophones is $x(t)$ given as:

$$x(t) = s(t) * r(t) \, , \tag{1.1}$$

where the * indicates convolution. This equation can be redefined in the frequency-domain as

$$X(\omega) = S(\omega)R(\omega), \qquad (1.2)$$

where ω is the angular frequency, since convolution in the time-domain is equal to multiplication in the frequency-domain.

In vibroseis acquisition the point source is a sweep, not an impulse as for a dynamite source. The sweep is defined as an oscillating signal with constant amplitude and a frequency that varies monotonically with time (Goupillaud, 1976). The embedded sweep makes it impossible to interpret the reflectivities of the earth without processing to remove or alter the source signal.

1.3 SWEEP REMOVAL: CROSSCORRELATION

Traditionally, the vibroseis sweep is compressed to a Klauder wavelet (sweep autocorrelation) with the use of crosscorrelation. Crosscorrelation is used to evaluate the similarity of two waveforms and mathematically is defined (e.g. Margrave, 1999) as

$$c_j = \sum_k s_k r_{k+j} . \qquad (1.3)$$

for discrete time sequences, r_t and s_t .

When two identical random waveforms are crosscorrelated the result is a spike. The crosscorrelation of the sweep with the convolved source sweep and the reflectivity is

$$cc(t) = r(t) * s(t) \otimes s(t), \qquad (1.4)$$

where $cc(t)$ is the result of the crosscorrelation and $\otimes$ indicates the procedure of crosscorrelation. This is equivalent to convolving the reflectivity with the autocorrelation of the sweep when any nonlinear earth effects are ignored. The autocorrelation function of the sweep is a zero-phase wavelet, and the shape of the wavelet is dependent on the sweep design. Sheriff (1990) states that the autocorrelation of a linear vibroseis sweep has the form of a Klauder wavelet. This definition also includes nonlinear sweeps as they can be characterized by the summation of numerous linear sweeps. The basic idea of vibroseis is very similar to that used in the chirp radar systems described by Klauder et al. (1960).

The autocorrelation function, which determines the wavelet shape, is important when designing the sweep. Improper design of the sweep affects the amount of side-lobe noise as well as the peak amplitude (Figure 1.1).

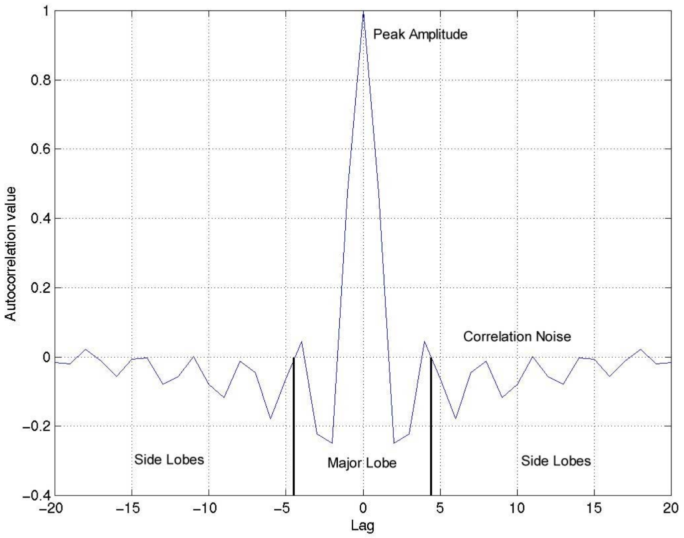

Figure 1.1: Autocorrelation of a linear sweep.

A linear sweep is the easiest to design for field acquisition. A linear sweep has an instantaneous frequency that is a linear function of time (i.e. $\omega = \omega_0 + kt$), where the correlation is the Klauder wavelet (Lines and Clayton, 1977). An important component of the sweep is the tapered ends which are designed with a $(1+\cos)^{2n}$ function to control the background levels of the sweep autocorrelation and the side-lobe reverberation (Goupillaud, 1976). For nonlinear sweeps, the frequency is not a linear function of time. When change in frequency is slowest, there will be depressed amplitudes. Generally speaking, nonlinear sweeps are designed to have amplitude spectra that counteract the effects of earth-attenuation, as shown later in Figure 1.2. When a nonlinear sweep is used, a different wavelet will be generated by the autocorrelation of the sweep than for a linear sweep. Alterations in the sweep can be used to assist in the removal of ground attenuation effects or to adjust the final wavelet shape. Associated with sweep design are the filtering effects of the Klauder wavelet during crosscorrelation. The inclusion of the Klauder wavelet in the convolutional equation controls the shape of the spectrum. Work completed by Goupillaud (1976) addresses the use of nonlinear sweeps to control the embedded wavelet. However, it is more difficult to transmit a nonlinear sweep into the ground and some of the spectral filtering can be completed as a component of the processing.

Crosscorrelation can also be written in the frequency-domain, which is important for examining the bandpass frequency-domain filtering effects of the sweep and the associated Klauder wavelet. When the sweep $s(t)$ is crosscorrelated with the recorded trace $x(t)$, the frequency-domain equation is

$$CC(\omega) = X(\omega)S^*(\omega) = R(\omega)S(\omega)S^*(\omega) = \left|S(\omega)\right|^2 R(\omega)\,, \qquad (1.5)$$

where $S^*(\omega)$ is the complex conjugate of the sweep and $|S(\omega)|^2$ is the power spectrum of the applied force. The data recovered by crosscorrelation are related to the power spectrum, with tapers of the sweep being squared.

1.4 SWEEP DESIGN

The shape of the designed vibroseis sweep has a significant effect on the resulting spectrum of the Klauder wavelet embedded in the seismic trace. Figure 1.2 shows the effect of sweep design on the wavelet when crosscorrelating to remove the vibroseis sweep.

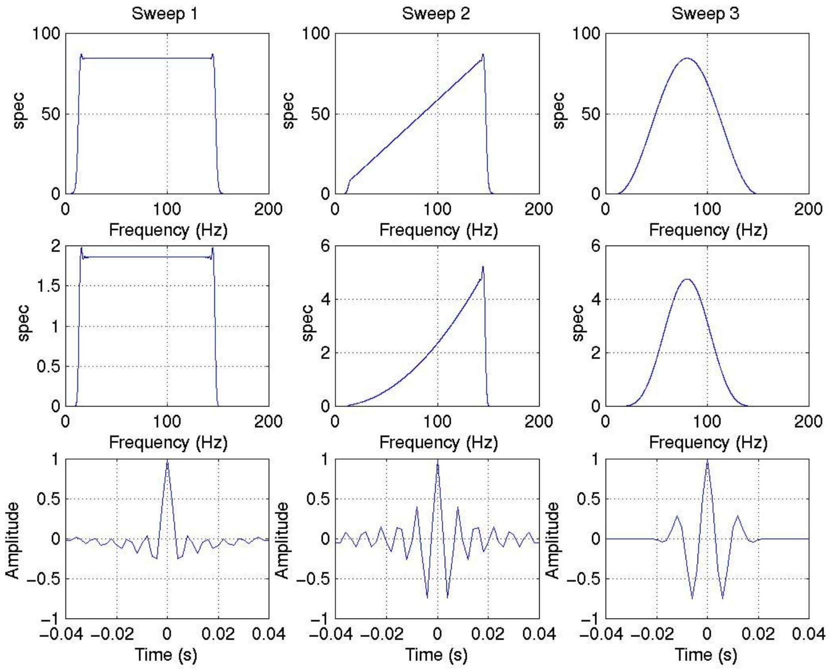

Figure 1.2: Effect of sweep design on the ability of crosscorrelation to remove the sweep due to the creation of a Klauder wavelet. The first row shows the amplitude spectra of the sweeps, the second row is the spectrum of the autocorrelation of the sweeps (Klauder wavelet) and the bottom row is the Klauder wavelet. Sweep 1 is a linear sweep with a 0.5 second taper, sweep 2 is a linear sweep with increasing amplitude with frequency and sweep 3 is a Gaussian sweep.

The linear sweep (1), with a 0.5-second taper, creates a Klauder wavelet with excellent peak amplitude and an insignificant amount of energy with negative amplitudes. However, it also has a large amount of side-lobe energy, which can be reduced by increasing the amount of tapering on the sides of the sweep. The taper length is the amount of time to reach the maximum amplitude of the oscillating signal in a vibroseis sweep (Sheriff, 1990). The second sweep, linear with an increasing amplitude for increasing frequencies has significant problems. The wavelet has a sizable amount of side-lobe noise and there is a large level of negative energy, which has the potential to mask thin beds. Since the white spectrum of the reflectivity is filtered by the power spectrum of the sweep during the crosscorrelation there is the loss of the low frequency data that is difficult to recover during subsequent processing. The final sweep (3) is designed with a Gaussian spectrum creating a wavelet with large negative amplitudes but no side-lobe noise. The filter effects of crosscorrelation are visible in the wavelet's spectrum.

For field data, a series of sweeps are recorded as auxiliary traces. This includes the sweeps generated by the computer, received by the vibrator truck, input by the electronics into the earth and often a measurement of the sweep from the baseplate. The ability of the vibrator to reproduce the sweep is important; however, it is limited by several factors. The sweep is altered by the electronic system and the hydraulics of the baseplate. Poor baseplate to ground coupling can also change the ideal sweep. This needs to be accounted for in the processing.

1.5 MINIMUM-PHASE

Minimum-phase wavelets are created naturally as waves propagate through an anelastic medium, which results in dispersion and attenuation of the seismic energy. Minimum-phase refers to the mathematical relationship that exists between the amplitude and phase spectra. This infers that knowledge of either the phase or amplitude spectra will allow the calculation of the other. Two assumptions are needed to show that attenuation in the earth is minimum-phase, linearity and causality (Futterman, 1962). The linearity refers to the validity of superposition. A causal time series is one that does not exist for $t < 0$ and the prototypical causal signal is the step function (eg. Margrave, 1999):

$$h(t) = \frac{1}{2} + \frac{1}{2}\operatorname{sgn}(t) \tag{1.6}$$

where the $\operatorname{sgn}(t) = \begin{bmatrix} +1 & t > 0 \\ 0 & t = 0 \\ -1 & t < 0 \end{bmatrix}$. The Fourier transform of the step function is

$$H(\omega) = \pi\delta(\omega) - \frac{i}{\omega}, \tag{1.7}$$

a spike at $\omega = 0$. If $f(t)$ is a causal function, then $f(t) = f(t)\ h(t)$. Therefore, the Fourier transform of any causal function, $f(t)$, is given by,

$$F(\omega) = F(\omega) * H(\omega). \tag{1.8}$$

Using equation (1.7) in equation (1.8), it follows (Margrave, 1999) that the real, $F_r(\omega)$, and imaginary, $F_i(\omega)$, parts of a causal function can be linked as,

$$F_r(\omega) = \frac{1}{\pi}\int_{-\infty}^{\infty}\frac{F_i(\mu)}{\omega-\mu}d\mu$$
$$\text{and} \quad . \tag{1.9}$$
$$F_i(\omega) = \frac{-1}{\pi}\int_{-\infty}^{\infty}\frac{F_r(\mu)}{\omega-\mu}d\mu$$

These two integrals are Hilbert transforms and the real and imaginary parts form a Hilbert transform pair. Letting *H* denote the abstract Hilbert operator defined by the first of equation 1.10, these become

$$F_r(\omega) = H(F_i)(\omega)$$
$$\text{and} \quad . \tag{1.10}$$
$$F_i(\omega) = H(F_r)(\omega)$$

However, we need to relate the amplitude and phase spectra, not the real and imaginary parts. The equation for a signal is a combination of the amplitude, $A(\omega)$, and phase spectra, $i\phi(\omega)$, defined as,

$$F(\omega) = A(\omega)e^{i\varphi(\omega)} . \tag{1.11}$$

If we take the logarithm of the signal, equation (1.11) can be written as,

$$\ln(F(\omega)) = \ln(A(\omega)) + i\varphi(\omega) , \tag{1.12}$$

where $\ln(A(\omega))$ is the real part of equation (1.9) and (1.10) and $i\phi(\omega)$ is the imaginary part. If equation 1.12 can be considered as the spectrum of a causal signal then the phase spectrum can be calculated with the Hilbert transform, *H*, such that,

$$\varphi(\omega) = H\left[\ln(A(\omega))\right]. \tag{1.13}$$

Equation (1.13) indicates that we need to determine the natural-logarithm amplitude spectrum to calculate the phase spectrum with the Hilbert transform. It also implies that the amplitude spectrum must have a stable inverse or that $A(\omega) \neq 0$ to satisfy the mathematical relationship between the amplitude and phase spectra.

The second condition is that the $\ln[F(\omega)]$ does not destroy the causality of the signal. The z transform of the signal $f(t)$ is defined as:

$$F(z) = \sum_{k=0}^{\infty} f_k z^k \; . \tag{1.14}$$

Through causality of the signal, $f(t)$, $F(z)$ will contain no negative powers of z. A Taylor series expansion of the natural logarithm of any function u is,

$$\ln(u) = \sum_{n=1}^{\infty} \frac{(-1)^{n-1}(1-u)^n}{n} \, , \tag{1.15}$$

which is valid only for $0 < u \leq 2$. Since $F(z)$ contains only positive powers of z and $\ln(u)$ contains only positive powers of u, then $\ln(F(z))$ contains only positive powers of z. Therefore, $\ln(F(\omega))$ is still a causal time-domain function.

Therefore, through this relationship we can define a minimum-phase wavelet as being a causal, stable function with a causal, stable inverse. The energy of a minimum-phase wavelet is maximally concentrated at the outset (Claerbout, 1976). Any change in the amplitude spectrum of a minimum-phase wavelet requires a change in the phase spectrum to maintain the minimum-phase relation. A causal stable time series, with a causal stable inverse can be completely determined with knowledge of either the phase or amplitude spectrum through the Hilbert transform. This is the basis of minimum-phase deconvolution in seismic data processing.

1.6 GROUND ATTENUATION

When designing the sweep for a vibroseis survey another important component to examine is the effect of ground attenuation. A ground attenuation factor, $e(t)$, can be included in the basic convolution equation as

$$x(t) = s(t) * r(t) * e(t) . \tag{1.16}$$

As the source signal penetrates into the ground, the signal is attenuated as the sediment absorbs some of the energy. The energy absorption occurs as the sediment grains move within the ground. The amount of energy lost is related to the sediment type. For example, with wave propagation through carbonates there is less energy loss than for soft sediment. There are two problems associated with the earth filtering. The first is the effect of minimum-phase attenuation on a zero-phase source and the second is the amplitude attenuation of the high frequencies.

The widespread industry success of minimum-phase deconvolution for impulsive dynamite sources suggests that earth filtering effects and the resulting seismic wavelet are minimum-phase. Crosscorrelation to remove the vibroseis sweep creates an embedded zero-phase Klauder wavelet. The convolution of the zero-phase Klauder wavelet with the minimum-phase earth filter results in a mixed-phase vibroseis wavelet. This wavelet cannot be removed by minimum-phase deconvolution unless phase filters are applied to convert mixed-phase wavelets to minimum-phase equivalents.

The second problem is the attenuation of the high frequencies, which degrades the wavelet associated with a linear sweep, and reduces the visibility of the thin beds that are important in heavy-oil and shallow reservoirs. If the earth filtering is assumed to be frequency-dependent, then a linear sweep with constant amplitude will degrade into a sweep with decreasing amplitudes in the higher frequencies. Performing deconvolution and whitening the spectrum can often correct the spectrum. However these procedures use the assumption, as discussed previously, that the wavelet is minimum-phase, not mixed-phase.

1.7 MINIMUM-PHASE DECONVOLUTION METHODS

Deconvolution is used in the processing of seismic data to improve the temporal resolution of the data by compressing the wavelet. The purpose of deconvolution is to replace the wavelet embedded in the seismic trace by a bandlimited spike. This process leaves a reflection coefficient wherever we have contrasts in the acoustic impedance.

For deconvolution, two main assumptions are usually made to create the inverse filter:

1. That the source waveform does not change as it travels through the subsurface. This assumption of stationarity is not always necessary. Methods developed by Margrave (1998) can deal with non-stationary (time-varying) wavefields.

2. That we know the source waveform or equivalently its amplitude and phase spectrum in the frequency domain. Assuming that the reflectivity is random allows the assumption of a white amplitude spectrum and the trace's amplitude

spectrum then equals the wavelet spectrum. The wavelet is assumed to be minimum-phase.

There are several different deconvolution methods, including frequency-domain and Wiener spiking deconvolution.

1.7.1 Frequency-domain deconvolution

The convolutional model, including the assumption that the trace is noise-free is:

$$x(t) = w(t) * r(t), \tag{1.17}$$

where $x(t)$ is the seismogram, $w(t)$ is the embedded wavelet and $r(t)$ is the reflectivity or the earth's response. This equation can be simplified by transforming it into the frequency domain as:

$$X(\omega) = W(\omega)R(\omega), \tag{1.18}$$

since convolution in the time-domain is equivalent to multiplication in the frequency-domain. Using the assumption that the reflectivity is random allows the conclusion that the spectral shape of the trace is due to the wavelet and not the reflectivity, which is white. The general spectral shape of the wavelet can be determined from the trace; however, the phase of the wavelet is still unknown. This leads to the assumption, that the wavelet is minimum-phase. The estimated wavelet can be defined as $W_e(\omega)$ and a simple division calculates the traces as:

$$X(\omega) = \frac{W(\omega)R(\omega)}{W_e(\omega)} = \overline{R}(\omega), \tag{1.19}$$

determining the estimated reflectivity $\overline{R}(\omega)$, with the wavelet removed.

1.7.2 Wiener spiking deconvolution

Wiener spiking deconvolution is a time-domain method involving the computation of a minimum-phase filter, given its autocorrelation. The autocorrelation of the wavelet is similar to that of the seismogram with the inclusion of the assumption of random reflectivity and noise (Yilmaz, 1987).

The autocorrelation of the seismic trace can be calculated with the noise, reflectivity and wavelet terms. The reflectivity and the noise can both be assumed as random series. The correlation of two random functions is equal to zero as there is no true similarity giving the following equation:

$$A_s(t) = A_w(t) * A_r(t) + A_n(t) \tag{1.20}$$

where the A_s is the autocorrelation of the seismic trace, A_w is the autocorrelation of the embedded wavelet, A_r the autocorrelation of the reflectivity and A_n the autocorrelation of the random noise (Margrave, 1999).

The autocorrelations of the random noise and reflectivity functions are equal to a Dirac delta function with power equal to that of the mean noise since the only similarity is at zero lag.

$$A_s(t) = A_w(t) + p_n \delta(t) \tag{1.21}$$

This shows that the autocorrelation of the seismogram should equal that of the wavelet with the exception of an increase in the zero lag power.

For Wiener spiking deconvolution there are several parameters that must be chosen, including the stability factor and the number of lags to allow in the autocorrelation (filter length). The stability factor eliminates the possibility of division by zero when the wavelet is inverted. For field data this stability factor may not be necessary depending on the data set. Truncating the autocorrelation at a certain lag is equivalent to smoothing the power spectrum of the seismic trace in frequency-domain deconvolution.

1.7.3 Surface-consistent deconvolution

In surface-consistent deconvolution, the seismic trace is decomposed into the convolutional effects of the source, receiver, reflectivity and offset. This accounts for the variations in the wavelet's shape as a result of near-source and near-receiver conditions, as well as receiver/source offset (Yilmaz, 1987). Following the decomposition, inverse filtering is applied in an attempt to recover the earth's impulse response. To apply surface-consistent deconvolution the wavelet shape is assumed to depend on the locations of the receivers and source and not on the raypaths. If the recorded seismogram $x(t)$ consists of the source waveform $w(t)$, the earth's impulse response $r(t)$ and the random noise $n(t)$ then the surface-consistent convolutional model is:

$$x_{ij}(t) = s_{j(t)} * h_{(i-j)/s}(t) * e_{(i+j)/2}(t) * q_i(t) + n(t)\,. \tag{1.22}$$

In the above equation $x_{ij}(t)$ is the seismogram, $s_j(t)$ is the waveform associated with the source location i, $q_i(t)$ is the waveform associated with the receiver at location j, and $h(t)$ is associated with the dependence of the waveform on the offset (Yilmaz, 1987).

If the minimum-phase assumption is applied then only the spectrum needs to be considered, such that,

$$A_x(\omega) = A_s(\omega)A_h(\omega)A_e(\omega)A_q(\omega)\,, \tag{1.23}$$

where the noise is assumed to be negligible.

The individual filters can be computed by least-squares minimization, where the energy is defined as:

$$L = \sum_{i,j,\omega}(\ln A_x - \ln \hat{A}_x)^2\,. \tag{1.24}$$

This solves for the individual spectral components associated with the receiver and source locations and the dependency on the offset. The final deconvolution operator is the minimum-phase inverse of $s(t)*q(t)$ (Yilmaz, 1987).

1.8 CHAPTER CONCLUSIONS

The effect of deconvolving the embedded vibroseis sweep by crosscorrelation is an embedded zero-phase Klauder wavelet. The Klauder wavelet results in the data being bandpass filtered with the power spectrum of the sweep. The design of the vibroseis sweep is important as it has a direct effect on the filtering of the data after crosscorrelation and the subsequent Klauder wavelet. The presence of earth-attenuation results in a mixed-phase wavelet, created by the convolution of the Klauder wavelet and the earth-attenuation minimum-phase wavelet.

CHAPTER 2

2 PROPOSED METHOD FOR VIBROSEIS SWEEP REMOVAL

2.0 CHAPTER SUMMARY

Frequency-domain sweep deconvolution (FDSD), as introduced in this chapter, is a method of removing the vibroseis sweep from the recorded data in the frequency-domain. The effect of this method with the addition of random noise and the inclusion of minimum-phase earth filtering is reviewed.

2.1 INTRODUCTION

As discussed in chapter 1, crosscorrelation is traditionally used to remove the vibroseis sweep from the recorded data. There are several problems with this method including the filtering effects that crosscorrelation imposes on the seismic trace and the resulting embedded Klauder wavelet. Another problem is the assumption that the embedded wavelet, when affected by ground attenuation is minimum-phase. However, the convolution of the Klauder wavelet with minimum-phase attenuation filter creates a mixed-phase wavelet. There are suggested methods by Gibson and Larner (1984) and Cambois (2000) to convert the Klauder wavelet to a minimum-phase equivalent eliminating the mixed-phase wavelet. A frequency-domain method is examined to take the place of crosscorrelation. Crosscorrelation is a processing technique, which is defined by Claerbout (1992) as a conjugate technique or mathematically, a matrix transpose that generally gives an imperfect result. The introduced frequency-domain method is an inversion technique. Inversion is related mathematically to matrix inversion (Claerbout, 1992). If an inversion technique is applied to perfect data it can give a perfect result.

2.2 FREQUENCY-DOMAIN SWEEP DECONVOLUTION

Frequency-domain sweep deconvolution (FDSD) utilizes the concept that convolution in the time-domain is equivalent to multiplication in the frequency domain. Deconvolution of the sweep in the time domain can be completed in the frequency domain through division. The basic convolution equation for a vibroseis source is

$$x(t) = s(t) * r(t), \tag{2.1}$$

where $x(t)$ is the trace recorded by the geophone, $s(t)$ is the source sweep and $r(t)$ is the reflectivity.

For FDSD it is easier to express the basic convolution equation for a vibroseis source in the frequency-domain as

$$X(\omega) = S(\omega)R(\omega). \tag{2.2}$$

The sweep can then be removed in the frequency-domain by dividing the trace by the sweep, $S(\omega)$, giving a solution of:

$$FDSD(\omega) = \frac{S(\omega)R(\omega)}{S(\omega)} . \qquad (2.3)$$

If the sweep input into the ground is equal to the sweep generated then the result is the exact reflectivity.

2.3 ADDITION OF RANDOM NOISE

The signal-to-noise ratio is critical for the acquisition of high-quality data. The noise can be controlled with proper source-receiver patterns, vibrator phase control and amplitude control in the field. There are two main categories for noise. The first is random noise, such as results from poorly planted geophones, wind motion and instrument noise. The second is coherent noise including ground roll, guided waves, side scatter, cable noise, airwaves, noise from power lines and multiples (Yilmaz, 1987). The noise, $n(t)$, is additive to the convolution equation in the time-domain, such that

$$x(t) = r(t) * s(t) + n(t) \ , \qquad (2.4)$$

and additive in the frequency-domain, such that

$$X(\omega) = R(\omega)S(\omega) + N(\omega) . \qquad (2.5)$$

If the sweep is removed with crosscorrelation both parts of the addition are convolved with the time-reversed sweep. This replaces the sweep on the left side of the addition with a Klauder wavelet but leaves the noise convolved with the time-reversed sweep,

$$cc(t) = r(t) * s(t) * s'(-t) + n(t) * s'(-t) . \qquad (2.6)$$

The effect of crosscorrelation can be examined for the addition of random noise, implying the effect on the result. For modelling, the signal-to-noise ratio is defined by the average power spectrum of the trace. With crosscorrelation the noise is filtered removing the frequencies excluded from the sweep (Figure 2.1).

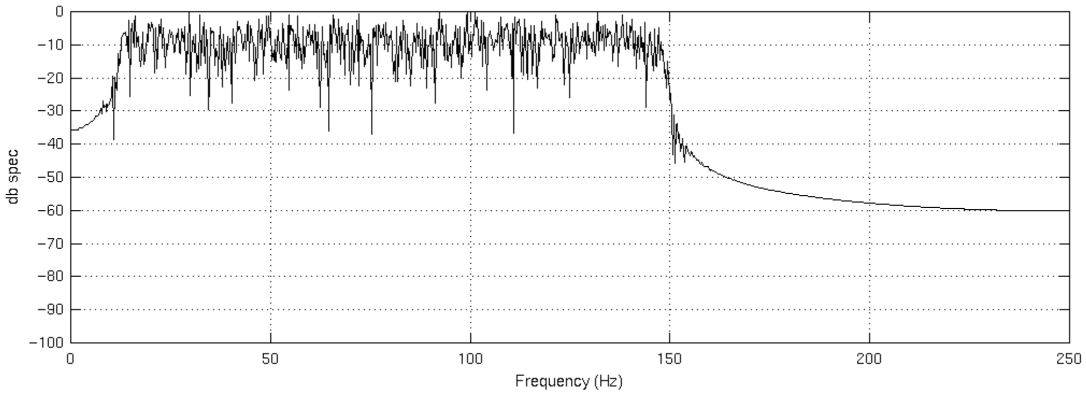

Figure 2.1: Effect of noise on crosscorrelation for a signal-to-noise ratio of 5:1. The plot is the decibel amplitude spectrum of the noise after being crosscorrelated with a linear sweep; the amplitude is 17% of the reflectivity.

For frequency-domain sweep deconvolution, the same convolution equations (2.4 and 2.5) as crosscorrelation are relevant. When the sweep is removed in the frequency-domain, the noise is divided by the sweep:

$$FDSD(\omega) = \frac{R(\omega)S(\omega)}{S(\omega)} + \frac{N(\omega)}{S(\omega)} = \overline{R(\omega)} + \frac{N(\omega)}{S(\omega)}. \tag{2.7}$$

The division of the noise by the sweep amplifies the noise for frequencies outside of the sweep's frequency range. If the result of FDSD is bandpass filtered, then the problematic amplified frequencies are removed from the data.

Adding a noise factor into the frequency-domain division can also reduce the amplification of the frequencies. This alters the FDSD equation to

$$\begin{aligned} FDSD(\omega) &= \frac{R(\omega)S(\omega)}{S(\omega)+b\max(|S(\omega)|)} + \frac{N(\omega)}{S(\omega)+b\max(|S(\omega)|)} \\ &= \overline{R(\omega)} + \frac{N(\omega)}{S_{stab}(\omega)} \end{aligned}, \tag{2.8}$$

where b is a stability factor and $S_{stab}(\omega)$ is the stabilized sweep. The stability factor level can be chosen through trial and error, with the preferential value being the lowest that will resolve the data. For the synthetic modelling done in this thesis, the lowest stability factor that will resolve the data is 0.1%.

After filtering the data, the noise in the section is almost completely eliminated (Figure 2.2).

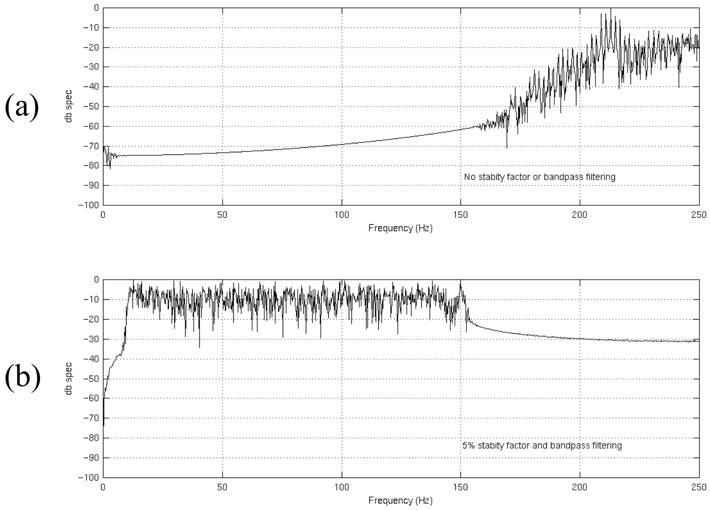

Figure 2.2: Frequency-domain sweep deconvolution of the noise. (a) shows the result of FDSD when no stability factor or bandpass filtering is applied to the data. (b) shows the result when a 5% stability factor is used and a bandpass filter is also applied to the data. The noise is slightly higher for the 5:1 signal-to-noise ratio than crosscorrelation, with the mean noise equal to 20% of the mean reflectivity.

Most of the random noise remaining in the traces will be removed after the data have been stacked.

The bit number of the digital acquisition system limits the decibel scale. A decibel is related to the maximum amplitude recorded where the decibel value, *dB*, at any frequency is equal to,

$$dB = 20\log\left({}^{A}\!/\!_{A_{\max}} \right), \tag{2.9}$$

where A is the amplitude at a given frequency and A_{max} is the maximum amplitude over the entire frequency range. The lowest decibel value that can be obtained from an 8-bit digital system is –48 dB and –144 dB for a 24-bit system. For the modelling in this thesis the limitation of the bit system needs to be considered.

2.4 EARTH ATTENUATION

As a source signal or wavelet penetrates the ground, the signal is altered as it travels through the sedimentary layers due to absorption before it is measured by a series of geophones. The earth filtering $e(t)$, is included in the basic convolution equation for a vibroseis source as,

$$x(t) = r(t) * e(t) * s(t). \tag{2.9}$$

In the frequency-domain the convolutional equation is defined as,

$$X(\omega) = R(\omega)E(\omega)S(\omega). \tag{2.10}$$

The effect of earth filtering has been discussed by both Gibson and Larner (1984) and Cambois (2000). All the authors identify problems associated with the earth effect and suggest that it creates an embedded minimum-phase wavelet. This conclusion is supported by the lack of problems associated with a dynamite source. Dynamite has an impulsive nature, in which the source spike is convolved with the earth-attenuation creating a phase (minimum) approximately equal to that of the earth filtering (Figure 2.3).

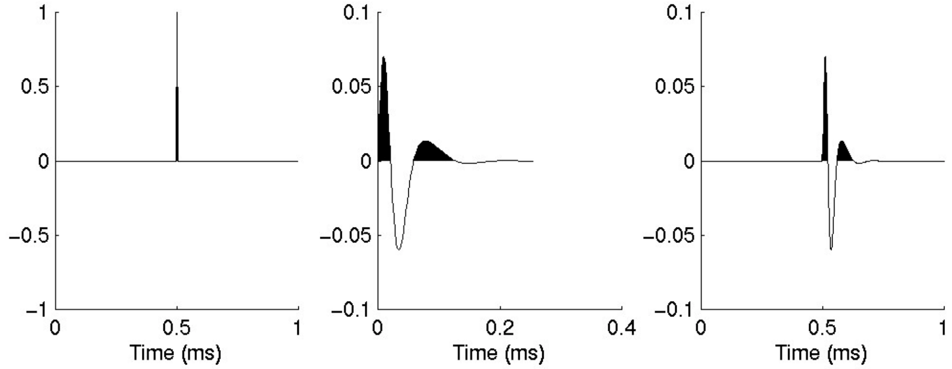

(a) (b) (c)

Figure 2.3: Idealized dynamite seismic signature. (a) is a basic idealized impulsive dynamite source; (b) is the wavelet associated with a minimum-phase earth filter. When they are convolved (c) is generated, which is equal to the recorded wavelet in dynamite source seismic, a minimum-phase wavelet.

However, a vibroseis source creates a zero-phase Klauder wavelet that is embedded in the data as a result of crosscorrelation. If as theory suggests, the earth filter is minimum-phase, the result is a mixed-phase wavelet (Figure 2.4).

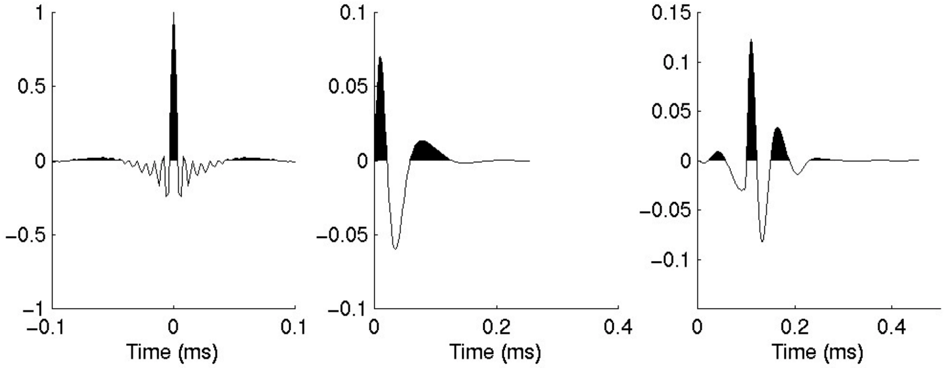

(a) (b) (c)

Figure 2.4: Vibroseis seismic signature. (a) is a Klauder wavelet from the processing of vibroseis source data while the (b) is a minimum-phase wavelet. When they are convolved (c) is generated, which would be the wavelet recorded in vibroseis acquisition.

Methods have been designed to remove the mixed-phase wavelet that is created through the initial vibroseis processing. Gibson and Larner (1994) suggest converting the mixed-phase wavelet to zero-phase by constructing a minimum-phase equivalent of the Klauder wavelet and filtering the vibroseis record to match the phase. Once this is completed, it is possible to use minimum-phase spiking deconvolution to remove the minimum-phase wavelet, creating a zero-phase record. Cambois (2000) suggests that the sequence of processes to convert the phase for linear sweeps is impractical as the conversion to minimum-phase is time-consuming and the low-frequency shape of the boxcar shaped spectrum for linear sweeps is too complicated. However, if nonlinear sweeps are used then the results are more successful.

When the vibroseis sweep is removed through crosscorrelation the equation for the seismic trace is

$$\begin{aligned} cc(t) &= r(t) * e(t) * s(t) * s(-t) \\ &= r(t) * e_{\min}(t) * k_{zero}(t) \quad , \\ &= r(t) * w_{mix}(t) \end{aligned} \tag{2.13}$$

where the earth filter, *e*(*t*), is minimum-phase and the Klauder wavelet, *k*(*t*), is zero-phase creating a mixed-phase wavelet $w_{mix}(t)$.

For FDSD in the frequency-domain the equation with the division of the sweep is

$$\begin{aligned} FDSD(\omega) &= \frac{S(\omega)R(\omega)E(\omega)}{S(\omega)} \\ &= R(\omega)E(\omega) \end{aligned} \quad . \qquad (2.14)$$

The result is the reflectivity convolved with the minimum-phase wavelet that is created by the earth-attenuation. If the data were not bandlimited, minimum-phase deconvolution should be able to completely remove the minimum-phase wavelet from the data. However, a non-bandlimited sweep is impossible and problems will arise when minimum-phase deconvolution is used for the frequencies at which the amplitude is zero.

2.5 CHAPTER CONCLUSIONS

Frequency-domain sweep deconvolution uses the frequency-domain to replace deconvolution with division. This eliminates the embedded Klauder wavelet that remains in the data when crosscorrelation is utilized. This assists in removing the problem of the mixed-phase wavelet associated with the Klauder wavelet and the minimum-phase earth filter. FDSD is bandlimited, diminishing the possibility of accurately estimating the minimum-phase wavelet.

CHAPTER 3

3 METHOD TESTING ON SYNTHETIC VIBROSEIS DATA

3.0 CHAPTER SUMMARY

In this chapter vibroseis data are modelled and the embedded sweep removed with both crosscorrelation and frequency-domain sweep deconvolution to examine the effects of the processes with different sweep types, the addition of random noise and inclusion of minimum-phase earth filtering.

3.1 INTRODUCTION

To understand the effects of both crosscorrelation and frequency-domain sweep deconvolution it is important to complete modelling to determine the effectiveness of frequency-domain sweep deconvolution (FDSD) for resolving the impedance of the earth. A series of four sweeps were designed with the MATLAB program *sweep.m* (G. Margrave). These sweeps, shown in Figure 3.1, include a variety of different taper lengths from 500 milliseconds to 8 seconds and one sweep that varies in amplitude over the frequency range. The tapers help to reduce the side-lobe noise that is associated with the sweep removal by crosscorrelation and they allow the vibrator to increase to maximum energy for the vibration time. The first sweep is linear with a 500-ms taper while the second sweep has a taper length of five seconds. The second sweep is also linear; however, the increased tapers alter the Klauder wavelet while allowing the vibrator more time to reach the maximum amplitude. The third sweep has a spectrum with increasing energy as the frequency increases. The initial and final amplitudes have a small 500-ms taper to help reduce the side-lobe energy. This sweep is often used in real acquisition to eliminate some of the earth-attenuation effects on the amplitude of the recorded data. As the rays pass through the ground the high frequency data are attenuated more than the low frequency data. The final sweep modelled has a Gaussian spectrum. All of the sweeps were designed with a sample rate of 2-ms, a length of 16 seconds and a frequency range of 10 to 150 Hz. The sweeps are shown in Figure 3.1.

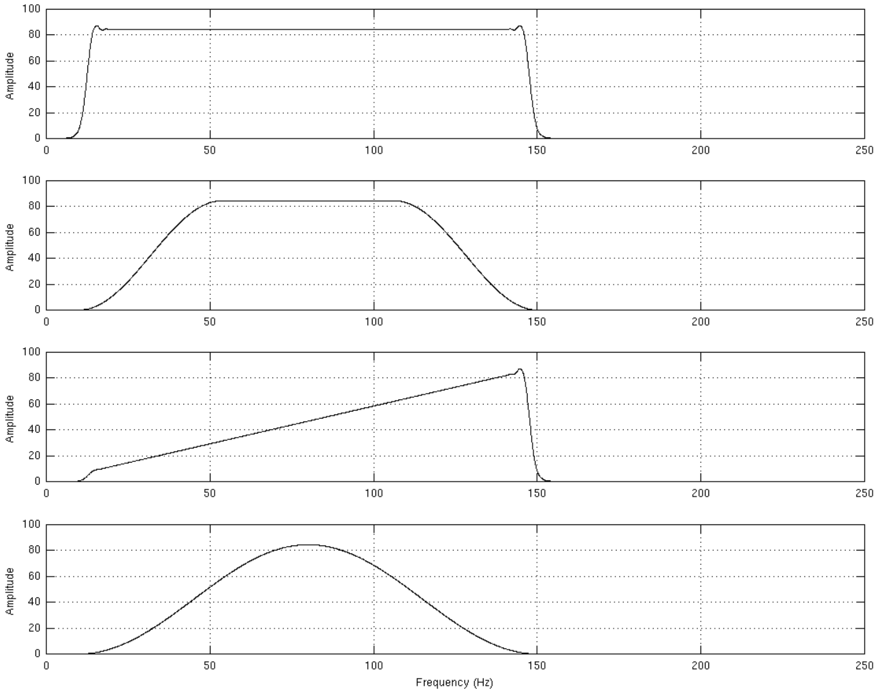

Figure 3.1: Synthetic modelled sweeps. From top to bottom: linear sweep with a 0.5-second taper, linear sweep with a 5 second taper, nonlinear sweep with increasing amplitude as the frequency increases with 0.5 second tapers and a Gaussian sweep.

These sweeps were convolved with a synthetic random reflectivity that was designed with G. Margrave's MATLAB program *reflec.m* with a two-millisecond sample rate and a four-second length. A single large reflectivity spike was then added at two-seconds for the result comparison between the deconvolved reflectivity and the true reflectivity but randomness is still maintained.

3.2 WITHOUT NOISE OR EARTH ATTENUATION

The first model completed in the synthetic testing was for a simple vibroseis earth model with no noise and no attenuation where

$$\begin{gathered} x(t) = s(t) * r(t) \\ \text{and} \\ X(\omega) = S(\omega)R(\omega) \end{gathered} \quad . \tag{3.1}$$

The length of the trace after the sweep and reflectivity are convolved is 20 seconds. The symbol for the sweep is $s(t)$ in the time-domain and $S(\omega)$ in the frequency-domain; the reflectivity is $r(t)$ and $R(\omega)$ and the recorded trace is $x(t)$ and $X(\omega)$. The sweep is input into the ground by the vibroseis truck. For modelling, the input sweep is exactly the same as the sweep that is recorded, an ideal case.

Following the convolution of the sweep with the reflectivity, creating the data recorded by the geophones at the surface, the sweep embedded in the trace is removed by both crosscorrelation and frequency-domain sweep deconvolution.

3.2.1 Crosscorrelation

The crosscorrelation results show that the reflectivity, *r*(*t*), is convolved with the Klauder wavelet, *k*(*t*). The Klauder wavelet is equal to the autocorrelation of the sweep. The crosscorrelation result is defined as:

$$cc(t) = r(t) * s(t) * s(-t) = r(t) * k(t), \tag{3.2}$$

where *cc* is the result of crosscorrelation. Crosscorrelation is dependent on the sweep shape, giving different results for all of the sweeps (Figure 3.2 to 3.4). All of the plots are normalized so that the maximum absolute value of the result is equal to one.

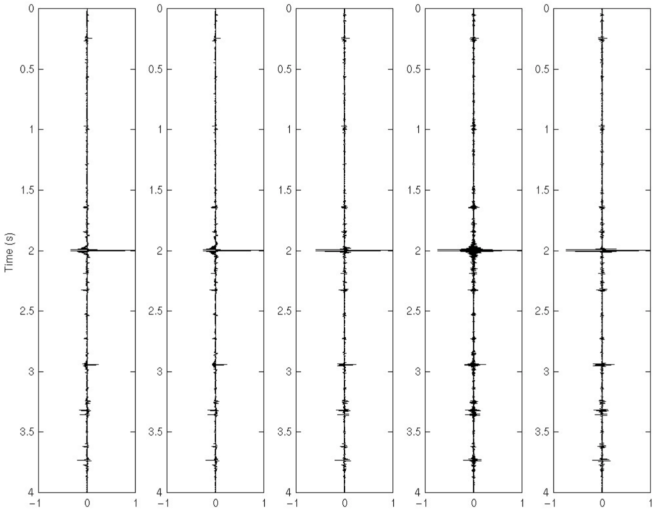

Figure 3.2: Results of crosscorrelation for the removal of the vibroseis sweep without noise or earth-attenuation. From the left to right: reflectivity, sweep 1, sweep 2, sweep 3 and sweep 4 as identified in Figure 3.1. The results are dependent on the Klauder wavelet created by the autocorrelation of the sweep.

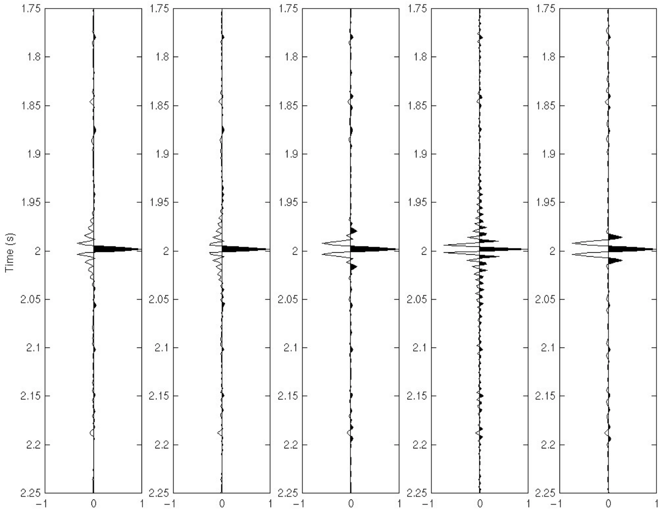

Figure 3.3: Results of the crosscorrelation with the plots zoomed in from 1.75 to 2.25 seconds on the large reflectivity spike. From the left to right: reflectivity, sweep 1, sweep 2, sweep 3 and sweep 4 as identified in Figure 3.1.

The plots indicate that the crosscorrelation result is dependent on the Klauder wavelet generated by the autocorrelation of the sweep. Sweep 1 produces a large amount of side-lobe energy but an insignificant amount of negative amplitudes while the rest of the sweeps have smaller side-lobes but a large amount of negative amplitudes. The large negative spike may obscure thin sedimentary beds. The Gaussian sweep produces only a few side-lobes but it does have a large amount of negative energy beside the main positive spike.

Plots of the correlated trace amplitude spectrum (Figure 3.4) show that the resulting spectrum is related to the sweep spectrum. The spectrum of the reflectivity is filtered by the power spectrum of the sweep.

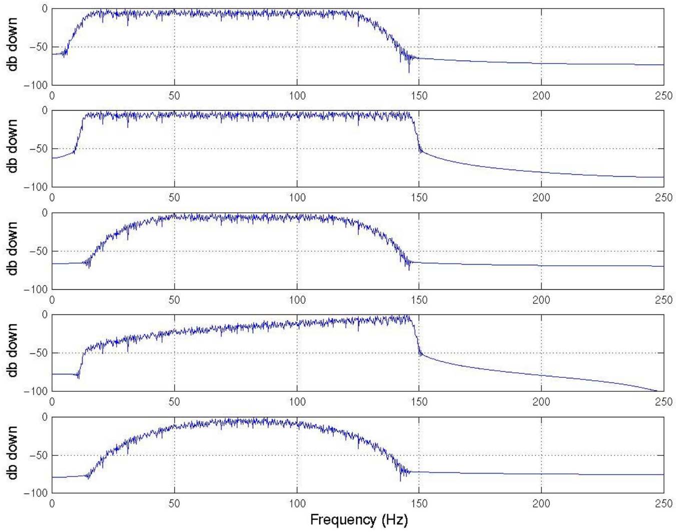

Figure 3.4: Decibel spectrum of the reflectivity and the results of the crosscorrelation. From top to bottom: the spectrum of the reflectivity, sweep 1, sweep 2, sweep 3 and sweep 4. The spectral shape for the deconvolved data are filtered by the power spectrum of the sweep as a result of the sweeps' autocorrelation.

3.2.2 Frequency-domain sweep deconvolution

For frequency-domain sweep deconvolution, FDSD, the results are independent of the sweep. When the sweep input into the ground is equal to the sweep used in FDSD the result is the reflectivity, such that:

$$FDSD(\omega) = \frac{R(\omega)S(\omega)}{S(\omega)} = R(\omega)\,. \qquad (3.3)$$

The result is limited by the sweep frequency range since there can be no data recorded outside of the sweep's bandwidth. For all of the FDSD examples the final results are bandpass filtered at 10-15-135-150 Hz to remove any energy recorded at frequencies outside the band of the sweep. Figure 3.5 and 3.6 indicate that an identical result is obtained for each sweep.

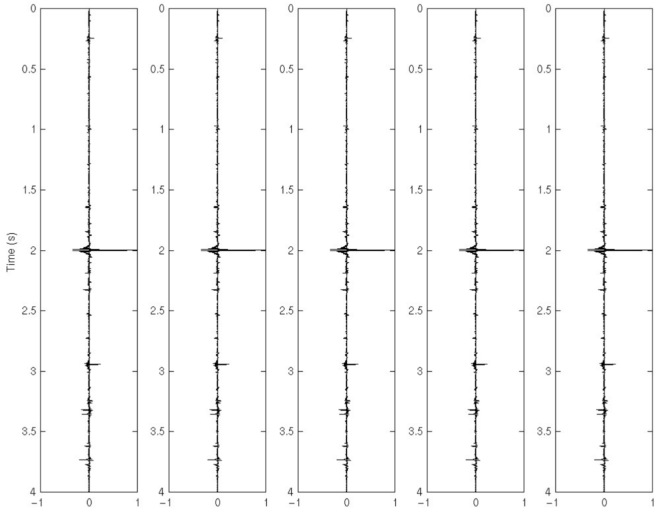

Figure 3.5: Results of frequency-domain deconvolution for the synthetic data with no noise and no earth-attenuation. From the left to right: reflectivity, sweep 1, sweep 2, sweep 3 and sweep 4 as identified in Figure 3.1. There is no discernible difference between the results.

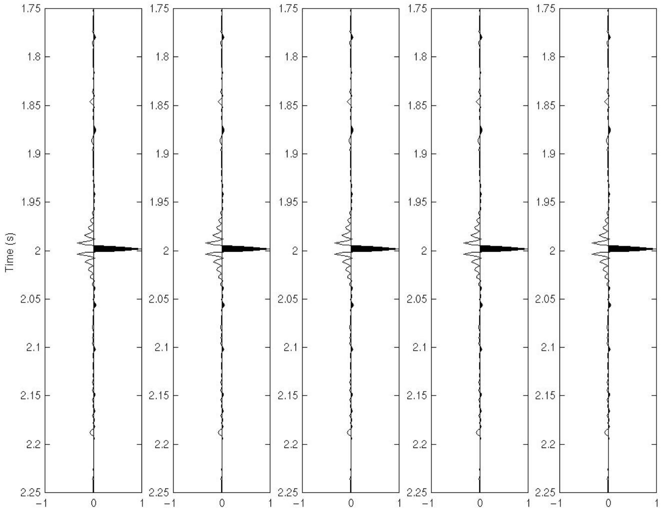

Figure 3.6: Results of the FDSD with the plots zoomed in from 1.75 to 2.25 seconds on the large reflectivity spike. From the left to right: reflectivity, sweep 1, sweep 2, sweep 3 and sweep 4 as identified in Figure 3.1. The results of the FDSD are identical with the wavelet of the reflectivity spike defined by the bandpass filtering of the data.

Due to the simple nature of this model, with no noise and no earth-attenuation, the sweep is completely divided out of the convolutional equation. For each sweep, the spectrum is identical, and prior to the necessary bandpass filtering, the spectrum is completely whitened, eliminating filtering effects by the sweep (Figure 3.7).

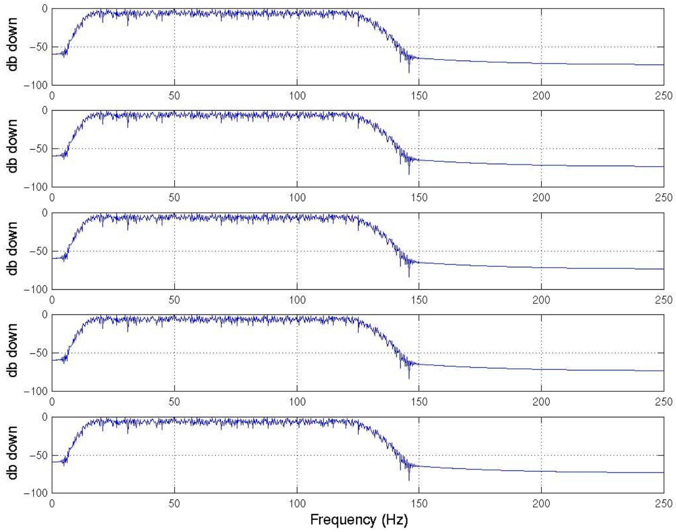

Figure 3.7: Decibel spectrum of the reflectivity and the results of FDSD. From the top to bottom: the spectrum of the reflectivity, sweep 1, sweep 2, sweep 3 and sweep 4. The spectrum shape is independent of the sweep. The spectrum shape is whitened prior to the application of the 10-15-135-150 bandpass filter applied to eliminate the ability of modelling to resolve the frequencies outside of the sweep frequency.

If the data include no noise and no earth-attenuation the result of FDSD is preferential to crosscorrelation since there are no filtering effects related to the sweep. The result has limited dependency on the sweep and is dependent only on the sweep's frequency range. The crosscorrelation results are dependent on the maximum and minimum sweep frequencies and the amplitude spectrum, which filters the data during the sweep removal. It is possible to whiten the data with deconvolution, removing the filtering effects of crosscorrelation to whiten the spectrum.

3.3 ADDITION OF RANDOM NOISE

The second model completed for the synthetic testing includes the addition of random noise to the convolutional equation. This alters the recorded trace equation to

$$\begin{gathered} x(t) = r(t) * s(t) + n(t) \\ \text{and} \\ X(\omega) = R(\omega)S(\omega) + N(\omega) \end{gathered} \quad , \tag{3.4}$$

where the noise *n*(*t*) is additive in both the time and frequency-domain. The noise is random and created with the use of G. Margrave's MATLAB program *rnoise.m*. The random noise level is defined by the signal-to-noise level based on the average power spectrum of the trace. The noise has the same amplitude over the entire spectrum. For the modelling, a signal-to-noise ratio of 5:1 is applied to the synthetic traces.

3.3.1 Crosscorrelation

When the noise is added to the convolutional equation the filtering effects of the crosscorrelation are important as the process will remove the noise excluded from the sweep bandwidth. The crosscorrelation equation is altered to

$$\begin{aligned} cc(t) &= \left(r(t) * s(t) + n(t)\right) * s(-t) \\ cc(t) &= r(t) * k(t) + n(t) * s(-t) \end{aligned} \quad . \tag{3.5}$$

The sweep is removed from the first component of the convolutional equation and replaced with the associated Klauder wavelet. However, the noise is also convolved with the time-reversed sweep. The convolution filters the noise by the spectrum of the inverse sweep, removing the high- and low-frequency noise. This removes a significant portion of the unwanted noise. This process is modelled in Figure 2.1. The result of the crosscorrelation for the synthetic data when there is random noise is shown in Figures 3.8 and 3.9. The spectra for the traces are displayed Figure 3.10.

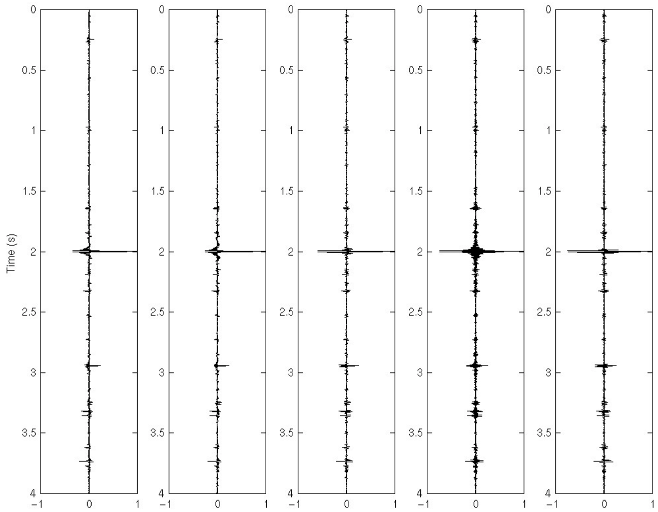

Figure 3.8: Results of the sweep removal by crosscorrelation when there is additive random noise in the convolutional equation. The results are dependent on the sweep shape and the Klauder wavelet created by the sweep autocorrelation. The noise is also filtered by the spectrum of the sweep removing the noise outside of the sweep frequencies. From the left to right: the reflectivity, sweep 1, sweep 2, sweep 3 and sweep 4.

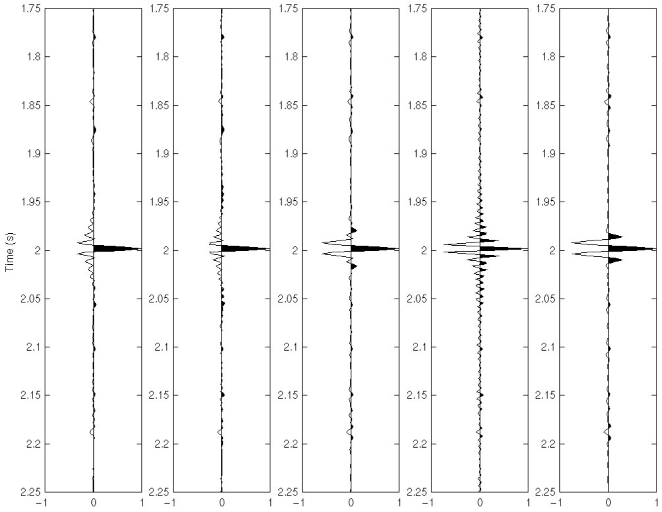

Figure 3.9: Results zoomed in from 1.75 to 2.25 seconds for the sweep removal by crosscorrelation when there is additive random noise in the convolutional equation. There is a small effect on the data related to the noise, with no noise remaining in the frequencies outside of the sweeps. From the left to right: the reflectivity, sweep 1, sweep 2, sweep 3 and sweep 4.

The amplitude spectrum for crosscorrelation with the additive random noise is comparable to the spectrum when there is no noise. The reflectivity is filtered by the power spectrum of the sweep, while the noise is filtered by the amplitude spectrum of the sweep due to the crosscorrelation. The deconvolution removes the data and the noise outside of the sweep bandwidth.

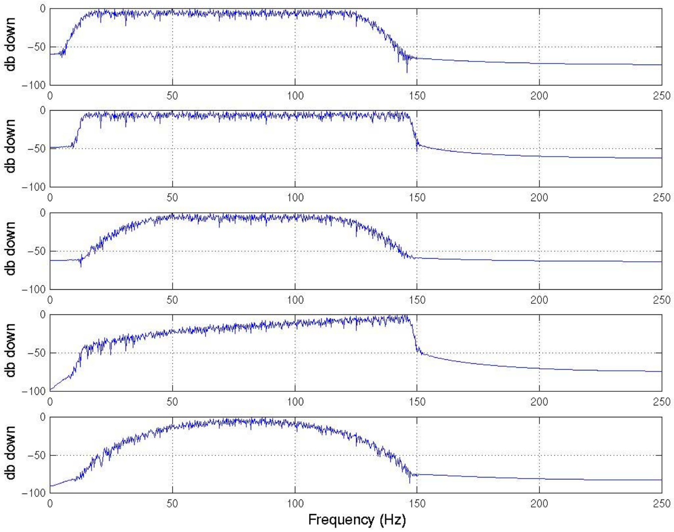

Figure 3.10: From top to bottom: the spectrum of the reflectivity, sweep 1, sweep 2, sweep 3 and sweep 4 from crosscorrelation with the addition of random noise to the convolutional equation. The reflectivity has been filtered by the power spectrum of the sweep and the noise has been filtered by the amplitude spectrum.

The results of crosscorrelation are dependent on the sweep shape. However, there is the advantage that crosscorrelation filters the noise during the sweep removal.

3.3.2 Frequency-domain sweep deconvolution

When there is noise added to the convolutional equation there is a significant effect on the results of FDSD. The equation of the process is altered to

$$\begin{aligned} FDSD(\omega) &= \frac{R(\omega)S(\omega)+N(\omega)}{S(\omega)} \\ FDSD(\omega) &= R(\omega)+\frac{N(\omega)}{S(\omega)} \end{aligned} \quad . \tag{3.6}$$

The sweep is still removed from the reflectivity component of the convolutional equation, as in the noise-free model. The second component of the equation involving the noise is a significant problem. The noise excluded from the bandwidth of the sweep is amplified during the division. There are several ways to handle the amplification of noise during the sweep deconvolution. This includes the use of a noise stability factor to remove the possibility of division by zero for the frequencies outside the sweep bandwidth. An alternative method is to apply a bandpass filter to remove any data not included in the bandwidth of the sweep. The preferred method is a combination of both noise-reduction techniques. The zero values in the sweep need to be removed with the stability factor. However, there will still be some noise outside of the sweep bandwidth that needs to be eliminated with the bandpass filter.

The result of the sweep removal with FDSD is shown in Figure 3.11 and 3.12. The spectra for the traces are plotted in Figure 3.13. The spike at two seconds is visible for all the cases; however, there are differences in the noise contents for the sweeps even though the same process was used. For all of the cases the amplitude spectrum of the noise is constant for all frequencies. When the sweep is nonlinear the signal-to-noise ratio is smaller for the frequencies where the sweep has a lower amplitude.

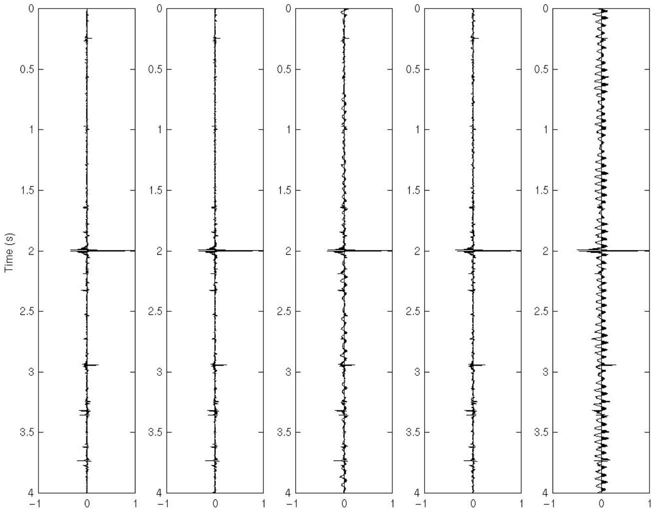

Figure 3.11: Frequency-domain sweep deconvolution for the synthetic data with the addition of noise. The differences in the deconvolved data are related to the different amplitudes of the sweeps over the frequencies. This allows different signal-to-noise ratios over the frequencies. From the left to right: the reflectivity, sweep 1, sweep 2, sweep 3 and sweep 4.

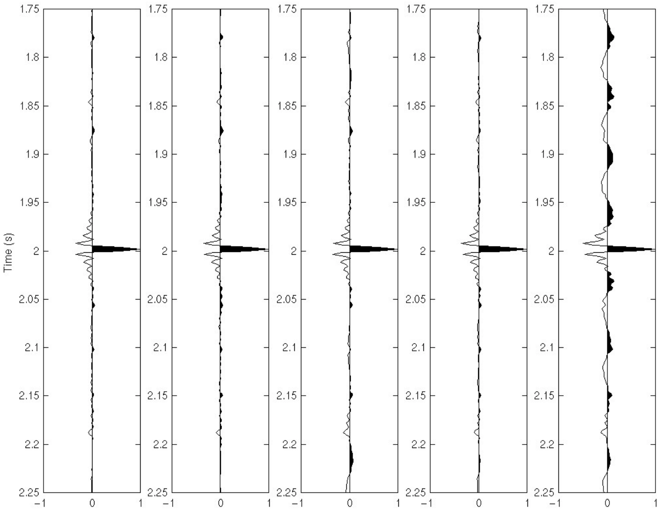

Figure 3.12: Zoomed in from 1.75 to 2.25 seconds for the frequency-domain sweep deconvolution for the synthetic data with the addition of noise. From the left to right: the reflectivity, sweep 1, sweep 2, sweep 3 and sweep 4.

There is a slight phase rotation of the data for frequency-domain deconvolution, visible for the spike. This is related to the pre-deconvolution filtering of the trace.

Similar to the noise-free synthetic example, the spectrum is whitened for the frequencies of the sweep. The final spectrum is not filtered by the shape of the sweep's power spectrum eliminating the dependency of the result on the sweep design.

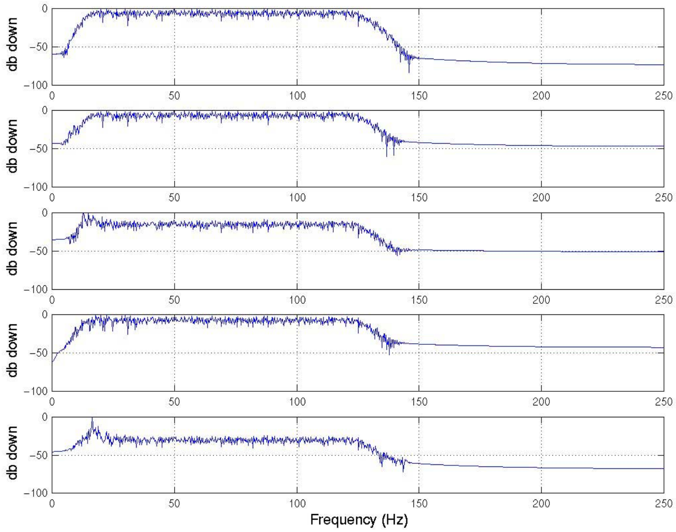

Figure 3.13: Amplitude spectrum of the frequency-domain sweep deconvolution for the synthetic model with the addition of noise. The spectrum is whitened by the sweep removal. From top to bottom: the spectrum of the reflectivity, sweep 1, sweep 2, sweep 3 and sweep 4.

Any differences in the results of the different sweeps are related to the program that applied the random noise. The signal-to-noise ratio used to create the random noise is based on the average power spectrum of the noise free trace. For the nonlinear sweeps, individual frequencies have differing signal-to-noise ratios. For the frequencies where the amplitude is lower than the maximum amplitude the signal-to-noise ratio is lower. This accounts for the slightly different spectra shown in Figure 3.13. The spikes in the spectra maybe removed with additional bandpass filtering; however, for the modelling the bandpass filters were kept the same for all sweeps.

3.4 STATIONARY MINIMUM-PHASE EARTH FILTER

To model a simple earth response, a stationary minimum-phase earth filter was included in the convolutional equation. Gibson and Larner (1984) and Cambois (2000) examine the problems associated with phase rotations in vibroseis data. The vibroseis source after crosscorrelation creates a zero-phase Klauder wavelet. In dynamite data the source is impulsive. However, the recorded data have an embedded minimum-phase wavelet. The minimum-phase wavelet is a result of earth attenuation. In vibroseis data the result of the earth attenuation is the convolution of a zero-phase and a minimum-phase wavelet creating a mixed-phase wavelet. The mixed-phase wavelet cannot be removed with minimum-phase deconvolution. For dynamite data the minimum-phase wavelet can be removed by minimum-phase deconvolution methods.

Another problem associated with the inclusion of earth-attenuation is the effect on the amplitude spectrum. The high frequencies are attenuated more than the low frequencies, changing the spectrum. Minimum-phase deconvolution whitens the spectrum of the data. However, if the data have previously been filtered due to the shape of the sweep in crosscorrelation, the minimum-phase wavelet determined during the deconvolution will be incorrect, creating errors.

The inclusion of the stationary minimum-phase earth-attenuation, $e(t)$ alters the convolutional equation to:

$$\begin{gathered} x(t) = r(t) * e(t) * s(t) \\ \text{and} \qquad . \\ X(\omega) = R(\omega)E(\omega)S(\omega) \end{gathered} \tag{3.7}$$

The minimum-phase earth filter was designed as a minimum-phase wavelet (Figure 3.14).

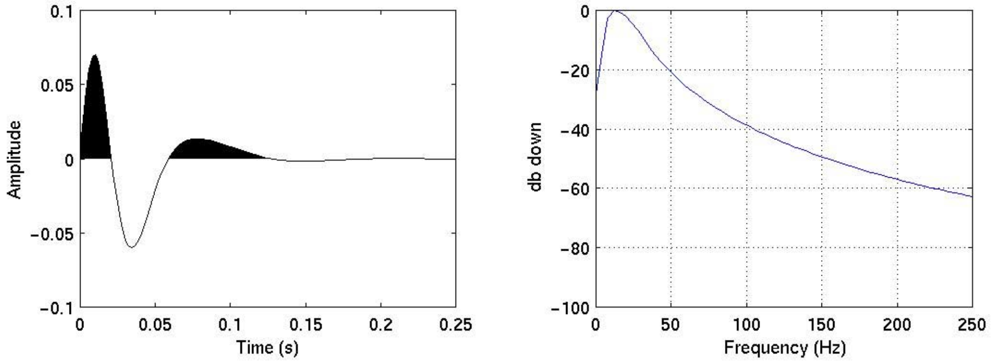

Figure 3.14: Synthetic minimum-phase wavelet created by earth-attenuation. Left plot is the wavelet in the time-domain and the right plot is the amplitude spectrum. The higher frequencies are more attenuated than the low frequencies.

3.4.1 Crosscorrelation

The inclusion of the minimum-phase earth filter to the convolutional equation alters the equation for crosscorrelation to:

$$\begin{aligned} cc(t) &= r(t) * e(t) * s(t) * s(-t) \\ cc(t) &= r(t) * e(t) * k(t) \end{aligned} . \qquad (3.8)$$

The effect of the minimum-phase earth filter being convolved with the Klauder wavelet generated as a result of crosscorrelation can be seen in the model in Figure 2.4.

There is a significant problem associated with the phase of the crosscorrelated data. The inclusion of the stationary minimum-phase attenuation creates a mixed-phase wavelet instead of a zero-phase Klauder wavelet. The differences associated with the sweeps cause different levels of frequency attenuation accounting for the wider wavelet at two-seconds for sweep one compared to the other sweeps (Figure 3.15 and 3.16). This can also be seen in Figure 3.17, the amplitude spectra.

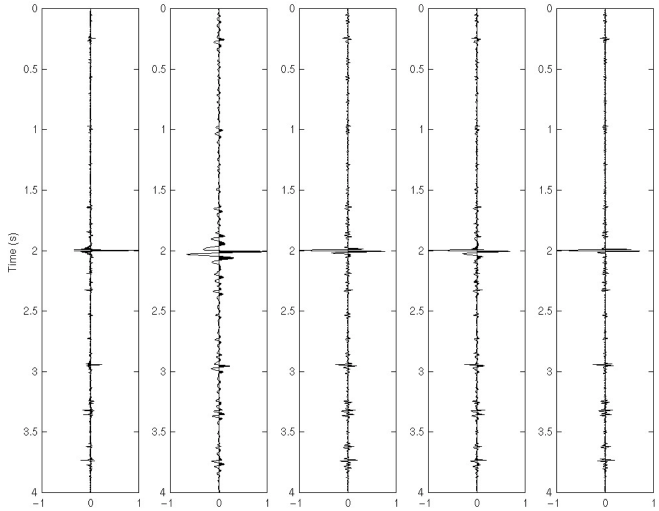

Figure 3.15: Crosscorrelation with a minimum-phase earth filter. The earth filter convolved with the Klauder wavelet creates a mixed-phase wavelet. From the left to right: the reflectivity, sweep 1, sweep 2, sweep 3 and sweep 4.

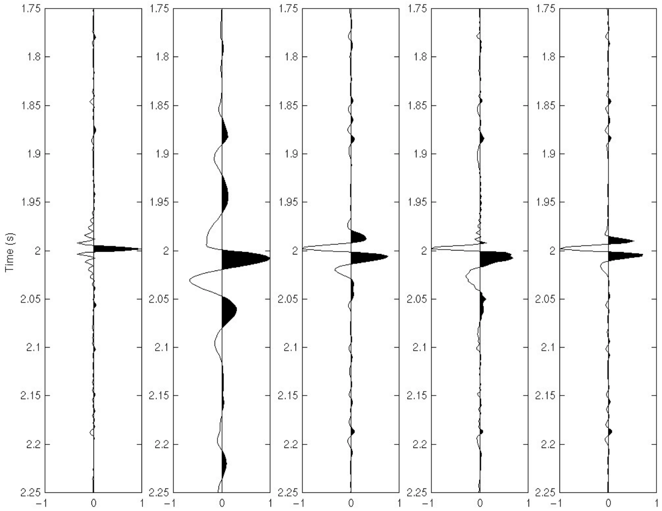

Figure 3.16: Time limited from 1.75 to 2.25 seconds for crosscorrelation with a minimum-phase earth filter. There is a significant difference between the results of the different sweeps and the spike is no longer zero-phase. From the left to right: the reflectivity, sweep 1, sweep 2, sweep 3 and sweep 4.

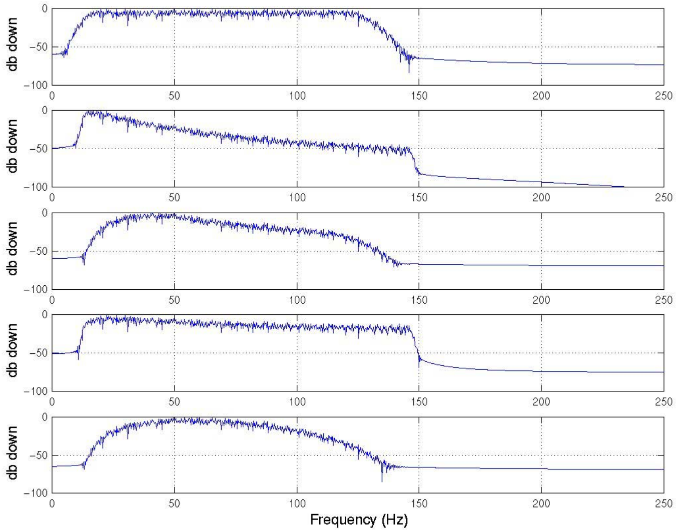

Figure 3.17: Amplitude spectrum for crosscorrelation with the inclusion of stationary earth-attenuation. There are significant differences associated with the sweeps controlling the amount of attenuation. From top to bottom: the spectrum of the reflectivity, sweep 1, sweep 2, sweep 3 and sweep 4.

For data acquisition, it is possible to design the sweep to compensate for the attenuation of the amplitudes due to earth-attenuation. A sweep can be designed to have lower amplitude at the low frequencies than the high frequencies. The earth-attenuation is greater for the upper frequencies, for which the sweep filtering effect will compensate. Knowledge from previous seismic surveys is required for proper sweep design.

To improve the amplitude spectrum and attempt to remove the earth-attenuation, minimum-phase deconvolution is applied to all of the crosscorrelation results. Frequency-domain minimum-phase deconvolution determines the amplitude spectrum of the embedded wavelet by estimating the spectrum from the data. This requires the assumption that the reflectivity is white. After the spectrum of the embedded wavelet has been determined the phase is assumed as minimum-phase. The estimated wavelet is then removed in the frequency domain, whitening the spectrum and attempting to remove the minimum-phase effects. Figure 3.18 and 3.19 show the result of the minimum-phase frequency-domain deconvolution of the crosscorrelated data. The minimum-phase frequency-domain deconvolution operator length is 100 samples and the stability factor is 1% for all cases.

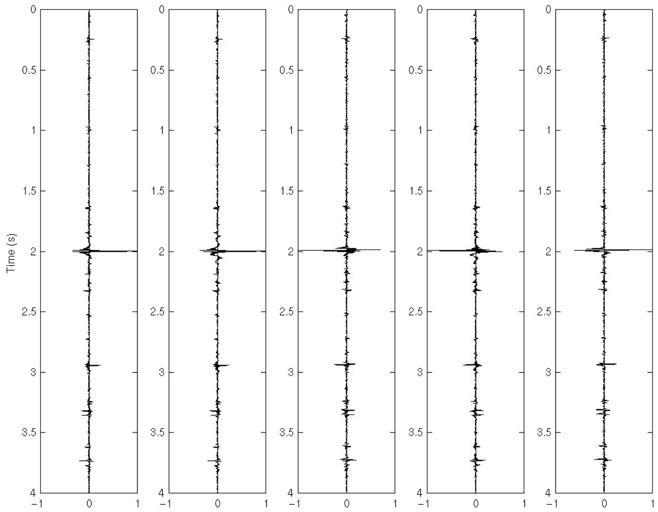

Figure 3.18: Result of minimum-phase frequency deconvolution on the crosscorrelated data. There is still a significant phase rotation for all of the sweeps. The phase rotations are also different since the embedded minimum-phase wavelet estimation differs due to filtering effects of the sweeps and incorrect wavelet spectra determined from the data. From the left to right: the reflectivity, sweep 1, sweep 2, sweep 3 and sweep 4.

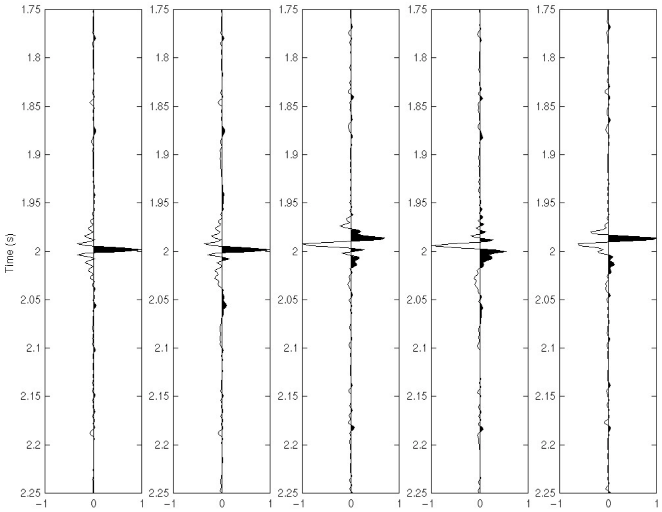

Figure 3.19: The phases for the crosscorrelated data after minimum-phase frequency deconvolution are incorrect for the single spike at 2 seconds. From the left to right: the reflectivity, sweep 1, sweep 2, sweep 3 and sweep 4.

All of the sweeps show an incorrect phase after the minimum-phase frequency-domain deconvolution. The actual phase rotation compared to the original reflectivity can be compared through *ProMAX's* 'Match filter operator' (Figure 3.20). For this process the synthetic trace was filtered to remove the high frequencies that cannot be recorded due to the sweep limitations.

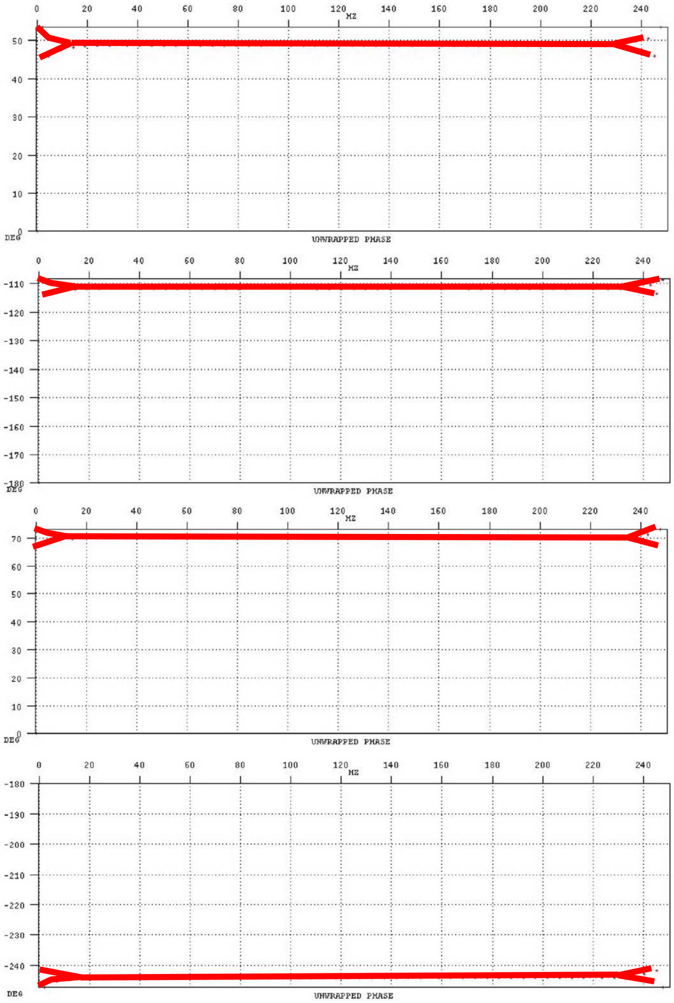

Figure 3.20: Phase rotations determined with ProMAX compared to the original reflectivity. The phase rotations vary for all of the sweeps. From top to bottom with approximate rotations: sweep 1 (50 degrees), sweep 2 (-110 degrees), sweep 3 (70 degrees) and sweep 4 (-250 degrees).

The rotations calculated vary from 50 to 250º. The calculated rotations are 50º for sweep 1, -110º for sweep 2, 70º for sweep 3 and -250º for sweep 4. The different phase rotations are a result of the incorrect minimum-phase wavelet estimation during the frequency-domain deconvolution due to the filtering effects of crosscorrelation.

The amplitude plots show that the spectrum has been substantially whitened for the frequencies of the sweep (Figure 3.21).

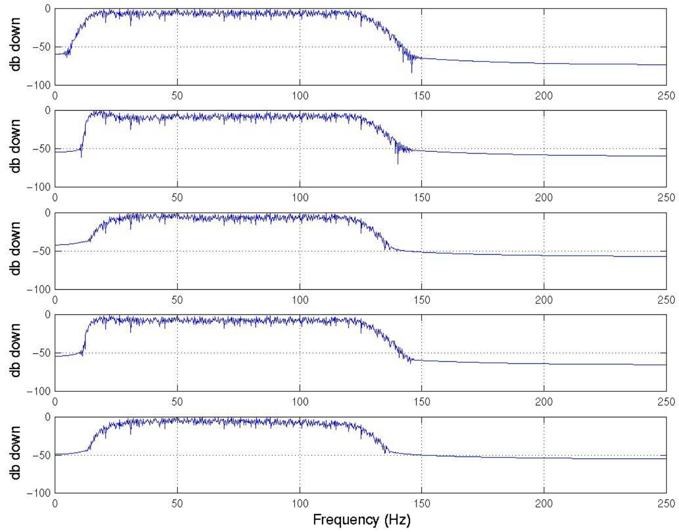

Figure 3.21: Spectra for the frequency-domain deconvolved crosscorrelated data where the spectra have been substantially whitened, incorrectly removing the spectrum effects for both the earth filter and the filtering effect of crosscorrelation. From top to bottom: the spectrum of the reflectivity, sweep 1, sweep 2, sweep 3 and sweep 4.

The spectra have been whitened for both the earth-attenuation and the filtering effects of the crosscorrelation. This is incorrect as the crosscorrelation is not a minimum-phase wavelet as assumed in minimum-phase frequency deconvolution.

3.4.2 Frequency-domain sweep deconvolution

The sweeps embedded in the minimum-phase earth-attenuated synthetic data were removed with FDSD. The inclusion of the earth-attenuation alters the equation for FDSD to:

$$FDSD(\omega) = \frac{R(\omega)E(\omega)S(\omega)}{S(\omega)}, \tag{3.9}$$

which simplifies to

$$FDSD(\omega) = R(\omega)E(\omega), \tag{3.10}$$

if the input sweep sent into the ground is identical to the sweep used to deconvolve the data. In the synthetic data, the sweep is the same as the sweep transmitted into the ground and therefore the only remaining embedded wavelet is the earth-attenuation. In field data, the sweep is attenuated as it progresses through the earth. However if the attenuation is minimum-phase then the change in sweep can be included in the overall earth-attenuation.

The results for all of the sweeps are identical, as there is no dependency on the sweep shape for filtering (Figure 3.22 to 3.24). The only wavelet in the data are the minimum-phase earth-attenuation. The data are filtered subsequent to the sweep deconvolution to account for the bandlimited nature of the sweep.

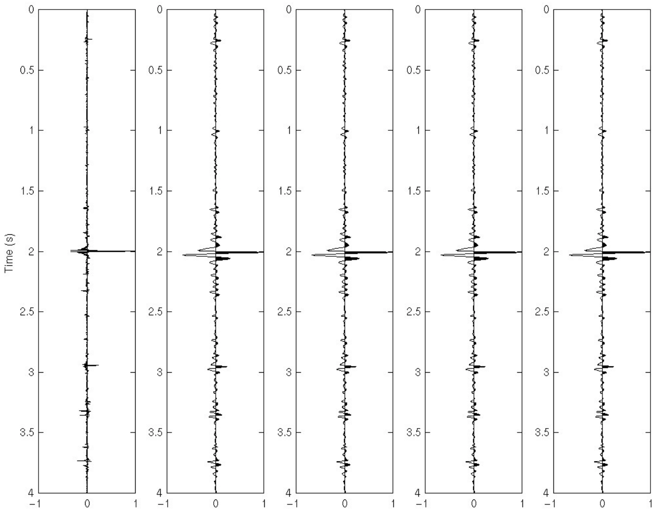

Figure 3.22: Results of frequency-domain sweep deconvolution on the synthetic data with the inclusion of the minimum-phase earth-attenuation. The sweep is completely removed from the data and the only remaining wavelet is the earth-attenuation. From the left to right: the reflectivity, sweep 1, sweep 2, sweep 3 and sweep 4.

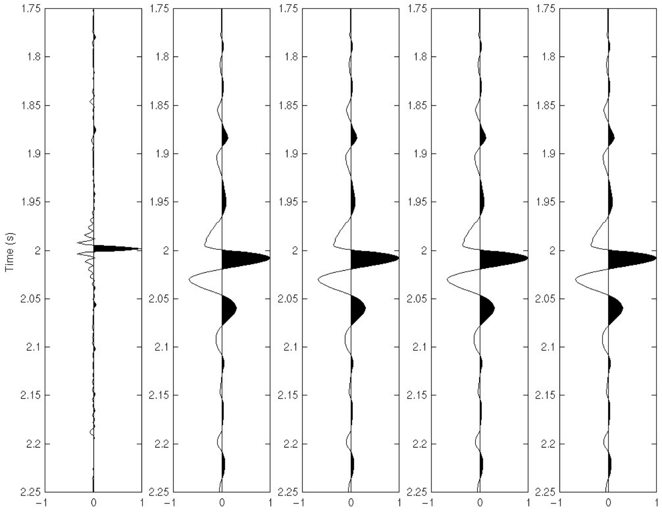

Figure 3.23: Results of frequency-domain sweep deconvolution on the synthetic data with the inclusion of the minimum-phase earth-attenuation from 1.75 to 2.25 seconds. FDSD provides the same results for each sweep, however there is a significant phase rotation due to the earth-attenuation. From the left to right: the reflectivity, sweep 1, sweep 2, sweep 3 and sweep 4.

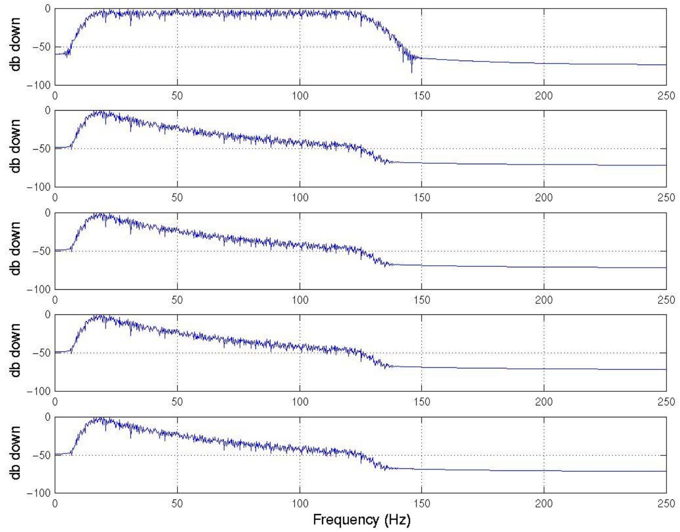

Figure 3.24: Spectra of the FDSD data with minimum-phase attenuation. The only remaining cause of the non-white spectrum is the earth filter leaving the same spectrum for all the sweeps.

The data for FDSD has been bandpass-filtered to remove the frequencies beyond the sweep frequency that are resolved due to the synthetic nature of the data. The amplitude spectrum after FDSD is non-white due to earth-attenuation. For the sweep frequencies it is possible to estimate the spectrum of the minimum-phase attenuation; however, it is not possible to estimate it outside of the sweep frequencies. The attempt to estimate the earth-attenuation is completed with minimum-phase frequency-domain deconvolution.

With minimum-phase frequency-domain deconvolution the earth-attenuation is estimated similar to the example with crosscorrelation. The data are then bandpass-filtered to remove the whitened high frequencies. The results (Figure 3.25 to 3.27) are excellent for the minimum-phase deconvolution. There is a small phase rotation that is associated with the inability to estimate the attenuation in the frequencies outside of the bandwidth of the sweep. The embedded minimum-phase wavelet's amplitudes are destroyed for the frequencies outside of the sweep's bandwidth. The phase rotation is a result of the incorrect estimation of the amplitude spectrum for the embedded wavelet, resulting in an incorrect phase calculation. The incorrect estimation causes the wrong minimum-phase wavelet to be removed from the trace during minimum-phase deconvolution.

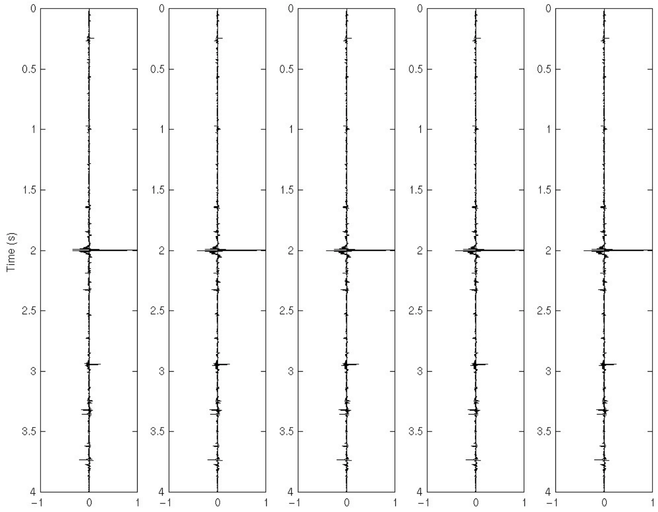

Figure 3.25: The FDSD data after minimum-phase deconvolution is applied to remove the earth-attenuation. From the left to right: the reflectivity, sweep 1, sweep 2, sweep 3 and sweep 4.

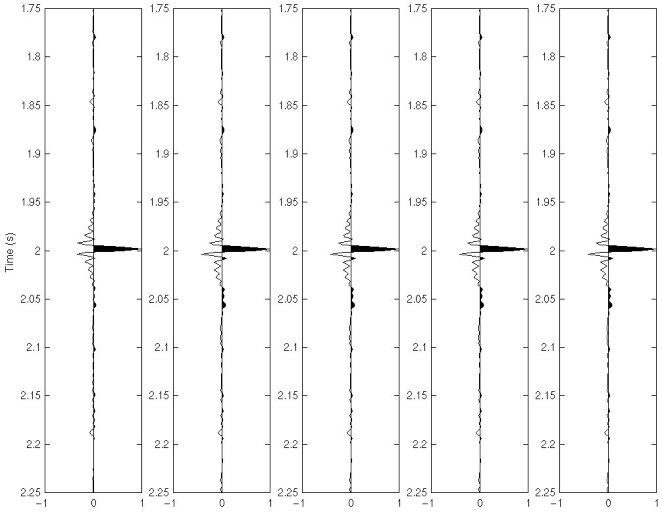

Figure 3.26: Concentrating on the large reflectivity between 1.75 and 2.25 seconds for the FDSD data after minimum-phase deconvolution to remove the earth-attenuation. There is a small phase rotation that is associated with the inability to determine the amplitude of the earth filtering outside of the sweep frequencies. From the left to right: the reflectivity, sweep 1, sweep 2, sweep 3 and sweep 4.

The minimum-phase frequency deconvolution whitens the spectrum of the data within the sweep spectrum. After FDSD, the cause of the non-white spectrum is the earth-attenuation and the bandwidth of the sweep. This can be compared to crosscorrelation where the spectrum also includes the filtering effects of the Klauder wavelet. FDSD allows an accurate minimum-phase wavelet to be determined from the data for the bandwidth of the sweep, leaving a white spectrum. The advantage of FDSD is the lack of sweep influence on the final result. All sweeps with identical bandwidth will create identical results.

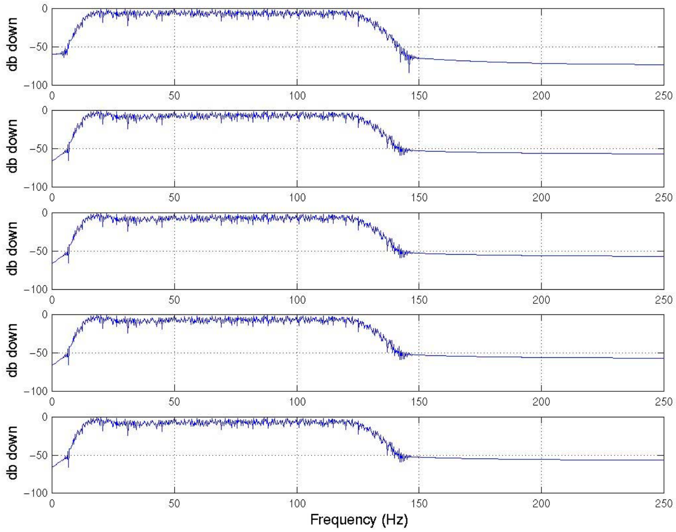

Figure 3.27: Spectrum of the whitened FDSD data. The data have been subsequently bandpass filtered to remove the whitened high frequency data. From the top to bottom: the reflectivity, sweep 1, sweep 2, sweep 3 and sweep 4.

It is possible to determine the amount of phase rotation caused by FDSD with *ProMAX* and the match filter operator (Figure 3.28). The results of the phase comparison show that the phase difference is approximately 10° for all the sweeps.

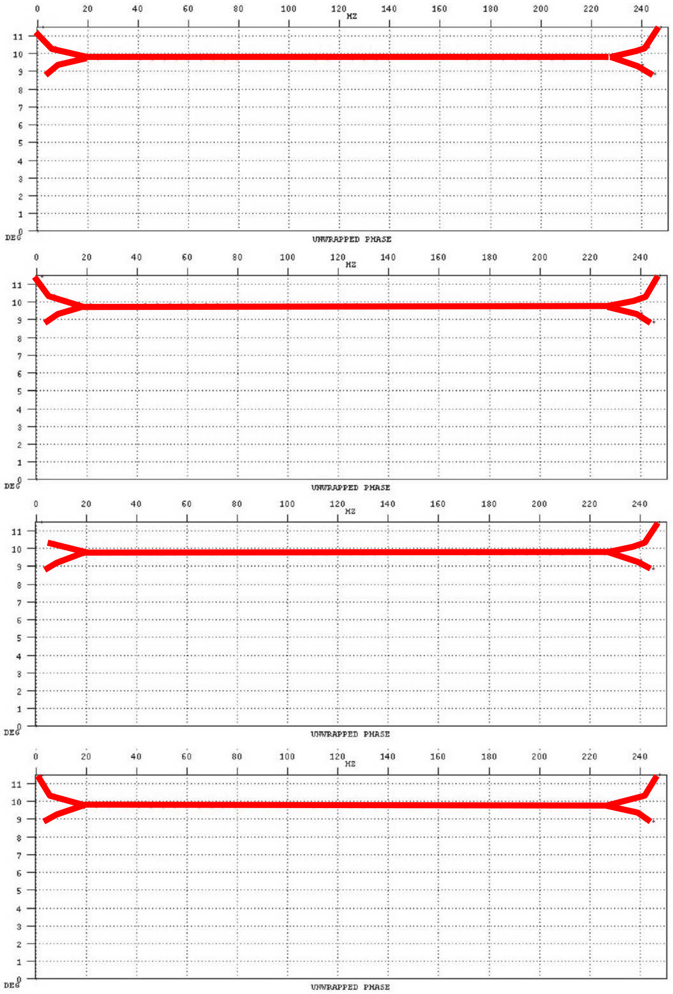

Figure 3.28: Phase rotations determined with ProMAX compared to the original reflectivity. The phase rotations are almost identical for all of the sweeps at 10 degrees. The phase rotation is due to the inability of the minimum-phase frequency deconvolution to estimate the amplitude spectrum outside of the frequency range of the sweep and therefore the embedded minimum-phase wavelet. From top to bottom with approximate rotations: sweep 1, sweep 2, sweep 3 and sweep 4.

The phase rotation of 10º is a result of the inability of minimum-phase deconvolution to estimate the spectrum for the earth-attenuation. If the spectrum is incorrect then the wavelet removed from the data will also be incorrect, resulting in a small phase rotation. The wider the bandwidth of the sweep, up to the Nyquist frequency, the better the minimum-phase deconvolution result.

3.5 COMPARISON OF DECONVOLUTION RESULTS

The deconvolution results can be compared to the reflectivity by completing a crosscorrelation of the reflectivity and the deconvolved data. The closer the result of the crosscorrelation to the autocorrelation of the reflectivity, the more accurate the deconvolution result. If the side-lobes on the crosscorrelation wavelet are not equal then there is a phase rotation associated with the data. When the maximum positive value is not at zero-lag there is a time shift. For better comparative results the reflectivity and the deconvolution results were set so the maximum absolute value was equal to 1.

For the synthetic example that assumes no noise and no earth-attenuation the FDSD results correlated to the reflectivity are identical to the autocorrelation of the filtered reflectivity. The reflectivity is filtered to remove the frequencies that cannot be recorded due to the limited bandwidth of the sweep. This indicates that there is no significant difference between the FDSD data and the filtered reflectivity. For crosscorrelation there are slight differences between the autocorrelation of the reflectivity and the reflectivity/crosscorrelated correlations. This indicates that for nonlinear sweeps there are small difference between the results and the ideal reflectivity. For both FDSD and crosscorrelation there are no phase rotations or time lags (Figure 3.29).

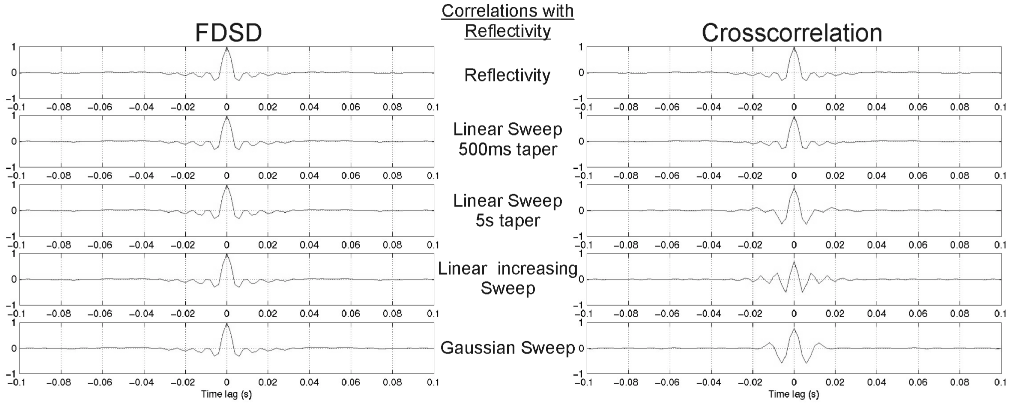

Figure 3.29: Comparison of FDSD to crosscorrelation for the noise and earth attenuated free synthetic model. All of the sweeps for FDSD show identical correlations as that of the autocorrelation of the filtered reflectivity. For crosscorrelation, the results differ from the autocorrelation of the reflectivity indicating differences in the results. There is no phase rotation or time lag for the results.

When random noise is added to the convolutional equation there is a slight phase rotation for the results of FDSD that is a result of the filtering necessary to remove the high signal-to-noise ratio in the high frequencies. This phase rotation is extremely small and can be controlled by adding white noise during FDSD. The results of crosscorrelation are similar to the noise-free synthetic example, with no phase rotation. The crosscorrelation results differ from the autocorrelation of the filtered reflectivity due to the filtering effects of the sweep (Figure 3.30).

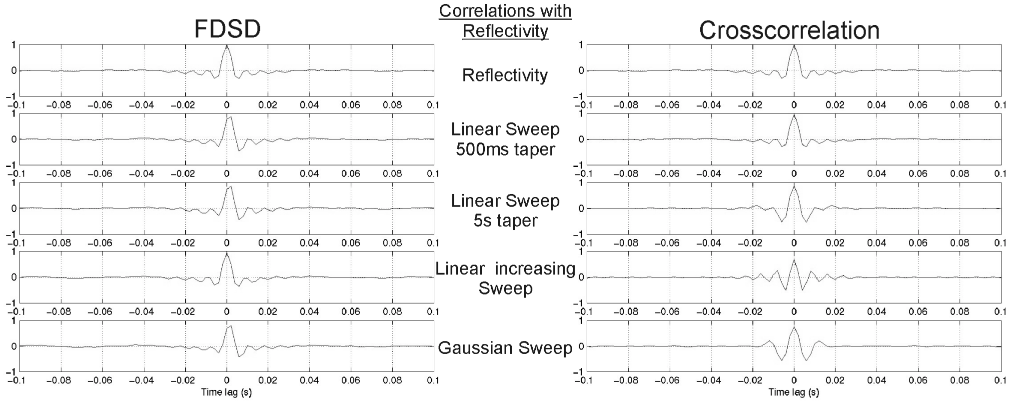

Figure 3.30: Comparison of FDSD and crosscorrelation for the synthetic model with the addition of noise. The correlations for the FDSD results are similar. There is a phase rotation associated with the filtering of the synthetic traces to remove the noise. The crosscorrelation results are similar to the noise-free case with difference due to the filtering effect of the sweep.

A comparison can be completed when a stationary minimum-phase earth-attenuation is included in the convolutional equation (before and after minimum-phase deconvolution). Prior to minimum-phase deconvolution there is a significant amount of phase rotation in the data as well as attenuation of the high frequency data. The FDSD correlations are all identical due to the spectrum whitening effects of the method. For crosscorrelation the data varies for each sweep due to both the attenuation and the filtering property of the method. When the sweep is linear the results are identical for both FDSD and crosscorrelation, as the sweep does not provide any significant filtering. Both methods are affected by the high frequency attenuation, resulting in a poor comparison with the original reflectivity (Figure 3.31).

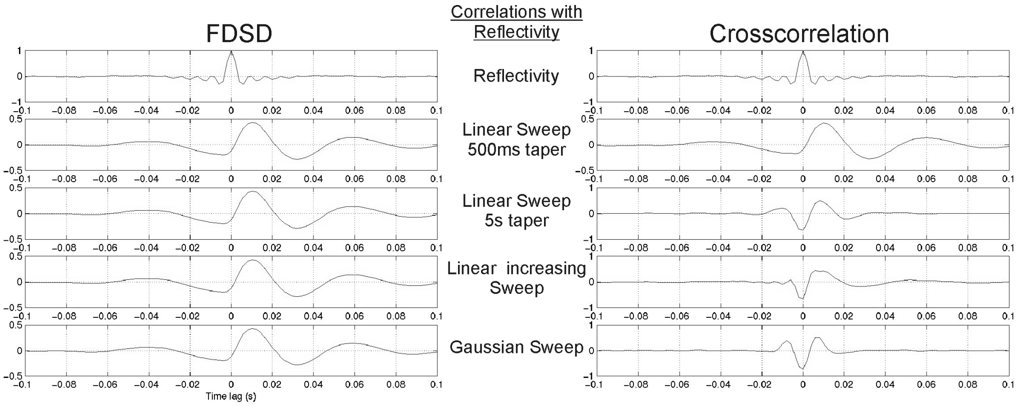

Figure 3.31: Comparison of FDSD to crosscorrelation for the synthetic model with the inclusion of stationary minimum-phase earth-attenuation. For FDSD there is a significant amount of phase rotation, however the rotation is equal for all sweeps. For the crosscorrelated results there is also a large amount of phase rotation and it differs for the different sweeps.

Minimum-phase deconvolution is used to remove the minimum-phase earth effects. The minimum-phase deconvolution is effective for the FDSD as there is no filtering associated with the sweep removal. There is a small phase rotation associated with the inability to estimate the embedded minimum-phase wavelet amplitude outside of the sweep bandwidth; however, the results are excellent. For crosscorrelation the attempt to remove the minimum-phase earth-attenuation is less successful as the filtering associated with the sweep during crosscorrelation causes an incorrect estimation of the minimum-phase wavelet. This is not significant for the linear sweep with the small taper in comparison to the other sweeps with increased taper lengths (Figure 3.32).

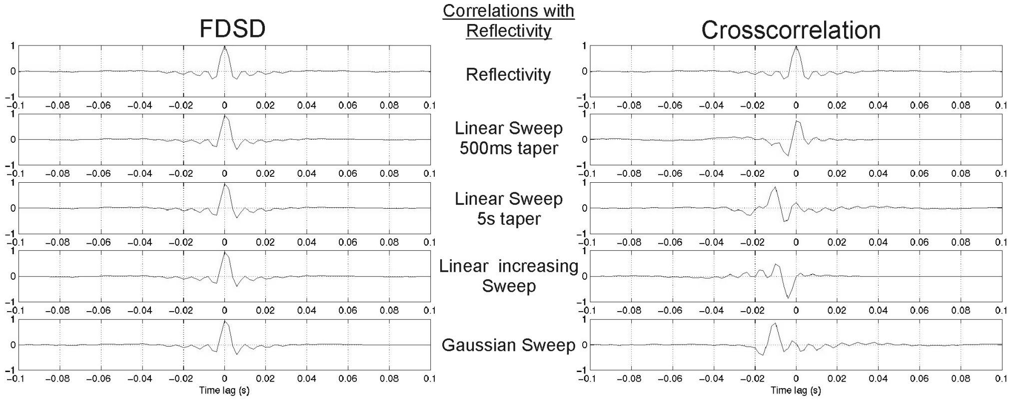

Figure 3.32: Comparison of FDSD and Crosscorrelation synthetic models with the inclusion of stationary minimum-phase earth-attenuation after minimum-phase frequency-domain deconvolution. FDSD is improved by the use of minimum-phase deconvolution, giving a result with only a small phase rotation. For CC the minimum-phase wavelet is incorrectly estimated due to the filtering effects of the sweep crosscorrelation.

The errors associated with minimum-phase deconvolution can be modelled and examined with the amplitude spectrum. It is possible to solve for the wavelet remaining after the sweep deconvolution. This is the wavelet that will be estimated by the minimum-phase deconvolution and subsequently removed.

For the trace with minimum-phase earth filtering the convolutional equation is

$$x(t) = r(t) * e_m(t) * s(t), \tag{3.11}$$

where $e_m(t)$ is the minimum-phase earth filter. During crosscorrelation the sweep is replaced by the Klauder wavelet and the data are subsequently bandpass filtered, $F(\omega)$, in normal processing. This alters the equation to

$$CC(\omega) = R(\omega)E_m(\omega)K(\omega)F(\omega). \tag{3.12}$$

The amplitude spectrum of the minimum-phase embedded wavelet is estimated from this equation as

$$\left|\hat{\boldsymbol{E}}_{\mathrm{m}}(\omega)\right| = \left|E_m(\omega)\right|\left|K(\omega)\right|\left|F(\omega)\right|, \tag{3.13}$$

where $\left|\hat{\boldsymbol{E}}_{\mathrm{m}}(\omega)\right|$ is the amplitude of the estimated minimum-phase embedded wavelet. The wavelet is assumed to be minimum-phase by the deconvolution process. When this wavelet is used in the minimum-phase deconvolution the result is

$$CC(\omega) = \frac{R(\omega)E_m(\omega)F(\omega)K(\omega)}{\hat{E}_m(\omega)}. \tag{3.14}$$

For FDSD the same process can be completed with the result initially being,

$$\begin{aligned} FDSD(\omega) &= \frac{R(\omega)E_m(\omega)S(\omega)}{S(\omega)}, \\ &= R(\omega)E_m(\omega) \end{aligned} \tag{3.15}$$

when the sweep input into the ground is equal to that used for FDSD. Similar to the process of crosscorrelation, a bandpass filter is applied to the data to remove the frequencies excluded from the sweep. This alters the equation to

$$FDSD(\omega) = R(\omega)E_m(\omega)F(\omega). \tag{3.16}$$

The minimum-phase embedded amplitude spectrum is estimated from this equation as,

$$\left|\hat{\boldsymbol{E}}_{\mathrm{m}}(\omega)\right| = \left|E_m(\omega)\right|\left|F(\omega)\right|. \tag{3.17}$$

After FDSD there is no Klauder wavelet embedded in the data. This gives the processor control for filtering the data with the potential to simulate a linear sweep with extremely small tapers. The result of the minimum-phase deconvolution for FDSD is

$$FDSD(\omega) = \frac{R(\omega)E_m(\omega)F(\omega)}{\hat{E}_m(\omega)}. \tag{3.18}$$

The estimated minimum-phase wavelets for the linear sweep with the 500-ms taper and the Gaussian sweep were determined for both FDSD and crosscorrelation (Figure 3.33). The amplitude spectrum was plotted with the real minimum-phase embedded wavelet. The estimation of the embedded wavelet is correct for the bandwidth of the sweep for both the sweep deconvolution methods when the sweep is linear. The plots also indicate that minimum-phase deconvolution will incorrectly estimate the spectrum (for the bandwidth of the sweep) when a nonlinear sweep is deconvolved with crosscorrelation. The estimate of the minimum-phase embedded wavelet after FDSD for the Gaussian sweep is accurate over the bandwidth of the source signal.

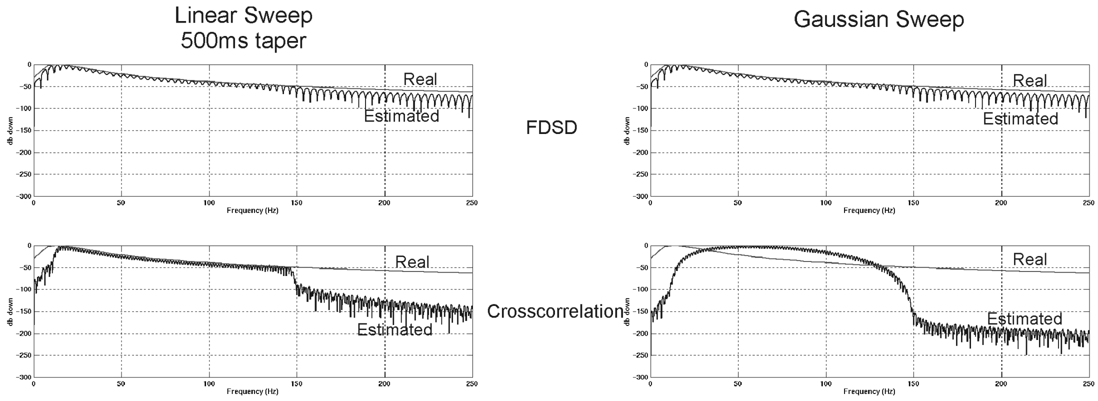

Figure 3.33: The quality of the minimum-phase estimation is dependent on the sweep shape for crosscorrelation but independent for FDSD

3.6 MINIMUM-PHASE EQUIVALENT METHOD

Gibson and Larner's (1984) method of removing the minimum-phase wavelet relies on the calculation of the minimum-phase equivalent of the Klauder wavelet. The associated filter is used to convert the embedded zero-phase wavelet in the trace after crosscorrelation to minimum-phase. This allows an accurate application of minimum-phase spiking deconvolution.

The results of this process are affected by the level of white noise that is added to the data as a stability factor (Figure 3.34).

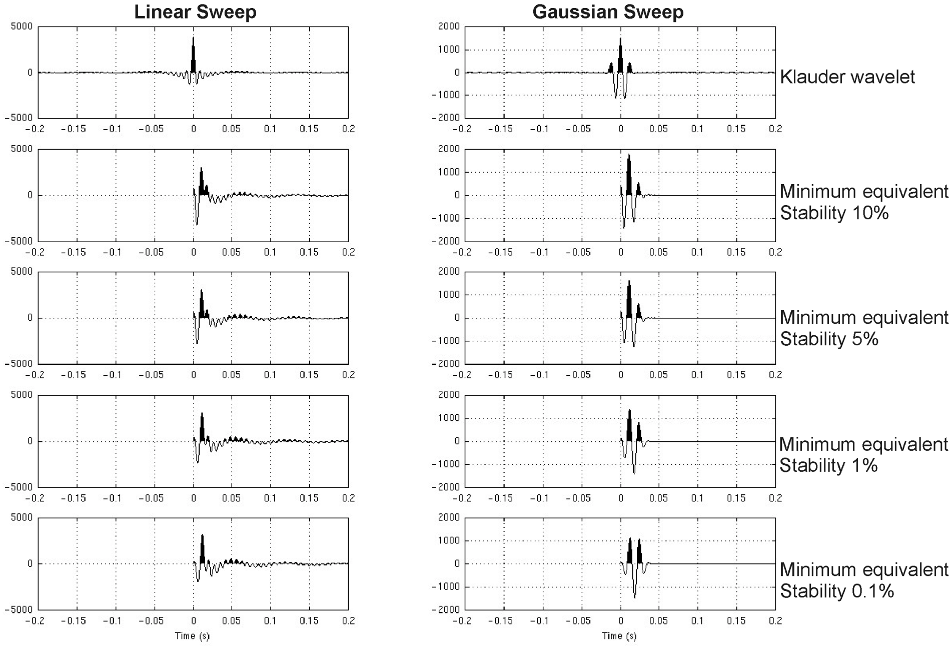

Figure 3.34: Minimum-phase equivalents with 10%, 5%, 1% and 0.1% stability factors for both the linear sweep and the Gaussian sweep. The minimum-phase equivalent depends on the amount of white noise that is added as a stability factor to the spectrum of the Klauder wavelet. The wavelets produced with different stability levels vary less for the linear sweep than for the Gaussian sweep. After Gibson and Larner (1984).

This has been modelled for both the linear and the Gaussian sweeps described in the previous sections of this paper. The linear sweep's minimum-phase equivalents vary with the level of white noise added to the Klauder wavelet's spectrum; however, the variation is greater for the Gaussian sweep.

The quality was examined for the minimum-phase wavelet removal from the modelled data to compare the results with and without the minimum-phase equivalent calculation. The minimum-phase equivalents at 10% and 0.1% white noise were determined for both the linear and Gaussian sweeps. A comparison can be completed between the noise levels required to efficiently determine the minimum-phase equivalent of the Klauder wavelet and the filter to eliminate the mixed-phase wavelet.

For a linear sweep, the results for a simple minimum-phase deconvolution for both the FDSD and crosscorrelated data show only slight phase rotations of ±10 degrees (Figure 3.35).

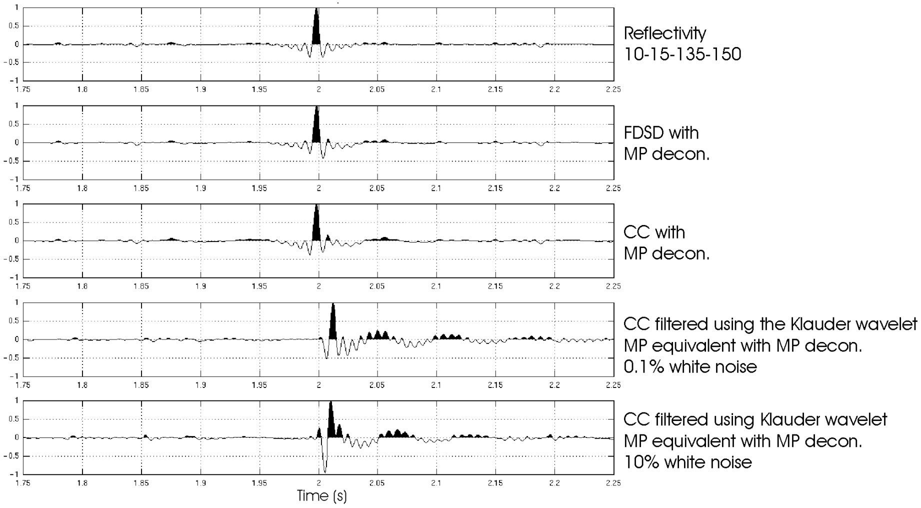

Figure 3.35: Comparison of crosscorrelation, FDSD, and effects of the white noise levels on the minimum-phase Klauder wavelet equivalent for a linear sweep.

If the minimum-phase equivalent for the Klauder wavelet is determined, and the appropriate filter is applied to the trace, the results show slight errors. The first error is a small time shift of 10 ms as a result of the filtering to minimum-phase and the subsequent minimum-phase deconvolution. As a result of the difficulties associated with determining the minimum-phase equivalent of the Klauder wavelet there is a significant amount of side-lobe reverberations in the trace and a phase rotation. The phase rotation is greater for the higher white noise level.

The same comparison can be made for a nonlinear sweep, such as the Gaussian sweep described in the previous sections of this paper (Figure 3.36).

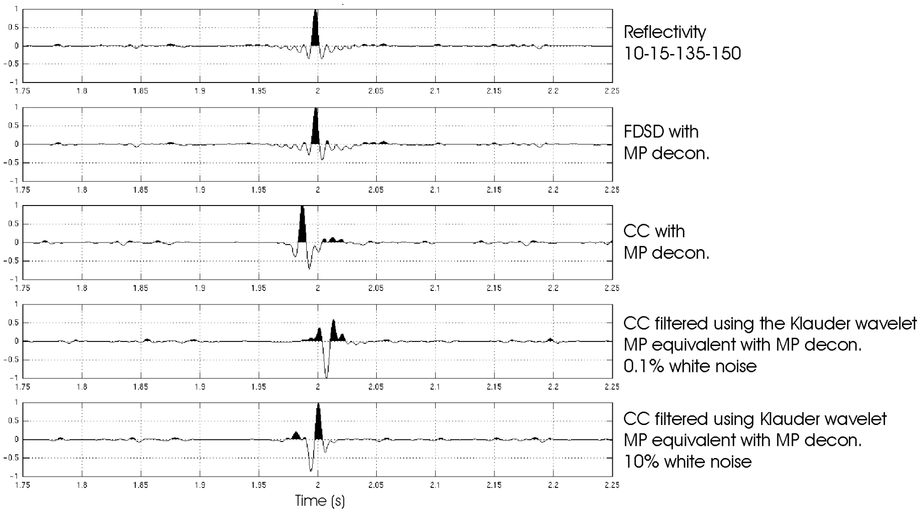

Figure 3.36: Comparison of crosscorrelation, FDSD, and effects of the white noise levels on the minimum-phase Klauder wavelet equivalent for a nonlinear sweep. The results for FDSD are independent of the sweep shape, but are dependent on the frequency content of the sweep and the data recovered.

For the Gaussian sweep, the results of FDSD are identical to that for a linear sweep. Crosscorrelation with minimum-phase deconvolution shows a larger phase shift compared to FDSD. The results when the minimum-phase equivalent method is implemented show extreme variations in quality depending on the amount of noise added as a stability factor. The low 0.1% stability factor gives a result that is approximately 180 degrees out of phase while the 10% stability factor improves the result significantly.

An advantage associated with the FDSD method is the complete removal of the sweep from the data eliminating some of the effects related to the zero-phase Klauder wavelet interacting with minimum-phase earth filtering. There will still be some phase rotation that is related to the bandpass limits of the sweep. The examples shown are for a 10-150 Hz sweep and give a phase rotation of 10 degrees. A sweep of 10-90 Hz increases the phase rotation to 40 degrees.

3.7 CHAPTER CONCLUSIONS

The results of the modelling on synthetic data for both crosscorrelation and frequency-domain sweep deconvolution show varied results when different sweep shapes, addition of random noise and the application of minimum-phase earth filtering are applied. FDSD provides excellent results for all sweep shapes, as the result is independent of the sweep. FDSD does amplify the random noise outside of the bandwidth of the sweep. This amplification is eliminated with the application of a noise factor, eliminating any possible division by zero and the application of bandpass filtering. When the minimum-phase earth filter is applied to the synthetic data the results vary. For a linear sweep, FDSD and crosscorrelation provide similar results. The nonlinear sweep deconvolved with crosscorrelation after minimum-phase deconvolution has a greater phase rotation than FDSD. The application of the minimum-phase equivalent with a linear sweep provides excellent results. However, for a nonlinear sweep, FDSD with minimum-phase deconvolution provides a more accurate reflectivity.

CHAPTER 4

4 VIBROSEIS DATA FROM PIKES PEAK - GEOLOGY AND PRODUCTION

4.0 CHAPTER SUMMARY

This thesis was completed as part of the 2000/2001 AOSTRA (Alberta Oil Sand Technical Research Authority) grant. A heavy-oil field was required to obtain both seismic data for this and other projects, specifically the Pikes Peak field owned by Husky Energy Inc. The data in this thesis, both the uncorrelated field data examined in chapter 6 and the VSP data in chapter 5 were obtained in this area. It is important to have an overview of the production zone for the analysis of the VSP and the seismic data.

4.1 AREA OF INTEREST

Pikes Peak is located 40 km east of Lloydminster in Saskatchewan (Figure 4.1). Similar heavy-oil fields are an important resource in Alberta for future oil reserves. In fact, heavy-oil and oil sands from the Cold Lake, Wabasca, and Athabasca oil sand deposits in Alberta have reserves of approximately one trillion barrels of oil. The oil in these areas are produced with the use of advanced method such as steam recovery. The production in the Pikes Peak area includes steam drive and cyclic steam methods.

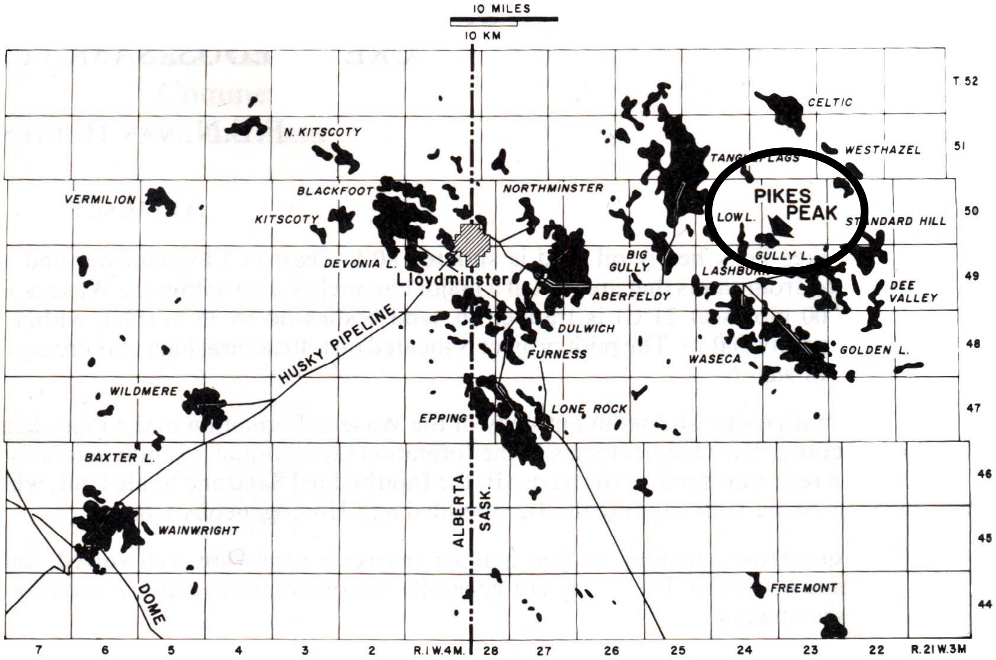

Figure 4.1: Map showing the location of the field of interest, Pikes Peak (Van Hulten, 1984).

Pikes Peak is stratigraphically located in a major channel within the Waseca formation of the Mannville group, Lower Cretaceous. The channel trends north-south and the trapping mechanism is a structural high created both by tilting and Devonian salt dissolution. The oil is classified as heavy with an oil gravity of 12° API at the reservoir temperature of 18 degrees Celsius (Sheppard et al., 1998). The oil saturation for the reservoir sands ranges from 80 to 90% with advanced recovery processes to remove 70% to 80% of the in place oil.

4.2 GEOLOGY

4.2.1 Regional structure and stratigraphy

Several events formed the structural high and subsequent oil trap in the area of Pikes Peak. The first event is the deposition of the Mannville sediments over a pre-Cretaceous unconformity and southwest dipping Paleozoic strata, where the Mannville formation contains the reservoir sands. The dip of the strata was increased in the southwest direction due to post Mannville tilting. After the sediment was tilted to the southwest the structure of the area was altered by dissolution of the middle Devonian prairie evaporite salt beds below the Mannville. The dissolution of the salt beds caused a northeast dip allowing a regional anticlinal structure to develop.

The sequence of interest in this area is the Mannville group, specifically the Waseca formation. Regionally the Waseca is 15-20m of silt and shale overlain by 1-4m of sand (Van Hulten, 1984). The upper sand is a regional oil reservoir. The lower silt and shales do not have any potential for oil production due to low porosity. The Waseca formation is underlain by the Sparky, a thin layer of coal, and is overlain by the McLaren, a shale sequence that forms the reservoir seal.

4.2.2 Channel stratigraphy

Pikes Peak is not a regional reservoir feature; rather it is interpreted as an estuarine channel that trends north-south. The channel contains three rock units that are of mappable size. These are the homogeneous sand, interbedded sand and shale and sideritic silty-shale unit. Figure 4.2 is a cross-section of the channel and shows the main stratigraphic units.

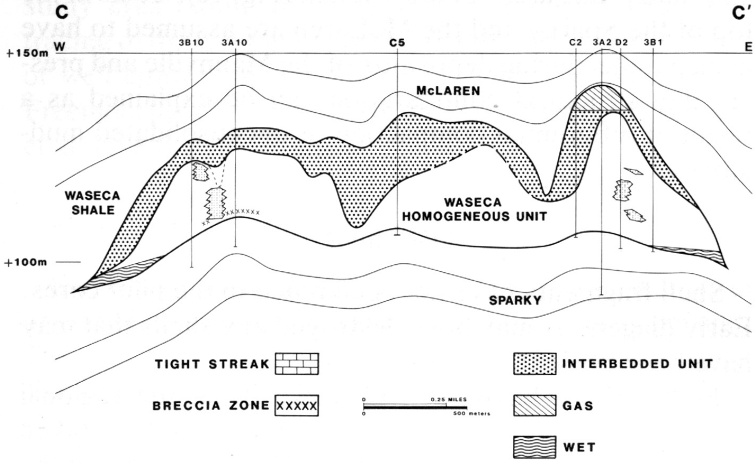

Figure 4.2: Cross-section of the Pikes Peak channel taken from Van Hulten (1984). The producing formation is the Waseca homogeneous sand.

The homogeneous sand is clean sandstone that reaches a thickness of 30 m and is fine to medium grained. The mineralogy of the sand is mainly quartz with some feldspar and heavy minerals. While this layer is labelled as homogeneous it does contain sideritic mudstone fragments, shale clasts and mud balls. The fragments are interpreted to be lag deposits and occur mainly at the base of the unit. One of the interesting features is the lack of sediment consolidation. The diagenetic history of the sand includes compaction and dissolution of unstable components and deposition of kaolinite and carbonates. The high viscosity of the oil may be the result of the low sediment compaction. The porosity of the sand ranges from 30 to 50% with the reservoir quality decreasing in the upper zones due to thin shale beds, with shale rip-up clasts. The permeability of the reservoir is extremely high at 5-10 Darcy. This sediment unit is the main reservoir at the Pikes Peak field. (Van Hulten, 1984)

Above this unit is the interbedded sand and shale, with a thickness of a few to 15 metres. This unit consists of sand with mudstone beds that vary in thickness from cm to dm with the mudstones becoming more prevalent upwards (Van Hulten, 1984).

Compared to the underlying sand, this unit contains more feldspar and clays, including kaolinite, illite and smectite. This creates a reservoir that is not as good as the homogeneous sand; however, the lower zone does produce oil. There is also increasing bioturbation in the upper zone of the unit.

The final unit of the Waseca channel formation is the sideritic shale unit. This unit contains silty shale up to 20m in thickness with visible bioturbation. There are rare coal laminae, sideritic concretions, banded layers and pyrite nodules. This unit forms the upper seal for the reservoir. The seal also includes the overlying McLaren formation, a shale/coal.

4.2.3 Environmental interpretation

The following interpretation is based on Van Hulten (1984).

The coal beds of the Sparky formation suggest that there was a flat Paleozoic surface during the deposition of the Mannville group with a shallow water or subareal depositional environment. The fossils that were examined by Van Hulten suggest that there was marine and tidal influence associated with the sediment deposition, specifically, an estuarine, open marine and shelf environment. The paleo-restoration of the channel is shown in Figure 4.3.

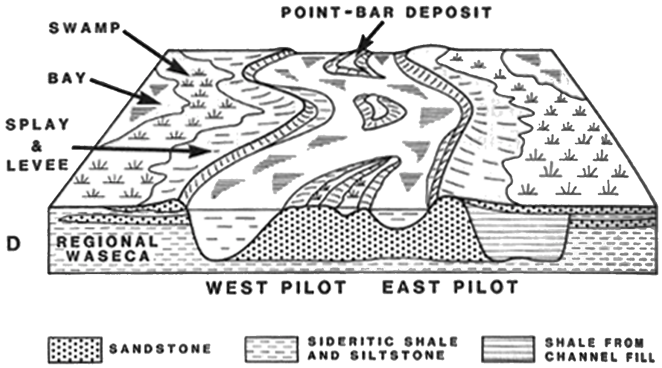

Figure 4.3: Paleo restoration of the Pikes Peak channel. (Van Hulten, 1984)

The Devonian salt dissolution is thought to have started before the deposition of the Waseca formation and may still be active today. The sediment deposits suggest that the Sparky and McLaren coal/shales were deposited during a period of regression, while the Waseca was created by a transgressive period.

Pikes Peak consists of channel deposits with a marine influence and the sediments are associated with deposits from deltaic distributaries, estuarine channels or tidal channels. Putnam (1982) believed that the drainage was into a boreal sea to the north west of the field location.

The channel evolution as interpreted by Van Hulten (1884) is summarized as follows.

i. Early erosion into the bottom unit of the regional Waseca creating lag deposits.

ii. This is followed by the deposition of the homogeneous sand where the structures suggest deposition under high-energy condition (low sea level).

iii. The breccias in the homogeneous sand may be a result of channel bank collapse.

iv. In the upper section of the homogeneous sand there is decreased grain size suggesting a reduction in the deposition energy.

v. Differences in the homogeneous and interbedded sand thickness suggest changes in the channel morphology including point bar deposition.

vi. The homogeneous sand is interpreted to be point bars in an estuarine system with the shaled out section indicating the location of the channel before abandonment.

vii. The channel developed into a sinuous system within the interbedded sand/shale and the shale units. This represents the channel's gradual abandonment.

4.3 RESERVOIR AND PRODUCTION

The Pikes Peak reservoir consists of unconsolidated sand and is located at a depth of approximately 500 metres. Husky Energy chose to produce this reservoir with the assistance of steam production. The lower homogeneous sand is the main reservoir with a mean porosity of 34%, high permeability of 5 Darcies and oil saturation of 80 to 90% (Sheppard et al., 1998). The channel sand contains a heavy oil at 12°API with a gas/oil ratio of 15 m^3/m^3 at the reservoir temperature of 18 degrees Celsius, with isolated gas caps at the structural highs (Sheppard, 1998). During steaming and production the oil in the reservoir is reduced from a viscosity 25 000 mPa·s to 20 mPa·s (Sheppard, 1998).

At the end of 1997, production volumes for the steam project included 13.3×10^6 m^3 of injected steam for a recovery of 4.8×10^6 m^3 of oil and 14.8×10^6 m^3 of water (Sheppard et al., 1998).

There are several different steam recovery methods in this reservoir. The first method is cyclic steam recovery. Steam is injected into the wells for several days to months and then placed on production with steam-to-oil recovery ratios (SOR) of 1.3 to 2.6 (Sheppard et al., 1998). The best SOR recovery ratio occurred during the second cycle due to the reduced viscosity of the oil from the first cycle and the presence of the oil in the steamed zone (Sheppard et al., 1998). Future cycles represent increases in the SOR and decreases in the oil recovered due to interwell communication.

Steam-drive recovery is also used at the Pikes Peak reservoir for oil recovery. The recovery wells are drilled in a hexagonal pattern with a steam injector well located in the centre (Figure 4.4). It is important to have good reservoir quality, thick pay, external pressure, interwell communication prior to initiation and pattern confinement (Sheppard, 1998). Several events must occur at the steam-front for this method to work. These include gas exsolution to create a foamy layer, viscosity reduction, oil distillation, mineralogical alteration, steam drag, gravity drainage, permeability changes and oil saturation dependence (Sheppard, 1998). The most important events are steam drag and gravity drainage. For this reservoir the SOR is approximately 5, which is expected to increase with decreasing oil saturation and reservoir pressures.

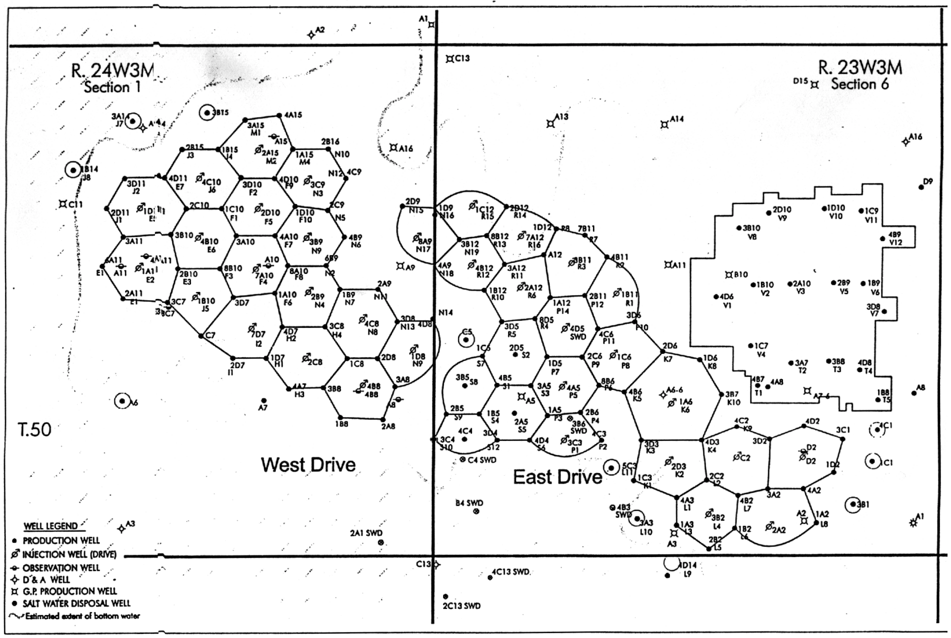

Figure 4.4: Map of the steam drive advanced production well layout at the Pikes Peak oil field. From Sheppard (1998).

4.4 CHAPTER CONCLUSIONS

The Pikes Peak field, operated by Husky Energy Inc. is a shallow estuarine reservoir at a depth of approximately 500 m. The reservoir formation, the Waseca is up to 30-m thick and is separated into three different beds; homogeneous sand, interbedded sand and a shale unit. The structure of the Pikes Peak field was created by the dissolution of Devonian salts on the flanks of the field. The oil is defined as 'heavy' at 12° API and is produced by both steam drive and cyclic steam methods. High-resolution accurate data are required to image the thin beds and the steam zones.

CHAPTER 5

5 VSP, ATTENUATION AND MODELLING

5.0 CHAPTER SUMMARY

In this chapter, the processing of the vertical seismic profile (VSP) is linked to the vibroseis data obtained at Pikes Peak, Saskatchewan. This includes the estimation of the stratigraphic *Q* inverse attenuation values. These values are subsequently used to model the attenuation expected in the area with a composite well-log. The attenuation values are used to model the reflectivity in order to simulate the results of both crosscorrelation and frequency-domain sweep deconvolution. The *Q* values derived from the VSP allow us to more realistically examine minimum-phase deconvolution and inverse *Q* filtering.

5.1 VSP ACQUISITION PARAMETERS

In association with Husky Energy Inc, a VSP survey was obtained in September 2000 at the Pikes Peak heavy-oil field. Pikes Peak is located in Saskatchewan, approximately 40 km east of Lloydminster. The VSP was obtained in well 141/15-06-50-23W3 (Figure 5.1). This well was drilled in 1978 and is suspended due to current uneconomical oil quantities. The total depth of the well is 583.1 m. The surface casing is located from 0 to

107.9 m [diameter = 244.5 mm] and the entire well is cased down to 582.8 m [diameter = 177.8 mm].

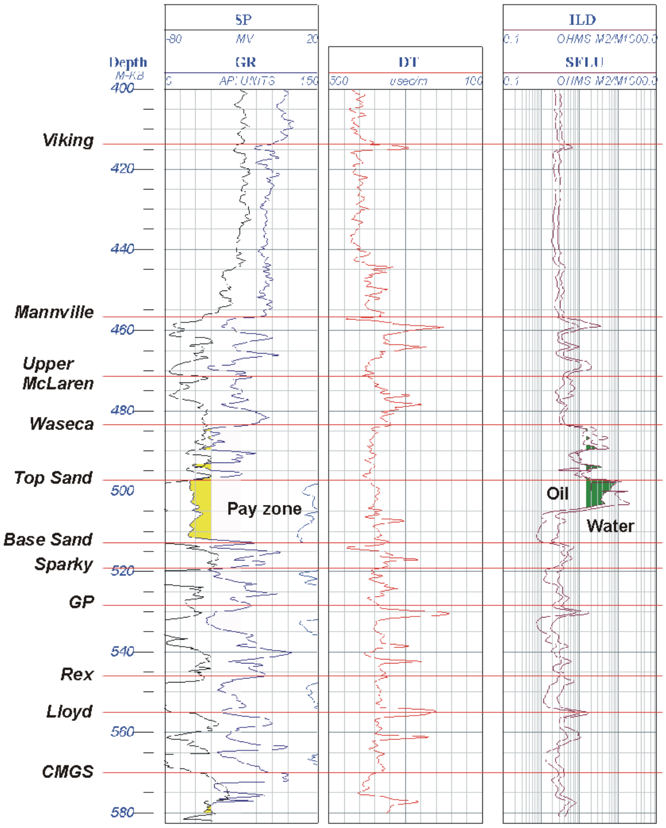

Figure 5.1: Well-log from 141/15-06-050-23W3 including the sonic, density and induction logs. The pay zone (Homogeneous sand) is marked in yellow as the porous zone. The corresponding oil and water zones are marked in green on the induction log.

Schlumberger Canada obtained the VSP with non-gimbaled 3-component, five-level ASI tool. A Mertz HD 18 buggy-mounted vertical vibrator produced a linear sweep from 8 to 200 Hz. A near zero-offset source location was recorded at 23 m as well as five offset locations from 90 to 450 m with 90 m increments. The down-hole geophone cable was clamped from 27 to 514.5 m, measured from the KB with 7.5 m spacing between geophones. An average of 7 sweeps were recorded for each receiver location. A total of 66 receiver locations were recorded with the VSP tool moving 14 times. One hundred and twelve different sweeps were produced to record a total of 510 traces, stacked into the 66 different receiver locations.

5.2 DECOMPOSED VSP

The VSP was recorded unsummed and uncorrelated. The zero-offset data were then processed with both crosscorrelation and frequency-domain sweep deconvolution to determine the velocity profile and the separated downgoing wave. A corridor stack of the zero-offset data are also useful for examining any possible phase rotation in field data due to the sweep deconvolution. The VSP data were processed in Landmark's *ProMax VSP* with the flow shown in Figure 5.2.

Stack of Receiver level data
Deconvolution of the embedded sweep
Bandpass filter (8-12-190-200)
First-break time pick
Velocity analysis
Amplitude Recovery and trace balance
Separation of downgoing and upgoing wave fields (2-D Median filter)
Downgoing waves to deconvolve upgoing waves
Align upgoing wave in two-way time
Enhance upgoing waves with median filter
Corridor stack

Figure 5.2: Processing flow for the decomposition and corridor stack for the zero-offset VSP.

The first step was to stack the data at the receiver level. This enhances the quality of the data by increasing the fold and consequently the signal-to-noise ratio. The next step is to deconvolve the embedded sweep in the data. From the stacked, deconvolved data the first-break picks are determined for both the sweep deconvolved with crosscorrelation (Figure 5.3) and FDSD (Figure 5.4).

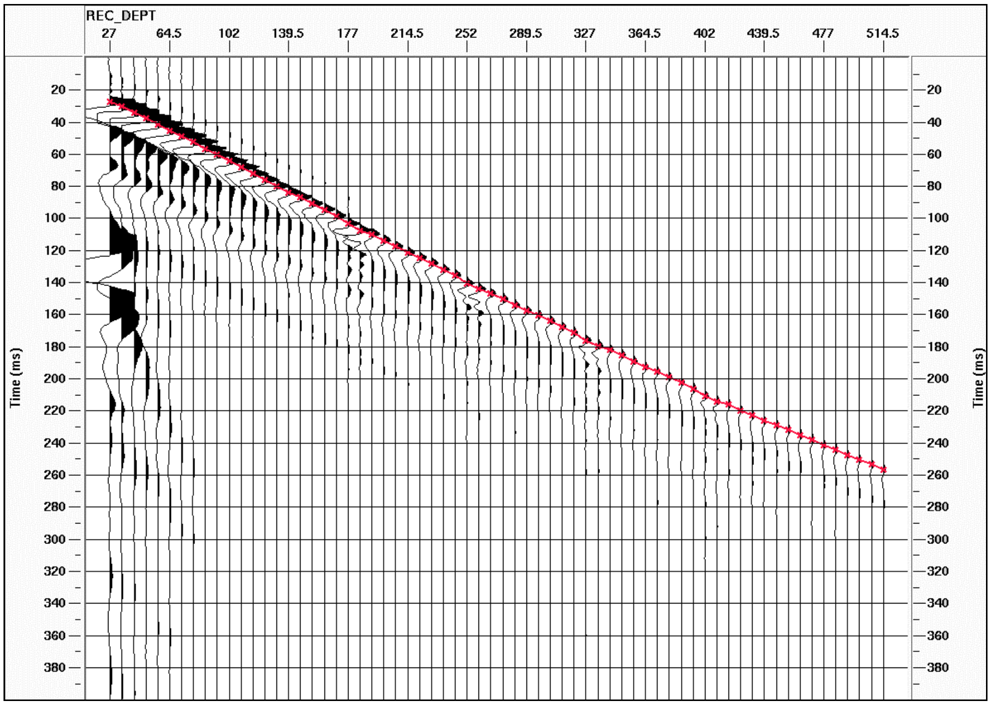

Figure 5.3: Crosscorrelation deconvolved receiver stack with first-break picks.

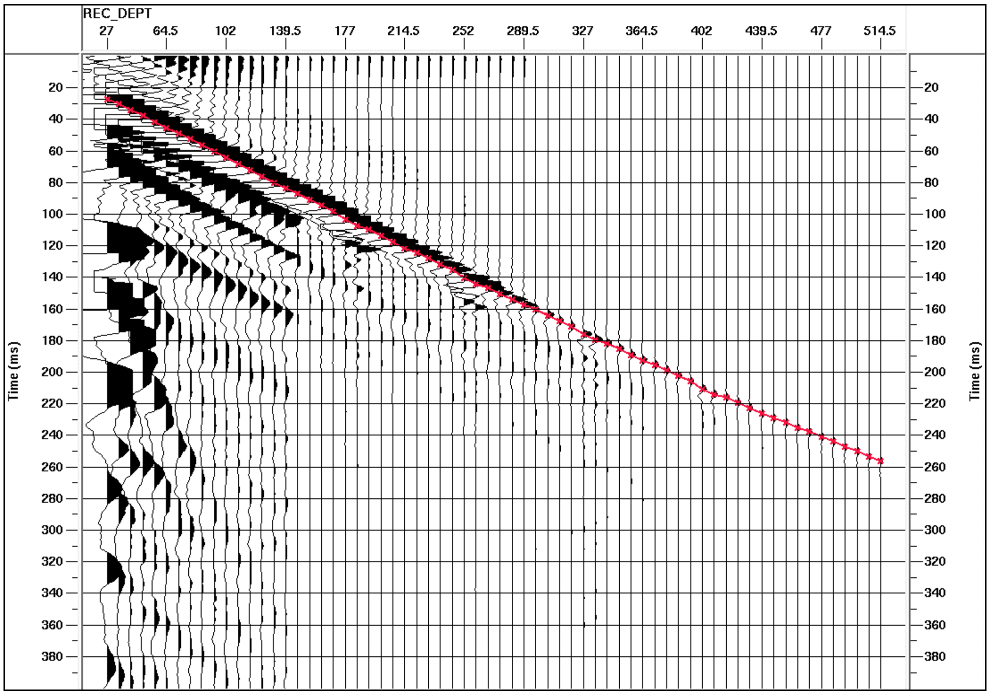

Figure 5.4: FDSD deconvolved receiver stack with first-break picks.

The first-break pick is the time for the wave to reach the receiver; this value is used to determine the interval velocity (V_{int}) as,

$$V_{\text{int}} = \frac{d_{n+1} - d_n}{FB_{n+1} - FB_n}, \qquad (5.1)$$

where d is the depth to the receiver and FB is the first-break time.

For the VSP at Pikes Peak the interval velocity values are shown in Figure 5.5, determined from the crosscorrelated data.

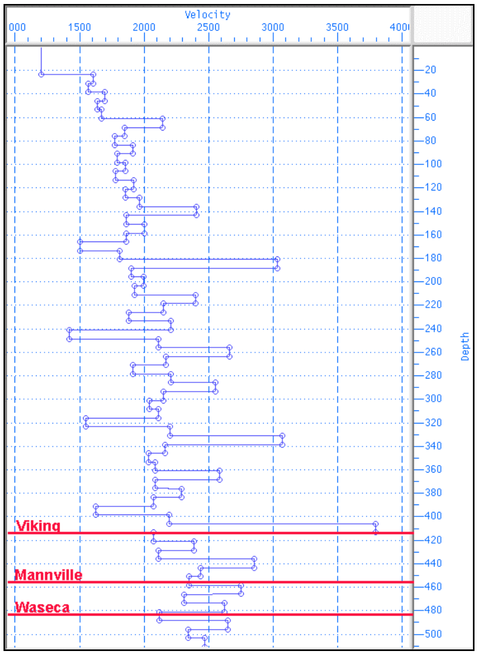

Figure 5.5: Interval velocity values for the Pikes Peak VSP

The interval velocity values generally increase with increasing depth and show both high and low thin-layer velocity changes. The major velocity change in the Pikes Peak area occurs at the Cretaceous unconformity, which is below the depth examined by the VSP. The velocity profile is dependent on the quality of the recording for each receiver location. Any problems, such as receiver coupling, will affect the quality of the first pick and subsequently the interval velocity value.

To eliminate the possibility of any data being lost due to time shifts less than zero during processing, the data are delayed by 100-ms. To separate the downgoing and upgoing wave fields a 3-sample by 7-trace median filter was applied. The median filter isolates the events of interest. For the downgoing wave field separation the filter is added to the data, while for the upgoing wave field a difference is used. If either the first-break picks or the median filter lengths are incorrectly chosen, the result will include processing artifacts. The first-break picks are used to flatten the data before the median filter is applied. For the median filter the sample length indicates the data window, for which the values within the input window are sorted according to their magnitude (Hinds et al., 1996). The centre value of the sort is the median value, the output value of the filter. The new point is then placed at the centre of the window and a new output time series is generated as the window slides both down and across the 2-D data. This method assists in removing the upgoing waves as they do not align with the first-break picks, rather they are anomalous. The upgoing events can then be filtered out while the amplitudes variations of the downgoing events are smoothed over several traces. The upgoing events are separated by the subtraction of the downgoing events from the initial data. The results of the separation are shown in Figure 5.6 and 5.7. The FDSD result shows more noise bursts than crosscorrelation, a result of the bandpass filtering. The extra noise can be removed with a more aggressive bandpass filter; however, to maintain identical processing flows the same bandpass filter is applied for both vibroseis deconvolution methods.

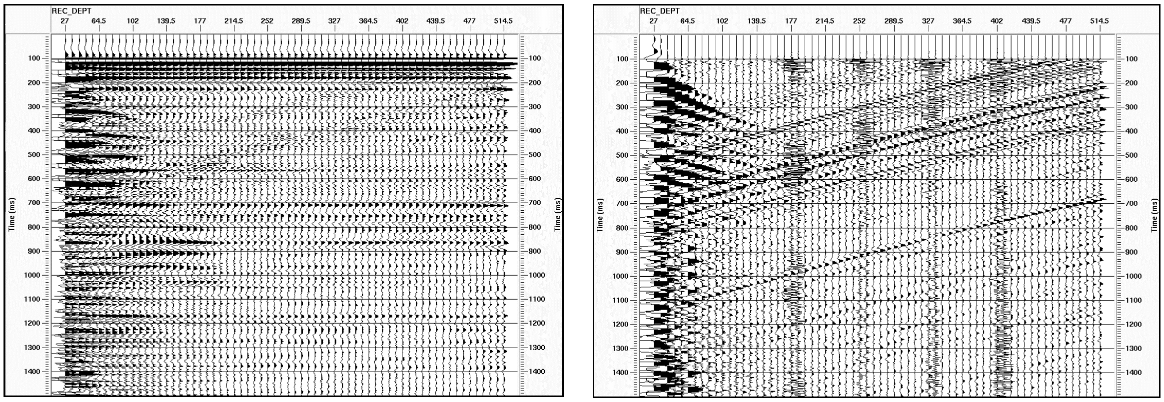

Figure 5.6: Separation of the wave field into downgoing (left) and upgoing (right) with the sweep deconvolution performed with crosscorrelation.

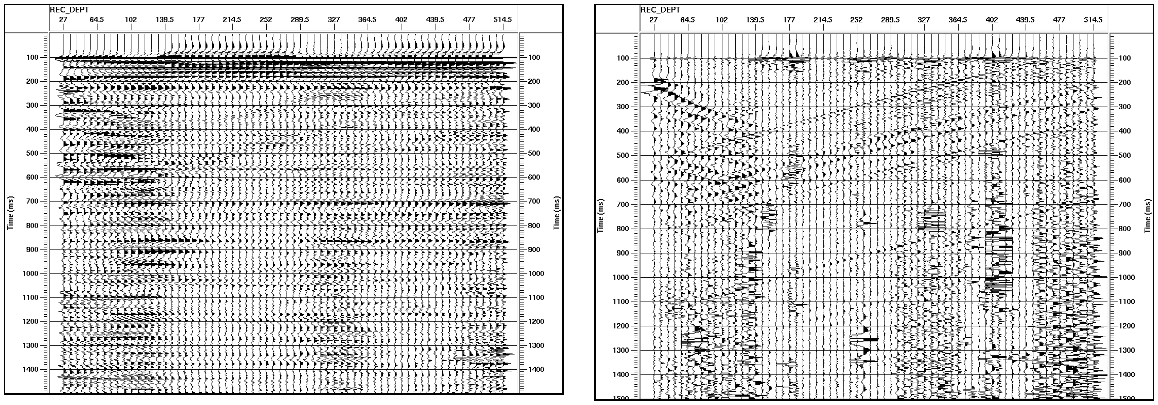

Figure 5.7: Separation of the wave field into downgoing (left) and upgoing (right) with the sweep deconvolution carried out with frequency-domain sweep deconvolution.

The downgoing wave field is used to estimate an impulse wavelet and filter with a 100-ms window. This is then used to deconvolve the upgoing wave field. The result is converted to two-way time with the first-break values (Figures 5.8 and 5.9).

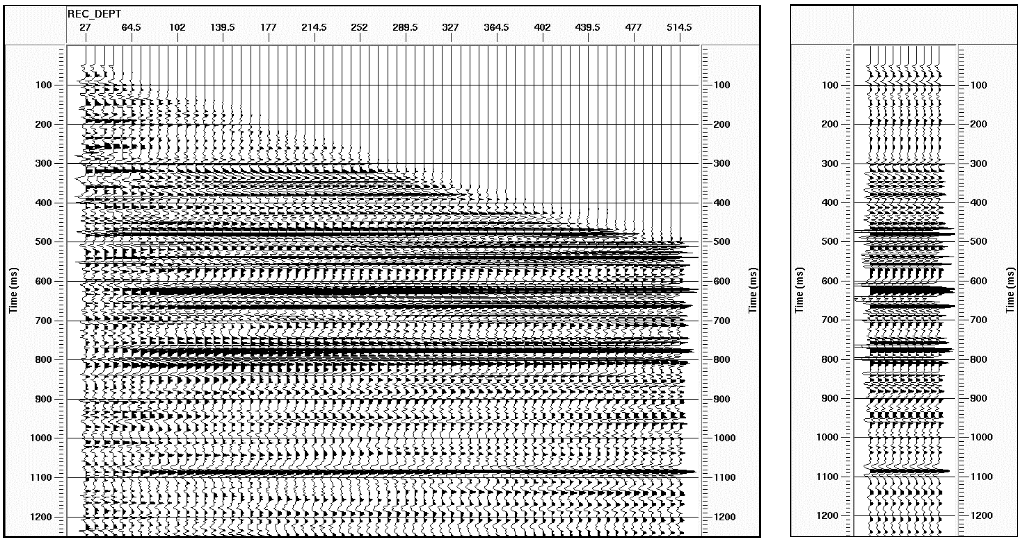

Figure 5.8: Deconvolved (with the wavelet determined from the downgoing wave field) upgoing events (left) and the corridor stack (right) with the sweep deconvolved with crosscorrelation.

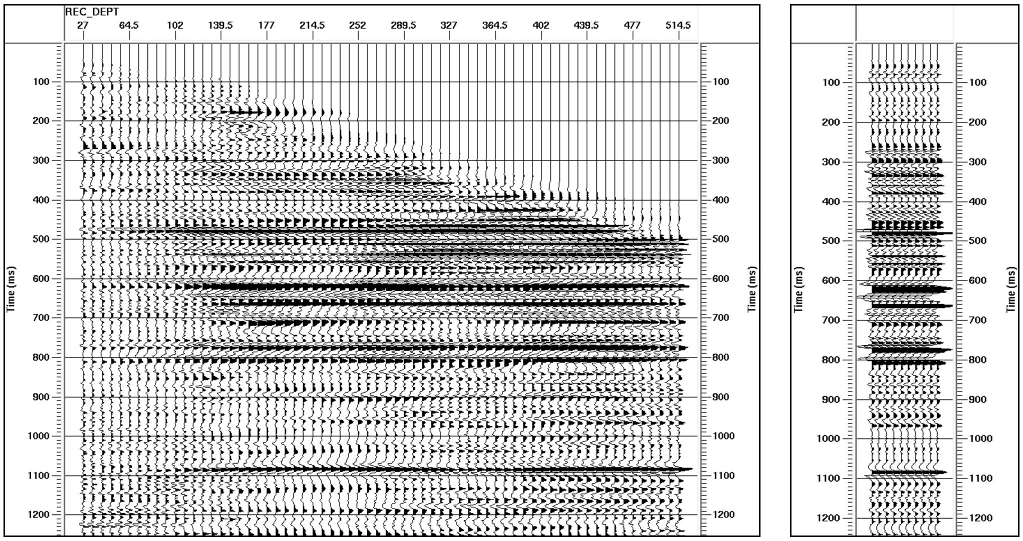

Figure 5.9: Deconvolved (with the wavelet determined from the downgoing wave field) upgoing events (left) and the corridor stack (right) with the sweep deconvolved with frequency-domain sweep deconvolution.

The results from the VSP separation for both crosscorrelation and frequency-domain sweep deconvolution can be compared to the well-log synthetic in order to examine the phase differences.

5.2.1 Comparison of VSP corridor stacks and well log

The calculated corridor stacks can be compared to a synthetic determined from a well log. Unfortunately, the 141/15-06-050-23W3/0 well log starts at 395 m, which is too deep to make an accurate comparison. The well log from 111/15-06-050-23W3/0 starts at a depth of 105 m and is close enough to the VSP for a comparison to be made.

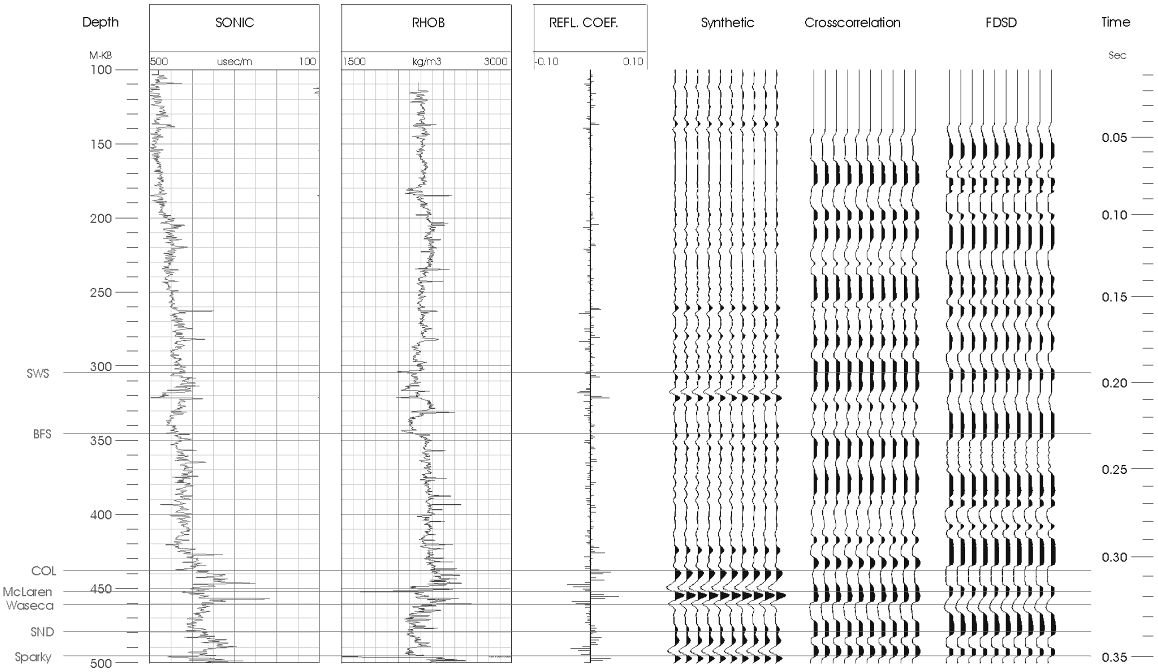

Figure 5.10: Comparison of the corridor stack with the synthetic generated with 111/15-06-050-23W3/0. The synthetic and the corridor are stacks correlated below 100 ms.

There are significant differences between the amplitudes in the two corridor stacks. However, the peaks in the corridor stack and the synthetic from the well-log do align. The amplitude differences are a result of the sweep deconvolution, as the crosscorrelated data are filtered by the Klauder wavelet. The VSP data are of poor quality above the Colorado (labelled COL in Figure 5.10), where there is a significant amount of source-generated noise.

The corridor stacks will be used in chapter 6 to examine the phase rotation of the crosscorrelated and frequency-domain sweep deconvolved seismic data from Pikes Peak. The corridor stack should be close to zero-phase as the downgoing wavelet estimation was used to deconvolve the upgoing wave field.

5.3 DETERMINATION OF *Q* AT PIKES PEAK

In an elastic medium, the energy of the propagating wavefield is conserved. However, the earth is not perfectly elastic and the energy of propagating seismic waves will diminish over time. This is a caused by the anelastic behavior of rocks. Anelastic absorption is the transformation of seismic energy into heat. The resulting attenuation is the absorption of the seismic energy as the seismic waves travel through the earth. The attenuation of the high frequencies increases with a longer travel time.

Absorption is described in geophysics by the absorption coefficient, α, and the seismic quality factor Q. For a perfectly elastic material Q is infinite while, for a perfectly absorptive material, Q is zero.

The initial definition of Q was determined from sinusoidal waves (Knopoff and MacDonald, 1958) as,

$$Q = 2\pi \frac{E_0}{\Delta E} \tag{5.1}$$

where E_0 is the maximum strain energy stored in the rock and ΔE is the energy dissipation in the cycle following the maximum. Strain energy can be defined as the potential associated with the deformation of a body.

For seismic waves, Futterman (1962) determined that Q could also be expressed as the fractional energy loss per cycle,

$$Q = 2\pi \frac{e_o}{\Delta e}, \tag{5.2}$$

where e_o is the amplitude of the maximum energy density and Δe is the dissipation of the kinetic-energy density over a cycle. Energy density is the energy per unit volume of a region of space.

According to Futterman (1962) the relationship between the absorption coefficient, α, and Q is given by,

$$Q = \frac{2\pi}{1 - \exp(-2\alpha\lambda)}, \tag{5.3}$$

where λ is the wavelength. Solving for the exponential in equation (5.3) yields,

$$\exp(-2\alpha\lambda) = 1 - \frac{2\pi}{Q} \tag{5.4}$$

Equation (5.4) can be simplified with the use of the exponential series expansion,

$$e^x = \sum_{n=0}^{\infty} \frac{x^n}{n!}, \tag{5.5}$$

and the assumption that the value of x is small, allowing the summation to be limited to the range from $n = 0$ to 1. This alters equation (5.4) to the approximation

$$1-2\alpha\lambda \approx 1-\frac{2\pi}{Q}, \tag{5.6}$$

which can be solved for both the absorption coefficient, α, as

$$\alpha \approx \frac{\pi}{\lambda Q}, \tag{5.7}$$

and Q as,

$$Q \approx \frac{\pi}{\lambda\alpha} \tag{5.8}$$

For constant-Q theory, the attenuation is independent of frequency but may still depend on time. The propagating waveform over distance, x, can be expressed with the absorption coefficient as (e.g. Margrave, 1999),

$$\left|W_p(f)\right| = \left|W(f)\right|e^{-\alpha x}, \tag{5.9}$$

where $\left|W(f)\right|$ is the input amplitude spectrum of the source waveform and $\left|W_p(f)\right|$ is the amplitude spectrum of the waveform after it has propagated over the distance x. Through the approximation of the absorption coefficient to Q (equation 5.8) this can also be expressed as,

$$\left|W_p(f)\right| \approx \left|W(f)\right|e^{-\pi f t/Q}. \tag{5.10}$$

With the relationship of $t = x / v$, where t is the time the waveform has propagated at a velocity, v, equation 5.10 can be modified to

$$\left|W_p(f)\right| \approx \left|W(f)\right| e^{-\pi f x / Q v}. \tag{5.11}$$

The seismic quality factor is generally assumed to be frequency-independent, apart from a slight dependency due to dispersion (Futterman, 1962). Dispersion is a result of the velocity variations for the different frequencies of a waveform. In determining a Q value from data, scattering and interference must be separated. An incomplete removal of these effects will distort the Q estimation. The methods of Q estimation determine the effective Q, the sum of the anelastic absorption and the apparent attenuation (Spencer et al. 1982).

There are also phase effects related to the propagating waveform. An input impulse is attenuated for all non-zero frequencies, implying dispersion. The amount of attenuation is also proportional to the time that the waveform has been travelling. The phase-shift in the wave, caused by the absorption, must have a causal arrival (Futterman, 1962). The causality invoked in Futterman's absorption-dispersion relation actually requires a minimum-phase attenuation filter, as shown by Aki and Richards (1980, p.172-175).

5.3.1 Spectral-ratio method

The spectral-ratio method (Båth, 1974) is widely accepted for determining the interval Q values from a VSP. This method was chosen based on the findings of Tonn (1991), where a comparison of different computation methods was completed and it was found to be the most reliable.

The first step in the spectral-ratio method is to determine the downgoing times from the VSP. These times are ascertained from the first-break picks of the VSP. The first-break picks indicate the amount of time for the energy to travel from the surface source to the specific receiver in the well. It is important that the VSP has not been altered by any amplitude gains.

For each receiver the amplitude spectrum is determined for the trace, specifically the initial downgoing arrival. For better results, the spectra can be smoothed with a boxcar function.

The natural logarithm of the ratio of the amplitude spectra for two receivers can be determined using equation (5.10), where the amplitude spectrum of receiver 1, $|W_1(f)|$, is related to the initial amplitude spectrum of the propagating waveform, $|W_o(f)|$, as

$$|W_1(f)| = |W_0(f)| e^{-\pi f t_1 / Q}. \tag{5.12}$$

The amplitude spectrum of receiver 2, $|W_2(f)|$, is related to the initial amplitude spectrum of the propagating waveform, $|W_o(f)|$, by

$$|W_2(f)| = |W_0(f)| e^{-\pi f t_2 / Q}. \tag{5.13}$$

where t_1 is the first break time for receiver 1 and t_2 is the first-break time for receiver 2. Receiver 2 is located further from the VSP source than receiver 1. The ratio, $r_{2/1}$, of the amplitude spectra for receiver 2 and receiver 1 is

$$r_{2/1} = \frac{|W_2(f)|}{|W_1(f)|} = \frac{|W_0(f)|e^{-\pi f t_2 / Q}}{|W_0(f)|e^{-\pi f t_1 / Q}}, \tag{5.14}$$

$|W_0(f)|$ is the same value for both receivers and cancels. The resulting ratio can be solved to

$$r_{2/1} = e^{-\pi f \Delta t / Q}, \tag{5.15}$$

where $\Delta t = t_2 - t_1$. By taking the natural logarithm of the ratio, $r_{2/1}$, this becomes

$$r_{2/1} = \frac{-\pi f \Delta t}{Q}. \tag{5.16}$$

Since the ratio of the amplitude spectra can be plotted with the frequency being the dependent value and the resulting equation being linear, the slope of the line, p, is

$$p = \frac{-\pi \Delta t}{Q}. \tag{5.17}$$

The value of Q related to the slope of the line for the ratio of the amplitude spectra is

$$Q = \frac{-\pi \Delta t}{p}. \tag{5.18}$$

The spectral ratio method is used on the VSP data obtained from the Pikes Peak field to obtain an attenuation estimation.

5.3.2 Q at Pikes Peak

The only VSP section used to determine the *Q* values is the near zero offset data, obtained with the source 23 m from the well. The amplitudes of the data have not been adjusted, allowing the spectral-ratio method to be more accurately obtained. The separated downgoing data are used to determine the attenuation of the waves through the earth. The first step was to pick the first-breaks, shown in Figure 5.11.

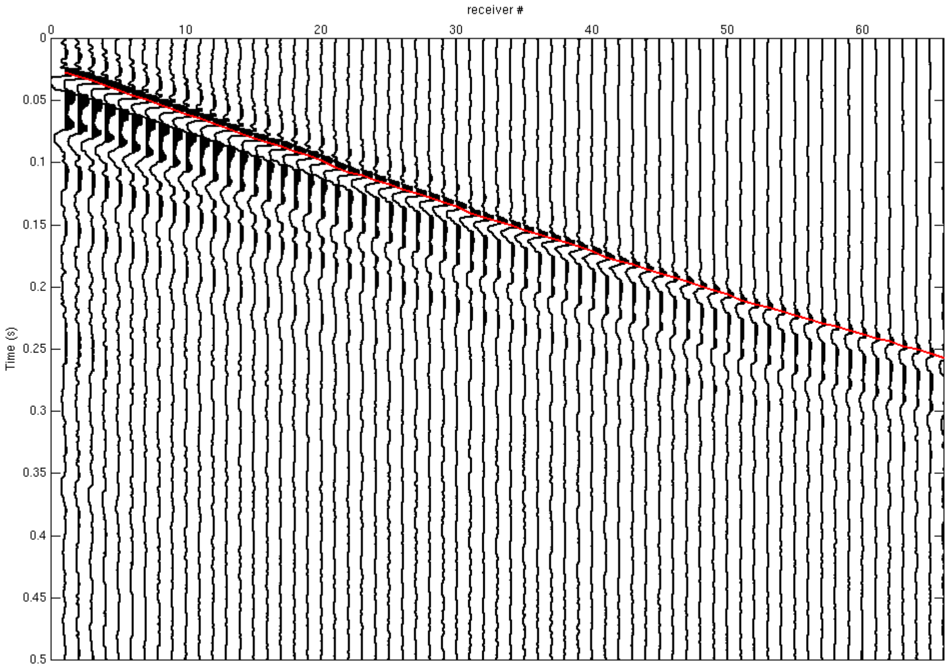

Figure 5.11: Plot of the separated downgoing waves with the first-breaks identified by the red line. The first-breaks are used to identify the location of the downgoing arrivals.

The first-break times or the receiver separation combined with the interval velocity can be used in the calculation of *Q*. The interval velocities are determined with the first-break values; therefore both methods are identical. Windowing of the first-breaks was done to ensure that only the downgoing seismic arrivals are included in the calculations. The window includes the data 25 ms before and 175 ms after the first-break time for each trace.

From analyzing the results associated with the spectral-ratio method it was determined that the sediment above the Colorado was too unconsolidated and that high noise levels resulted in an inability to determine the values of *Q*. However, below this it is possible to determine the values of *Q*. This method is dependent on a frequency smoother that is applied to the data. In Figure 5.12, a series of frequency smoother lengths have been applied to show the differences in the calculated *Q*. The *Q* value is initially determined from the top of the Colorado (receiver 35) to the top of the Waseca (receiver 64). The final parameter is the frequency range to use when determining the slope of the spectral-ratio. The VSP data were acquired with an 8-200 Hz vibroseis sweep. However, in examining the data there are changes in the linear nature of the ratio at 100 Hz. This value was chosen as the upper limit and 10 Hz as the lower limit for the *Q* estimation.

The spectra obtained from the data measured by a VSP survey are the combination of both the attenuation in a dissipative system and a nondissipative system. The linear trend required is an estimate of the dissipative system. Spencer et al. (1982) also found that there is an increase in the variability of the amplitude ratios with an increase in frequency, where the straight-line approximation was a good fit up to approximately 90 Hz. If the frequency band was chosen to include higher frequencies the models show that it would overestimate the actual dissipation. From this they determined that the attenuation obtained from the amplitude ratio is dependent on the frequency bandwidth used for the linear fit and that the ideal bandwidth is not necessary the limits of the signal. They believe that for small receiver separation the dissipation at high frequencies is offset by the increase in the variability of the locally generated interference (primaries and multiples) related to the stratigraphy.

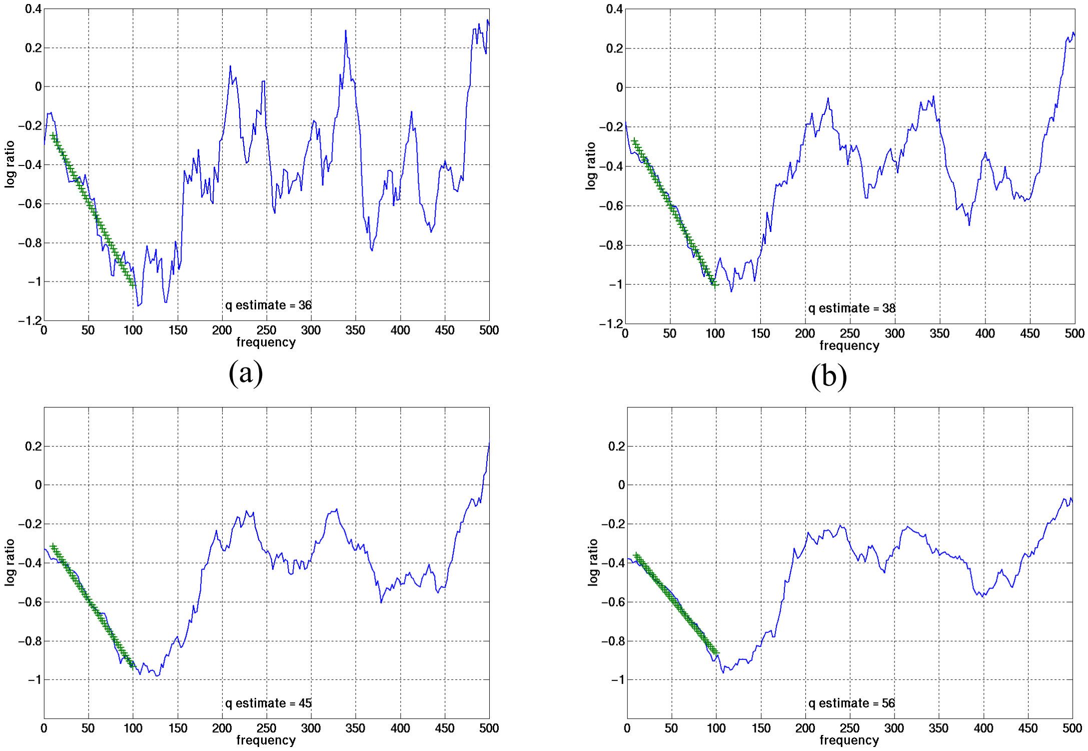

(a) (b) (c) (d)

Figure 5.12: Q value determined with the spectral-ratio method. The plots show the ratios when different boxcar lengths are used on the data. The lengths of the boxcar smoothers are (a) 20 Hz, (b) 40 Hz, (c) 60 Hz and (d) 80 Hz. The value of Q varies from 36 to 56, increasing with the length of the boxcar smoother.

The calculated values for Q increase with the increased length of the boxcar smoother. There is no ideal length for the smoother; instead a compromise must be made. A longer smoother will create a better spectrum for a linear trend line; however, it will also cause information beyond the chosen frequency range (10-100 Hz) to be included in the slope of the linear trend line. A boxcar smoother of 80 Hz was chosen as it creates a smoothed amplitude spectrum for which a linear trend can easily be determined.

This VSP example gives a Q value for the interval from the top of the Colorado to the top of the Waseca. However, for modelling purposes it is of interest to examine the Q values for the entire well-log, separating it into several Q values. This is possible by choosing a receiver spacing and determining the Q values across the receiver spacing moving the receiver location downward by one for each calculation. This was done for several different receiver spreads, including those of 2, 6, 10 and 14 receivers. The receiver-spread value is the number of receiver intervals between the two receivers (Figure 5.13).

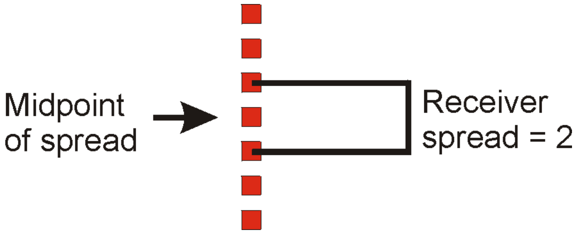

Figure 5.13: Diagram indicating the designation of a receiver-spread

The results of the single receivers with differing spreads are shown in Figure 5.14.

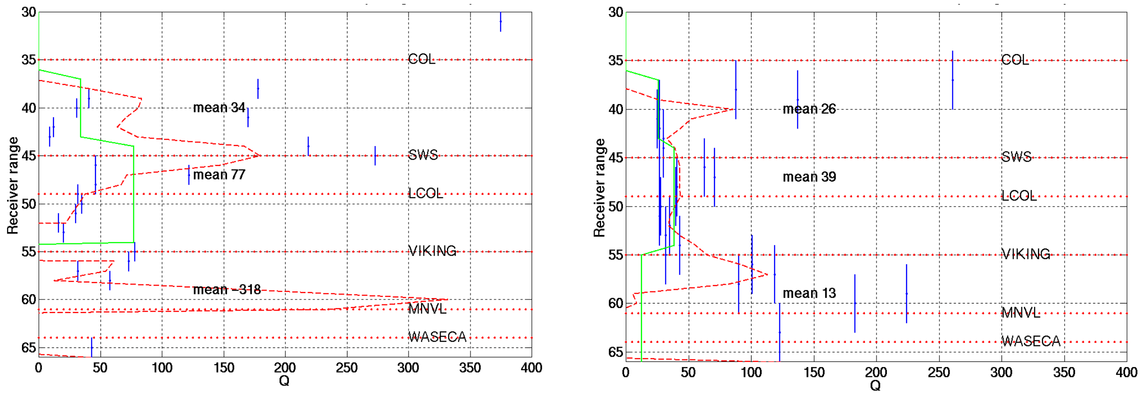

(a) 2-receiver spread (b) 6-receiver spread

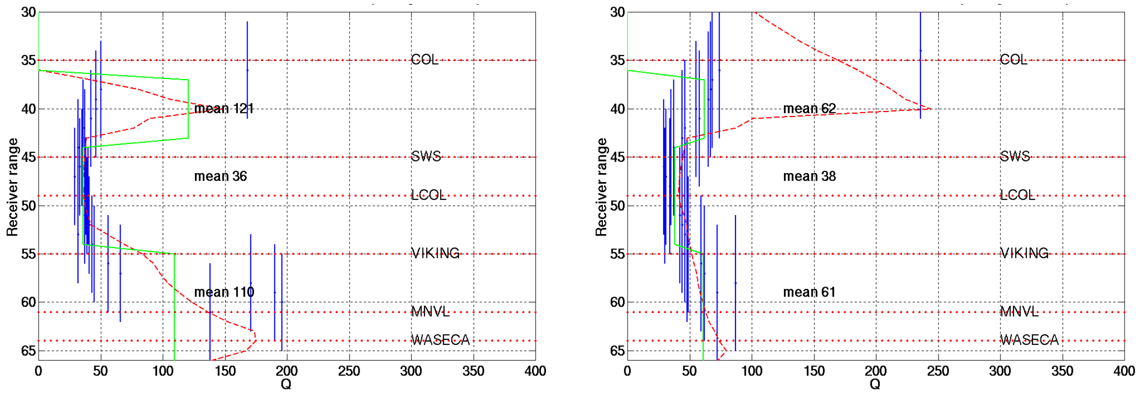

(c) 10-receiver spread (d) 14-receiver spread

Figure 5.14: Receiver ratios over a series of different receiver spacings. The values obtained include the vertical lines which indicate the range over which the interval Q value was obtained and the value itself. The dashed line is the average Q for each point determined from the multiple calculated Q values for each interval. The dotted line is the mean values for blocked zones for which similar Q values were obtained based on the geology.

The results when a receiver spread of two is used show considerable scatter in the Q values obtained. This scatter makes it difficult to determine the blocked interval Q values. This is also applicable when a receiver spread of six is used. The receiver spread of 14 is over-smoothed, possibly hiding the true Q values. Unfortunately, it is not possible to assign numerical criteria to this process. The interpretive process involves changing and choosing the receiver spread for which it is possible to see ideally blocked Q values for the geological formations. The best receiver spread was estimated to be ten as it is still possible to see distinct zones of changing Q values. It is also possible to separate the results into three separate zones for *Q,* the top zone, from receiver 36 to 44, is found to have a *Q* of about 120, the second zone, from receiver 45 to 54, a lower *Q* value of about 40 and the bottom section a *Q* value of about 120.

These values are only based on the ratios between two receivers. There is a large possibility of errors in the data, which can be reduced by calculating the average spectrum of more than one receiver (Figure 5.15). This was carried out for the ten-receiver spread for an average calculated with three- and five-receivers (Figure 5.16).

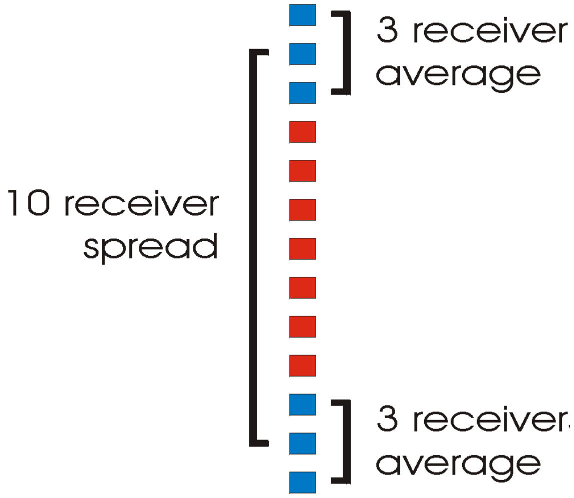

Figure 5.15: Averaging of spectrum to provide a smoother Q analysis of the data

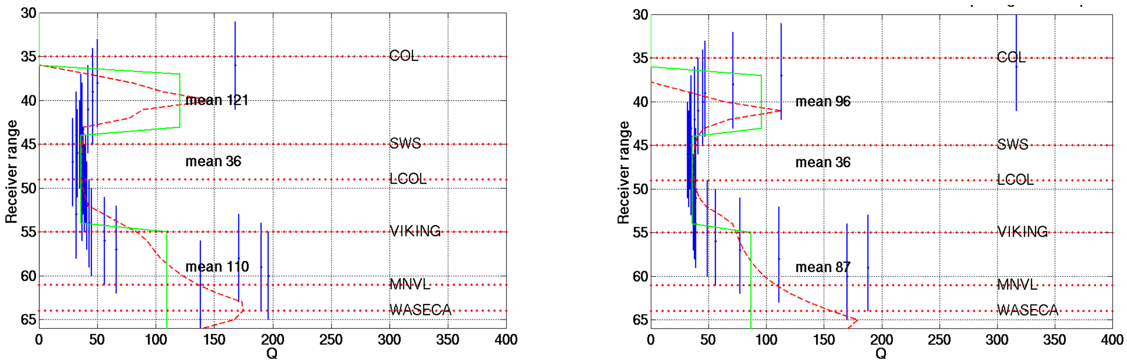

(a) with 1-receiver averaging (b) with 3-receiver averaging

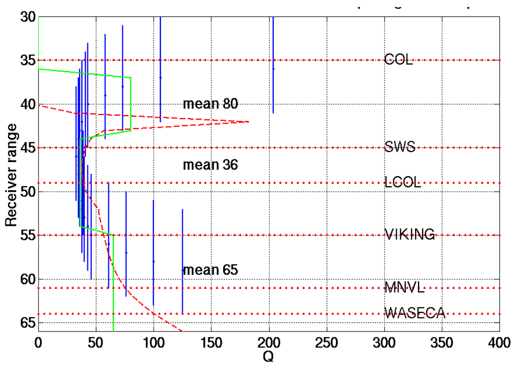

(c) with 5-receiver averaging

Figure 5.16: Multiple receivers averaged to determine the Q values over a ten-receiver spacing. The values obtained include the vertical lines which indicate the range over which the interval Q value was obtained and the value itself. The dashed line is the average Q for each point determined from the multiple calculated Q values for each interval. The dotted line is the mean values for blocked zones for which similar Q values were obtained based on the geology.

The vertical lines indicate that the values of Q over the specified spread become less varied over the changing depths. This alters the Q value and also provides a better value for the interval Q. With an increase in the number of receivers averaged, there is a tendency to remove any fluctuations in Q. For further analysis and modelling, the interval values with the three-receiver average and the ten-receiver spread will be applied. Above the Colorado there were no values obtained due to the soft nature of the sediment and source-generated noise. This value of Q was set to 150, a value close to the underlying Q but not low enough to significantly change the seismic data. The quality of the Q values for the different spreads and receiver averaging can be compared to the value estimated for the interval *Q* value obtained over the entire VSP. This value includes all the receivers below the Colorado and was estimated as approximately 60. The final values for *Q* are shown in Figure 5.17 with the tops from the composite well log used in the following modelling analyses.

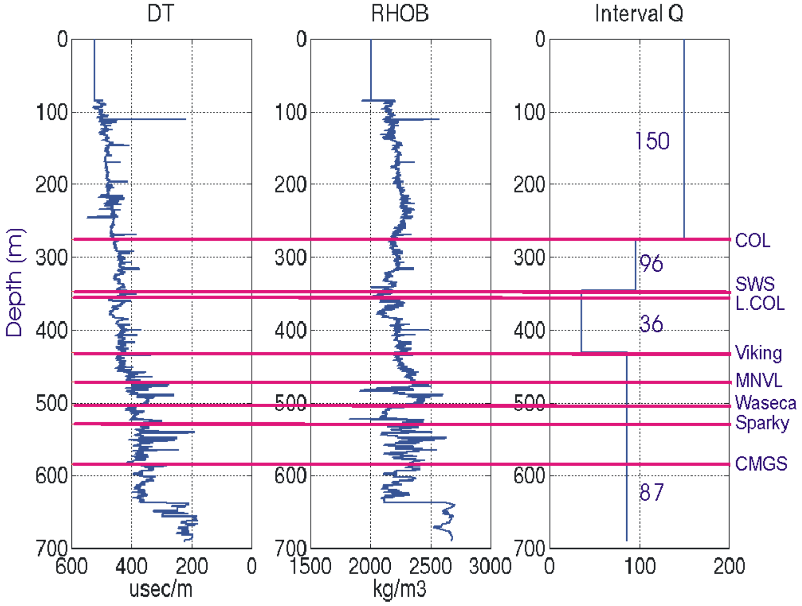

Figure 5.17: Well-log data used for the seismic modelling and the associated Q values obtained from the VSP at Pikes Peak.

5.4 APPLICATION OF THE AVERAGE Q TO THE COMPOSITE WELL-LOG

The attenuation values from the VSP can be used with the composite well log shown in Figure 5.8 to create a synthetic reflectivity. This reflectivity can then be used with a series of sweeps and the *Q* values to model earth-attenuated data in the Pikes Peak area. This allows the sweep deconvolution methods to be tested with the inclusion of minimum-phase earth filtering. The first step is to convert the sonic and density logs into a reflectivity series as well as to convert the *Q* values from depth to time (Figure 5.18). The *Q* values are converted to time based on the location of the tops.

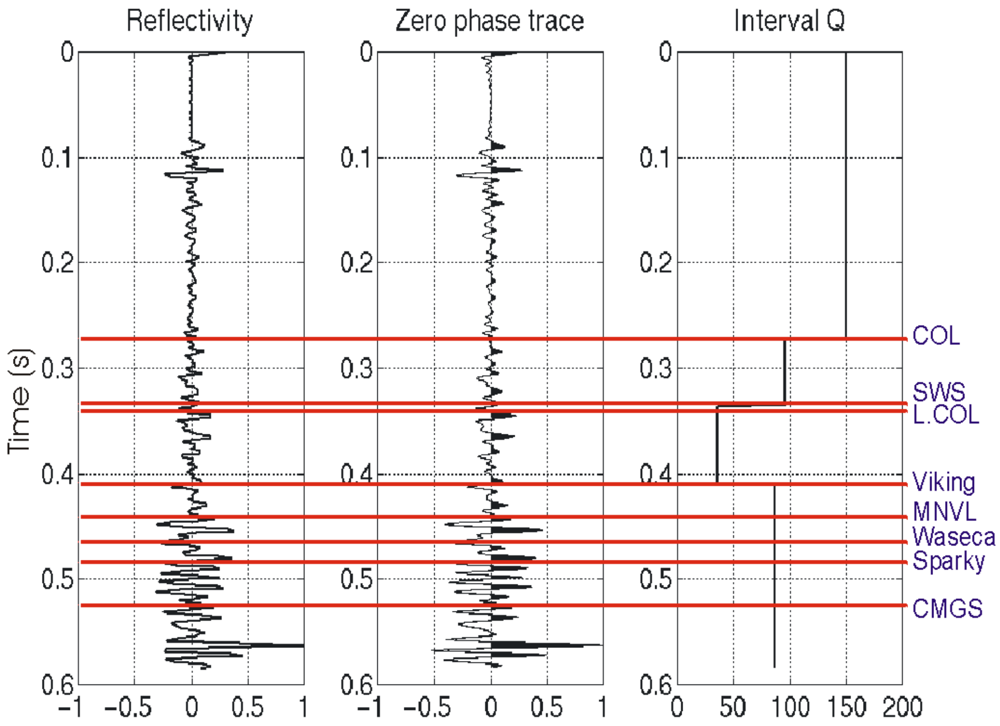

Figure 5.18: Reflectivity, zero-phase trace and the corresponding Q values in time for the composite well-log.

The attenuation values obtained from the VSP are interval Q values. Attenuation is the absorption of the seismic energy as the seismic waves travel through the earth. These values must be converted into average Q values at each time sample. If for simplicity, we assume both time and frequency independence, at the first time sample the attenuation, $a(t)$, is

$$a(t) = e^{\left(\frac{-\pi f t_1}{Q_1}\right)}, \tag{5.19}$$

while at the second time sample the equation is,

$$a(t) = e^{\left(\frac{-\pi f t_1}{Q_1}\right)} e^{\left(\frac{-\pi f (t_2 - t_1)}{Q2}\right)}. \tag{5.20}$$

where f is the dominant frequency, t_1 is the time of sample 1 (2 ms) and t_2 is the time for sample 2 (4 ms). Q_1 is the interval Q value at sample 1 and Q_2 is the interval Q value at sample 2.

Therefore the average Q value, Q_{ave}, at time t_n can be solved as

$$\frac{t_n}{Q_{ave}} = \sum_{k=1}^{n} \frac{t_k - t_{k-1}}{Q_k}, \tag{5.21}$$

where $t_o = 0$. This was calculated for the Q interval values obtained from the VSP, resulting in the Q average values shown in Figure 5.19.

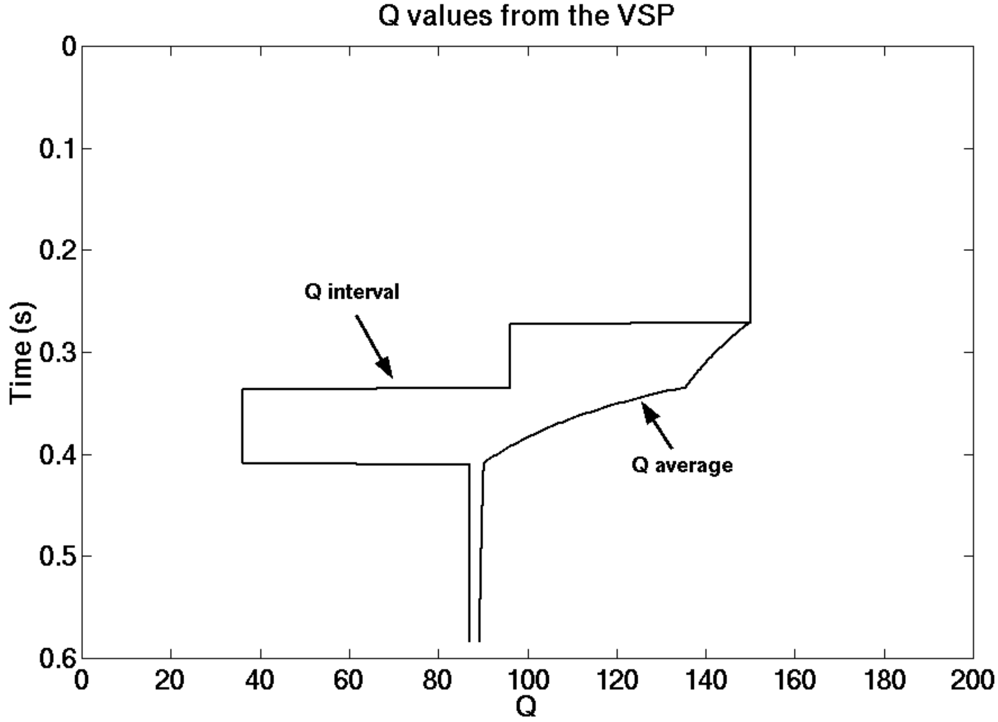

Figure 5.19: Calculated interval and average Q values

With the Q average determined it is possible to use the reflectivity modelled from the well-log and apply the attenuation. This is determined with the creation of a time-variant matrix with a minimum-phase wavelet thereby creating all of the synthetic minimum-phase attenuation wavelets at each time sample. This matrix is then multiplied by the reflectivity to create the attenuated reflectivity. This can then be modelled as vibroseis data by convolving the attenuated reflectivity with a sweep. For the purposes of the modelling, two sweeps from chapter 3 have been chosen, the linear (with 0.5-second taper) and the Gaussian (Figure 5.20).

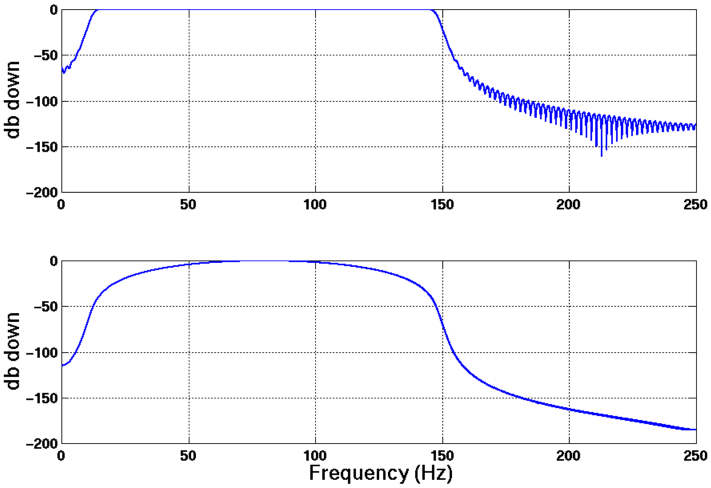

Figure 5.20: Sweeps used for the modelling. Both sweeps are designed with a 10-150 Hz frequency range, a 16 second length and 2-ms sampling. The top sweep is linear with a 500-ms taper and the bottom sweep is Gaussian.

These two sweeps are convolved with the reflectivity and the attenuated reflectivity to create the synthetic traces. The amplitude spectra of the traces before and after the incorporation of attenuation are shown in Figure 5.21. The dashed line is the data before attenuation and the solid line is after the inclusion of the minimum-phase filter.

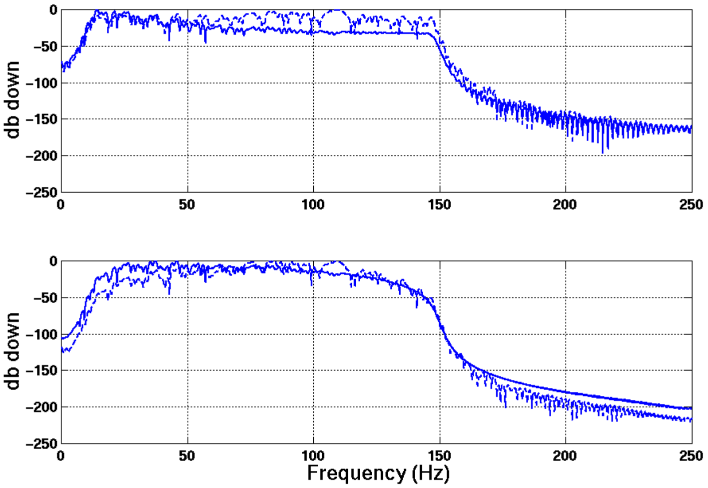

Figure 5.21: Amplitude spectra of the traces. The top plot is for the linear sweep and the bottom for the Gaussian sweep. In both plots the solid line is the attenuated data while the dashed line indicates the non-attenuated trace.

The synthetic traces must then be deconvolved to remove the sweep from the trace. The first step is to use both crosscorrelation and frequency-domain sweep deconvolution (FDSD) to remove the sweep. The deconvolved trace can then be compared to the reflectivity from the initial model. The final step is to perform minimum-phase deconvolution in an attempt to whiten the spectrum and to remove the minimum-phase wavelet.

For the linear vibroseis sweep the results of crosscorrelation and frequency-domain sweep deconvolution are shown in Figure 5.22 and 5.23. The results for both sweep deconvolution methods for the linear sweep provide similar results.

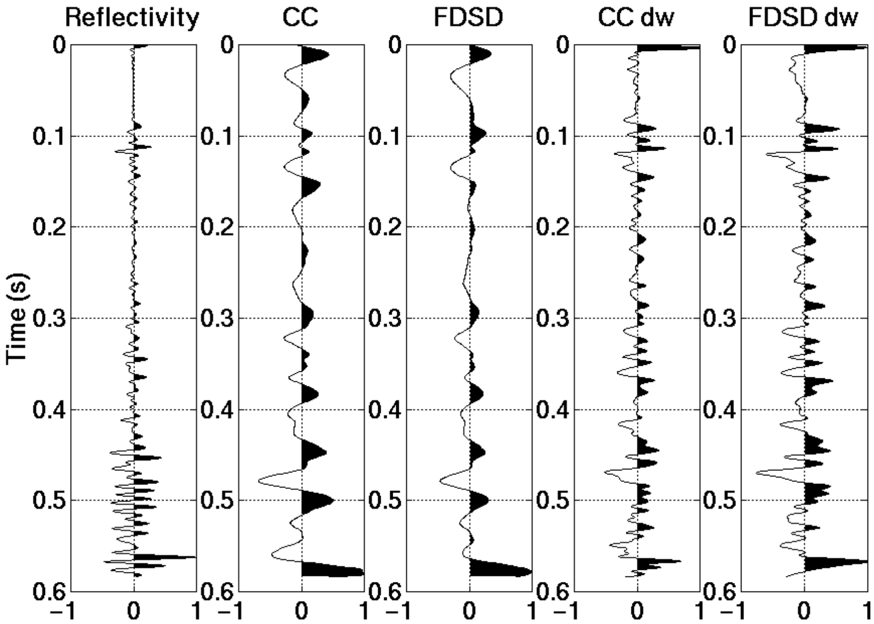

Figure 5.22: Modelled reflectivity with crosscorrelation (CC) and frequency-domain sweep deconvolution (FDSD) for the linear sweep. The two traces on the right are crosscorrelation and FDSD with Wiener deconvolution (n=100m stab=0.0001) and a 5-10-145-155 bandpass filter.

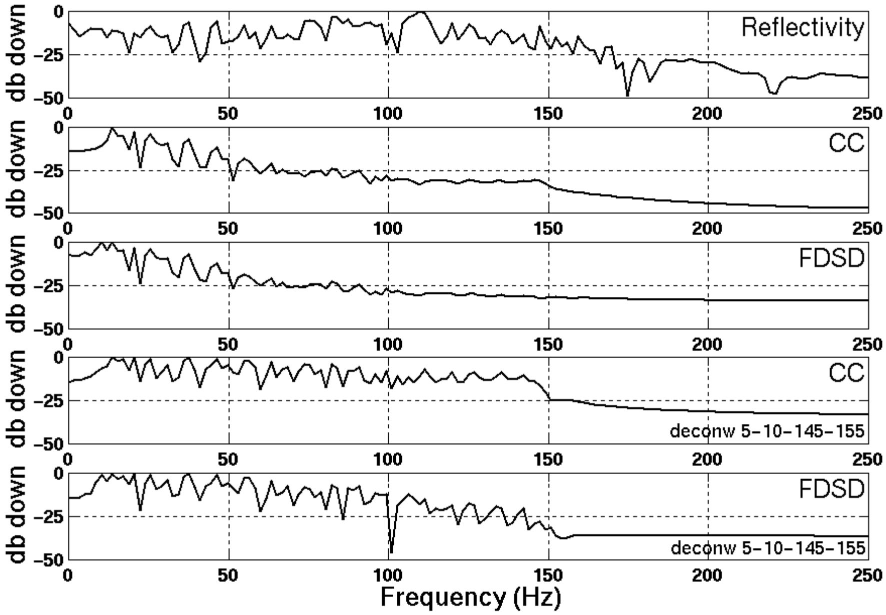

Figure 5.23: Spectrum of the modelled reflectivity with crosscorrelation (CC) and frequency-domain sweep deconvolution (FDSD) for the linear sweep. The two bottom figures are crosscorrelation and FDSD with Wiener deconvolution (n=100m stab=0.0001) and a 5-10-145-155 bandpass filter.

The results of the deconvolution are drastically affected by the *Q* attenuation. There is very little similarity between the reflectivity and the deconvolved traces. Both crosscorrelation and FDSD show comparable results for the linear sweep. This is due to the limited filtering effect of the linear sweep during crosscorrelation. The results with the use of minimum-phase Wiener deconvolution improve the resolution of the data through whitening. There is a slight time shift associated with sweep deconvolution methods, shown in Figure 5.24.

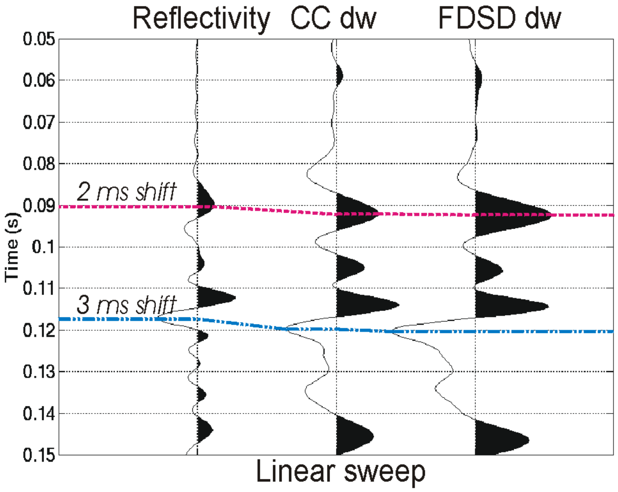

Figure 5.24: 50 to 150-ms section for the reflectivity and minimum-phase deconvolution of FDSD and CC. There is a small time lag associated with both of the deconvolution methods.

The same modelling process was applied for the Gaussian sweep with different results (Figure 5.25 and 5.26).

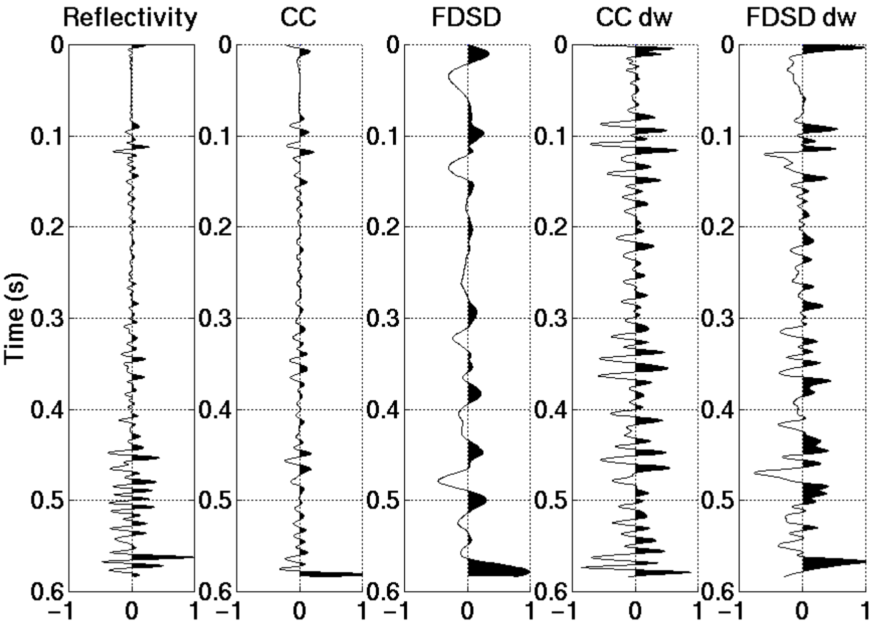

Figure 5.25: Modelled reflectivity with crosscorrelation (CC) and frequency-domain sweep deconvolution (FDSD) for the Gaussian sweep. The two traces on the far right are crosscorrelation and FDSD with Wiener deconvolution (n=100m stab=0.0001) and a 5-10-145-155 bandpass filter.

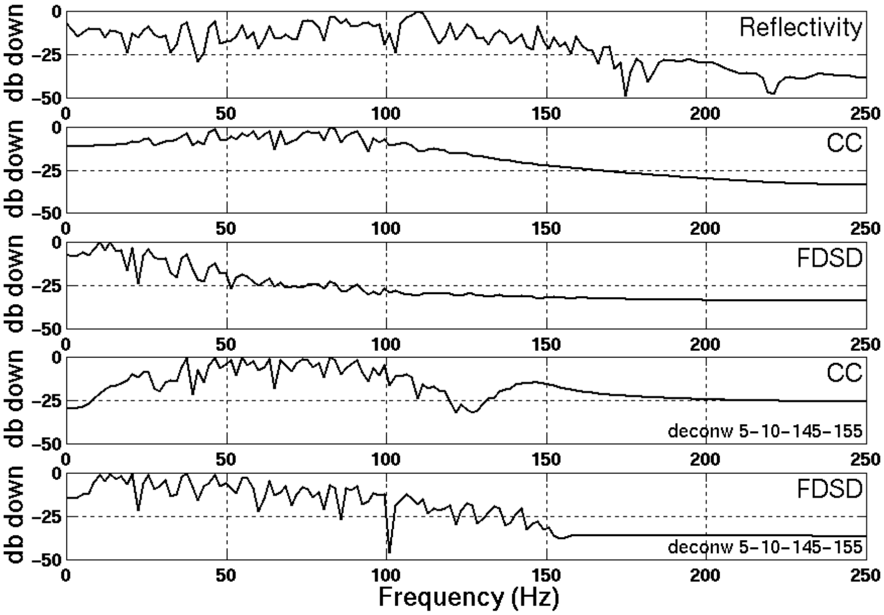

Figure 5.26: Spectrum of modelled reflectivity with crosscorrelation (CC) and frequency-domain sweep deconvolution (FDSD) for the Gaussian sweep. The two bottom amplitude spectra are crosscorrelation and FDSD with Wiener deconvolution (n=100m stab=0.0001) and a 5-10-145-155 bandpass filter.

The result obtained from FDSD for the Gaussian sweep is indistinguishable from the linear sweep result. This is due to the complete division of the sweep from the trace during application of FDSD. The results of crosscorrelation before minimum-phase deconvolution are significantly better than for to the linear sweep. This is due to the filtering effect of crosscorrelation and the embedded Klauder wavelet. The low frequency values are decreased in amplitude compared to the centre frequencies (80 Hz). Therefore, the result is a more flattened spectrum for the higher frequencies, providing a trace similar to the reflectivity.

For the crosscorrelation result there is a phase rotation associated with the earth-attenuation's minimum-phase wavelet (Figure 5.27). This needs to be corrected with minimum-phase deconvolution. When this is finished the result of crosscorrelation is degraded and there is still a significant amount of phase rotation associated with the data. The result of minimum-phase deconvolution on FDSD is identical to that of the linear sweep. The phase rotation is smaller than the result from crosscorrelation. There is a 2-ms lag associated with the deconvolution of the Gaussian sweep.

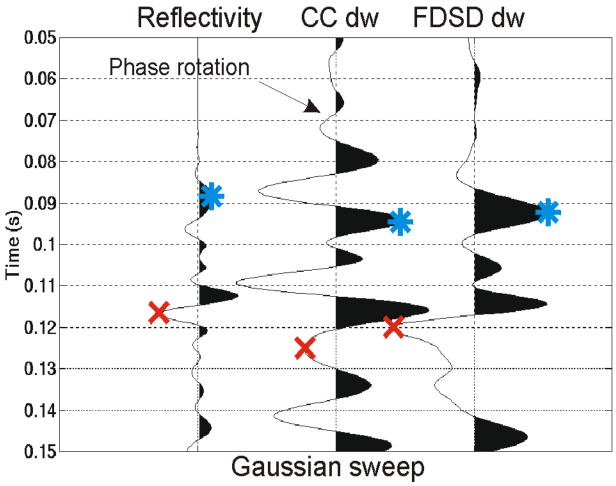

Figure 5.27: 50 to 150-ms section for the reflectivity and minimum-phase deconvolution of FDSD and CC. There is a small time lag (2-ms) associated with FDSD; however, there is a significant phase rotation (approximately 60°) for the crosscorrelation result.

The modelling indicates that with minimum-phase *Q* attenuation there is a significant problem associated with both the amplitude spectrum and the phase when the sweep is removed from the data. The results from the linear sweep show the deconvolved traces from both crosscorrelation and FDSD to be similar with a small 2- to 3-ms lag associated with the data. The inclusion of minimum-phase deconvolution increases the frequency content of the data, removes some of the phase rotation and leaves the small time lag.

With the Gaussian sweep the results are not as encouraging. The result of crosscorrelation before minimum-phase deconvolution shows a good frequency content as a result of the filtering during the sweep removal. The FDSD result for the Gaussian sweep is identical to that of the linear sweep, both before and after minimum-phase deconvolution. When minimum-phase deconvolution is applied to the crosscorrelation result there is a significant phase rotation remaining in the data. This is caused by the incorrect calculation of the minimum-phase wavelet for the entire spectrum.

For FDSD the phase rotation is related to the frequency range of the sweep. The closer the high frequency limit reached by the vibrator to the Nyquist value, the better the calculation of the minimum-phase wavelet embedded in the data. For crosscorrelation the phase rotation is based on the same criteria as FDSD; however, there is the inclusion of the sweep shape. A nonlinear sweep will cause a more significant error in the calculation of the embedded minimum-phase wavelet, increasing the phase rotation of the result.

There will be an advantage with the sweep independence of the FDSD minimum-phase deconvolution result in time-lapse seismic, where it may not be possible to recreate the sweep identically for all surveys.

5.4.1 Application of inverse Q filters

An alternative method to minimum-phase deconvolution for removing the Q attenuation is an inverse Q filter. This can be used in areas for which the Q values are known for the geological section. For the modelling, the Q values are known, as they were applied to the data in the previous section. To remove the minimum-phase attenuation, three different inverse Q filters will be implemented. The first is for the Q values that were applied to the data, the second for Q values 20% lower and the final Q values all constant at 200.

The entire modelling process for the removal of the Q values is shown in Figure 5.28. The Q matrix values are the average Q values previously calculated for the modelling. It is necessary to apply an identical bandpass filter to both the data and Q matrix values to take into account the bandlimited nature of the data.

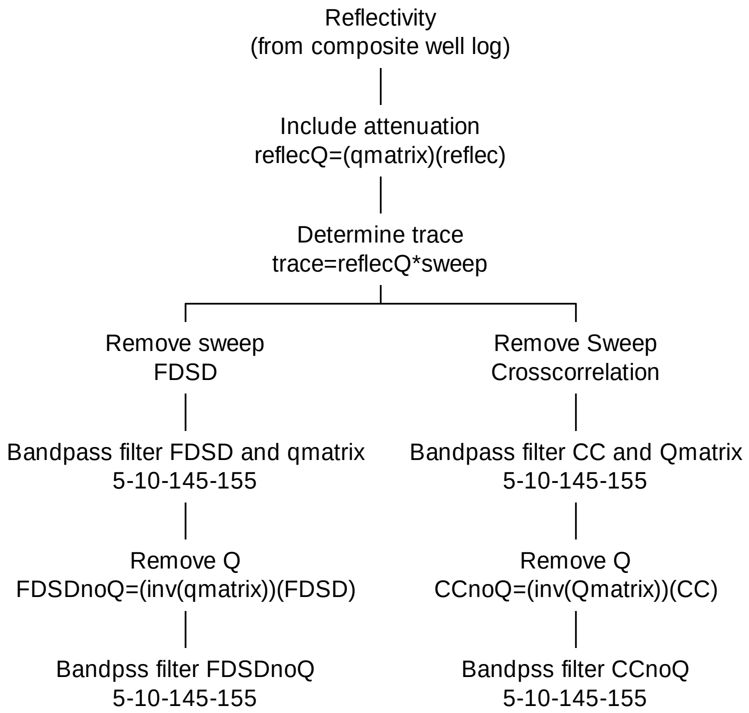

Figure 5.28: Flow chart of the processing flow used to model and subsequently remove the Q attenuation.

This processing flow was done for both the linear and Gaussian-shaped sweeps. The removal of the *Q* values with the identical *Q* matrix that was modelled into the data resulted in the FDSD values being close to the initial reflectivity for both sweep types. The crosscorrelation results are unsatisfactory: the reflections are indeed imaged, but the amplitudes do not match those of the initial reflectivity (Figures 5.29 and 5.30).

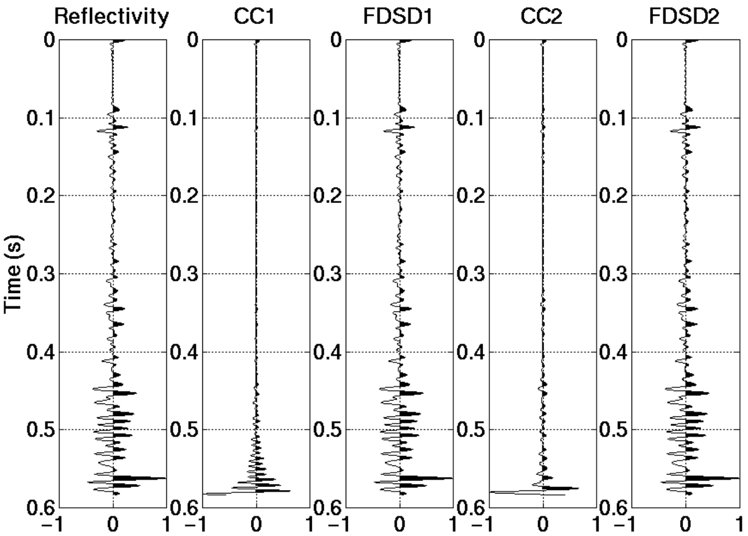

Figure 5.29: Application of an inverse Q filter to remove the minimum-phase filtering effects. CC1 and FDSD1 are the results for the removal of the linear sweep and application of the inverse Q filter. CC2 and FDSD2 are the results of the Gaussian sweep.

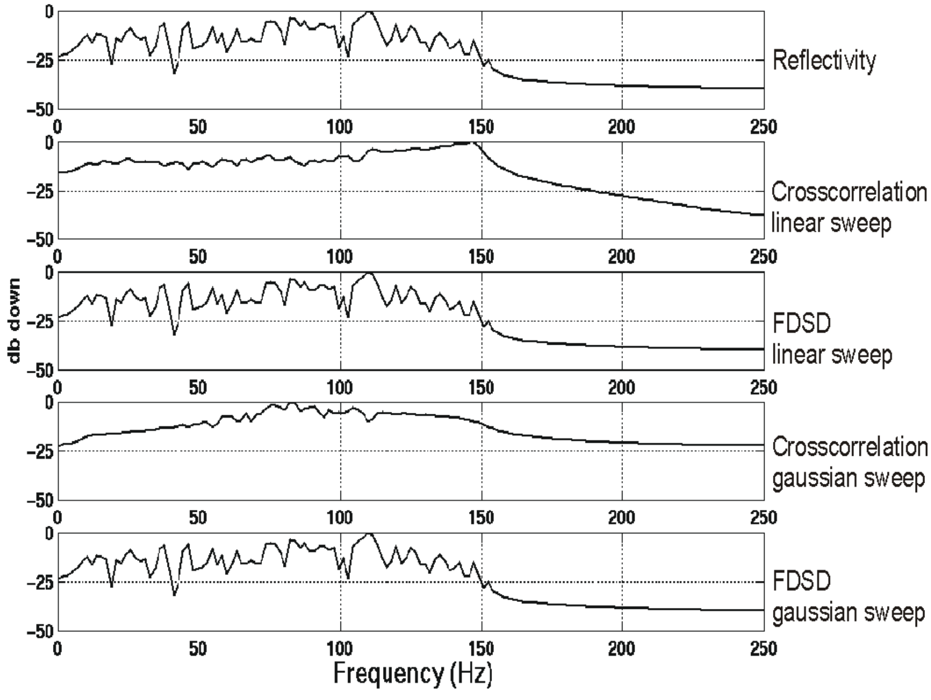

Figure 5.30: Amplitude spectrum for the application of an inverse Q filter to remove the minimum-phase filtering effects for both the linear and Gaussian sweeps. There are significant problems associated with the amplitudes for the traces with the sweep removed by crosscorrelation.

The same process of removing the minimum-phase attenuation was performed with a Q estimate equal to 80% of the original value. By doing this it is possible to predict any problems that would be associated with an error in the *Q* values for the inverse filter. The results (Figure 5.31 and 5.32) show that a 20% error in the attenuation estimate does not significantly affect the results. As in the previous case, the results of the sweep removal by FDSD and the subsequent inverse *Q* filter provide excellent results. Crosscorrelation imparts results that are in phase but do not have a correct amplitude spectrum, an implication of the embedded Klauder wavelet.

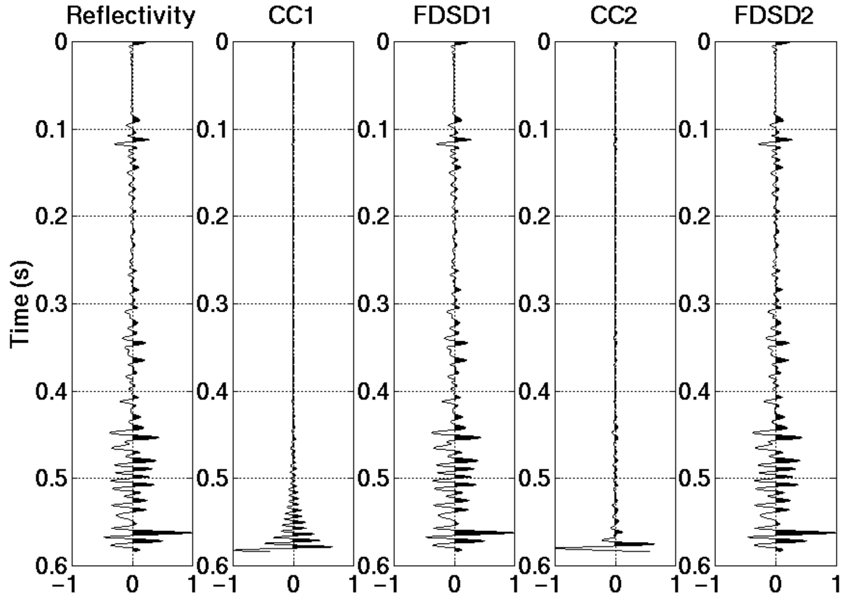

Figure 5.31: Application of an inverse Q filter with Q values equal to 80% of the values actually determined to remove the minimum-phase filtering effects. CC1 and FDSD1 are the results for the removal of the linear sweep and application of the inverse Q filter. CC2 and FDSD2 are the results of the Gaussian sweep

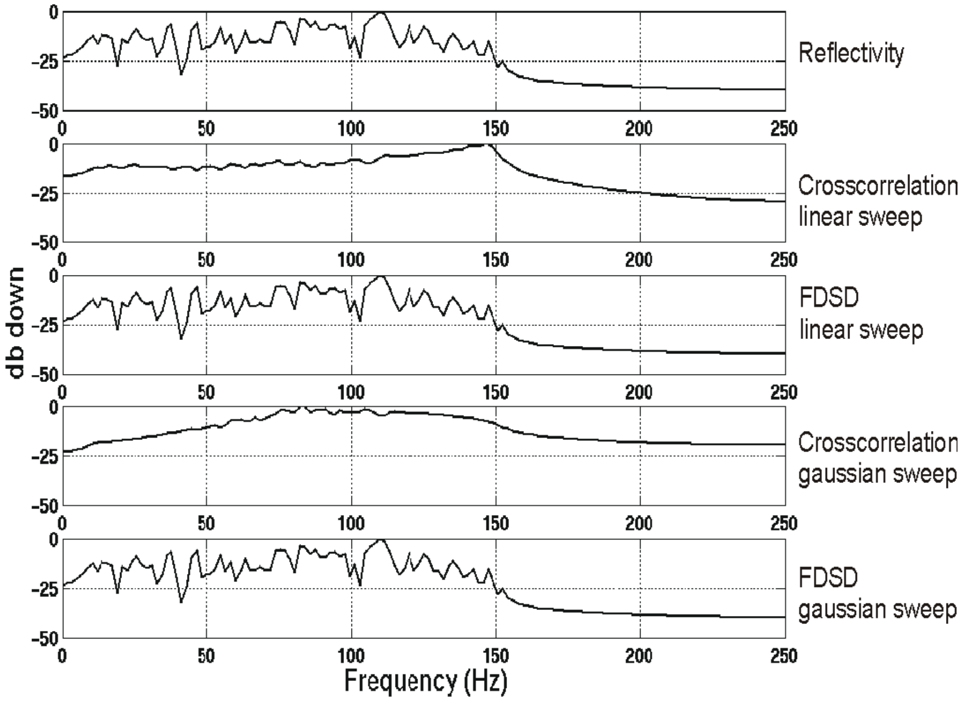

Figure 5.32: Amplitude spectrum for the application of an inverse Q filter equal to 80% of the original values to remove the minimum-phase filtering effects for both the linear and Gaussian sweeps. There are significant problems associated with the amplitudes for the traces with the sweep removed by crosscorrelation.

Another simulation can be completed with a constant *Q* value of 200. This value is too high for the area as the geology consists of clastic sediment. The results are significantly better than the previous two inverse *Q* filters attempts (Figures 5.33 and 5.34). However, the results from the crosscorrelated sweep removal attempt still show anomalies in the trace and the amplitude spectrum, although they are not as significant.

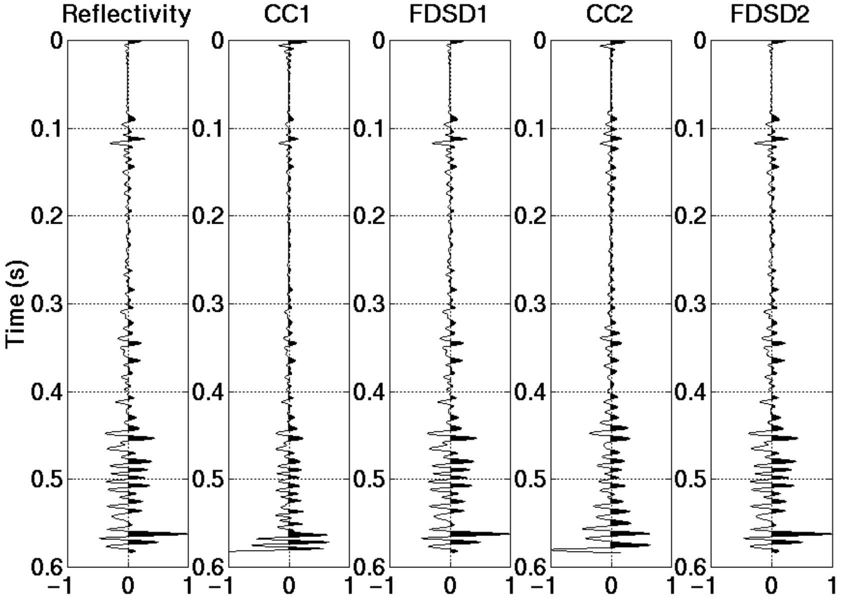

Figure 5.33: Application of an inverse filter for a constant Q of 200 to remove the minimum-phase filtering effects. CC1 and FDSD1 are the results for the removal of the linear sweep and application of the inverse Q filter. CC2 and FDSD2 are the results of the Gaussian sweep.

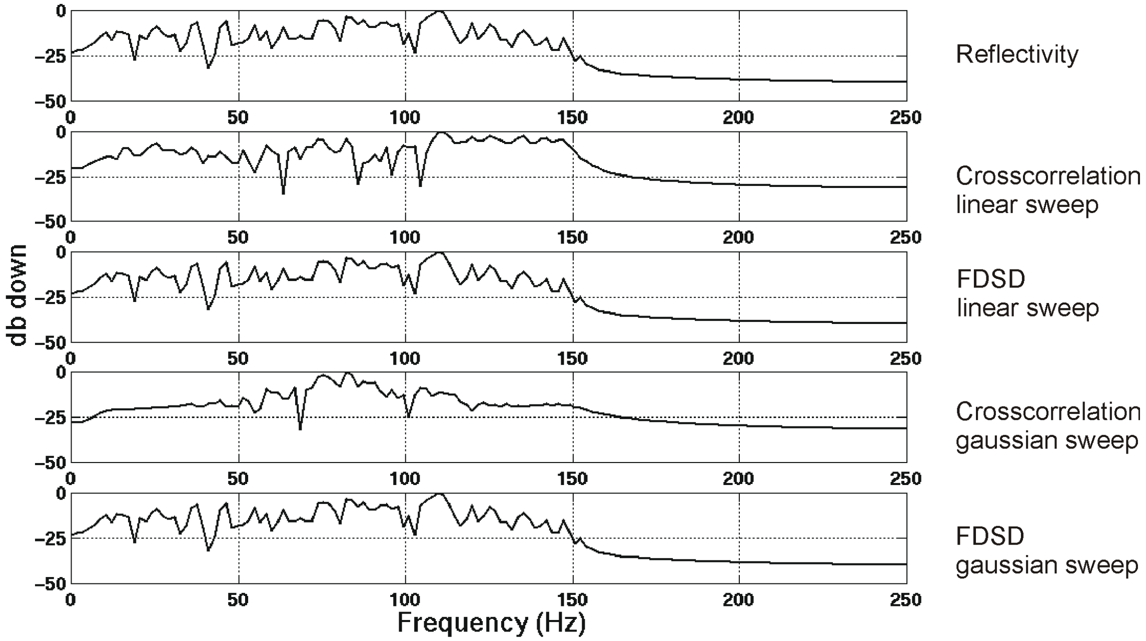

Figure 5.34: Amplitude spectrum for the application of inverse filter with a constant Q of 200 to remove the minimum-phase filtering effects for both the linear and Gaussian sweeps. There are fewer problems associated with the amplitudes for the traces with the sweep removed by crosscorrelation than the previous models.

The application of the inverse *Q* filter is dependent on the amplitude spectrum of the data recovered from the sweep deconvolution method. The application of FDSD has no final sweep dependency and for all of the modelled inverse filters provides excellent results. There are significant amplitude errors associated with crosscorrelation, creating an incorrect trace. This trace can be improved by whitening the spectrum, assuming that the reflectivity is white.

5.5 CHAPTER CONCLUSIONS

The results of the VSP analysis provide *Q* values from approximately 35 to 95 below the Colorado and above the reservoir zone. It was not possible to calculate the *Q* values above the Colorado due to interference by source-generated noise. The VSP data processed with both crosscorrelation and frequency-domain sweep deconvolution provide similar results, with the exception of amplitude variations. A comparison of the corridor stacks for crosscorrelation and FDSD show variations above the Colorado, a result of increased noise. The removal of the *Q* attenuation from the modelled data by minimum-phase deconvolution indicates that the sweep type is significant in obtaining superior results. For a linear sweep the results were similar for both crosscorrelation and FDSD, while the results for the Gaussian sweep with both sweep-removal methods differed. The FDSD results for the *Q* attenuation removal with inverse *Q* filters were superior to crosscorrelation. The embedded Klauder wavelet caused by crosscorrelation resulted in significant amplitude problems, reducing the effectiveness of the inverse *Q* filter.

CHAPTER 6

6 PROCESSING OF FIELD DATA

6.0 CHAPTER SUMMARY

This chapter includes the processing of two seismic lines donated by Petro-Canada and a third acquired by Husky Energy Inc., with the assistance of the University of Calgary AOSTRA grant.

6.1 PETRO-CANADA LINE 25FX

The first data set was acquired by Petro-Canada in 1999 in Alberta, Canada. The data were acquired with a linear 10-80 Hz sweep at a sample rate of 2 ms and a sweep length of 16 s (Figure 6.1). A partial section of line 25 FX was obtained for this research.

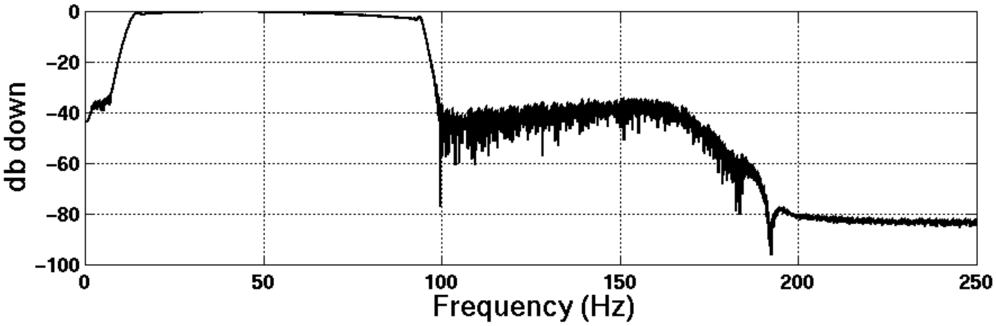

Figure 6.1: Amplitude spectrum of the sweep used for the seismic acquisition of line 25FX.

The taper length both at the start and end of the sweep is 300 ms. The shot point interval is 25 metres and the geophone interval is 5 metres.

The data were processed twice with identical flows, with the exception of the initial sweep removal of crosscorrelation and frequency-domain sweep deconvolution. By retaining identical processing flows, it is possible to make a direct comparison between crosscorrelation and FDSD. The one exception to this is for the values obtained by the residual statics, which were calculated with the same parameters but provided slightly different results. The processing flow used to process both Petro-Canada lines is shown in Figure 6.2.

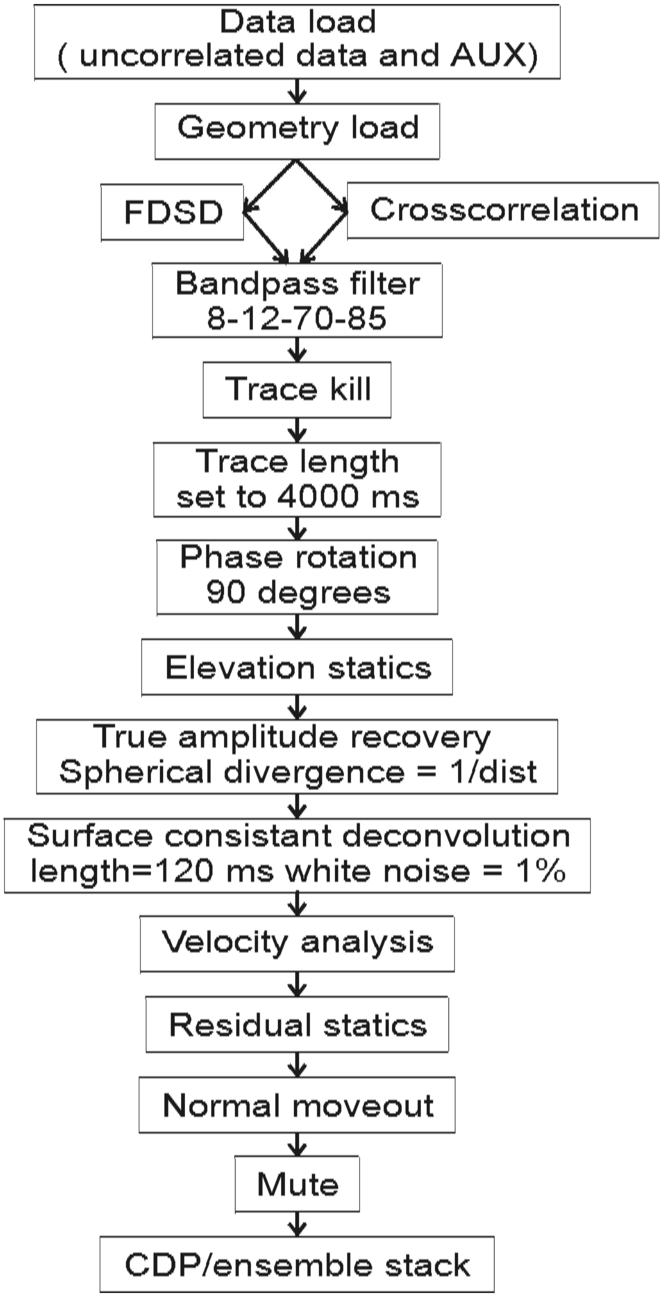

Figure 6.2: Processing flow for both Petro-Canada seismic lines.

A comparison of the data are made at three different points in the processing flow. The first is directly after the trace kill, the second after surface-consistent deconvolution and a final comparison is made with the stacked sections including the residual statics.

6.1.1 Crosscorrelation

For the processing, Landmark's *ProMAX 2D* was utilized; this includes the vibroseis crosscorrelation module. For comparative purposes source 300 on line 25FX is shown for the shot gathers in the all of the figures.

The first two figures (6.3 and 6.4) are the source gather and the corresponding amplitude spectrum for the gather, where the sweep is removed by crosscorrelation and an 8-12-70-85 bandpass filter is applied.

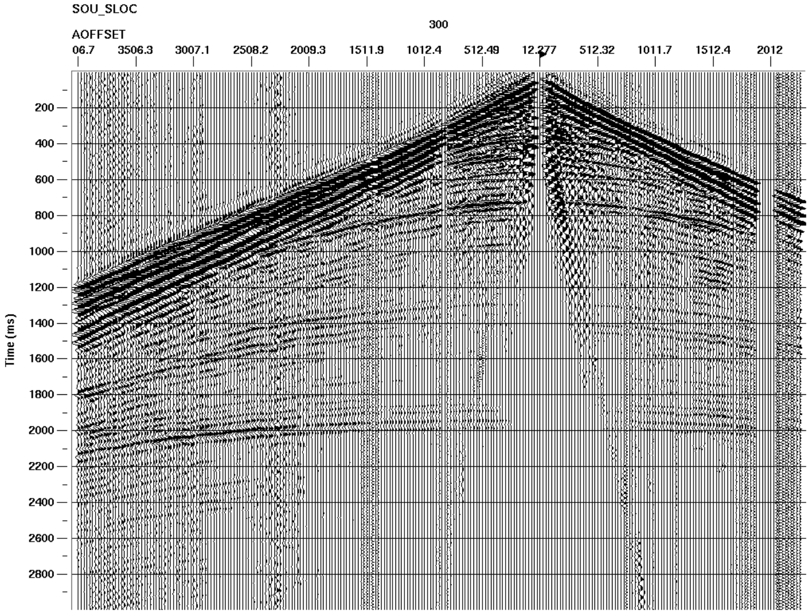

Figure 6.3: Crosscorrelation of source 300 for line 25FX

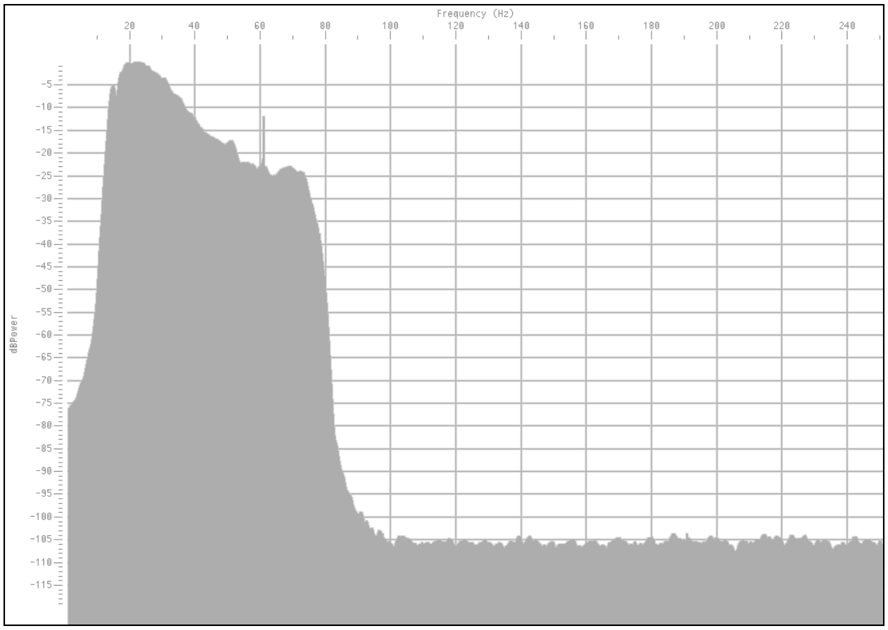

Figure 6.4: Amplitude spectrum of source 300 for line 25FX after crosscorrelation.

Following the removal of the vibroseis sweep, minimum-phase surface-consistent deconvolution is applied in an attempt to remove the minimum-phase earth filtering effects (Figures 6.5 and 6.6). The earth filtering causes attenuation of the high frequencies and the inclusion of an embedded minimum-phase wavelet. After the minimum-phase deconvolution, the data are whitened increasing the resolution and the earth filter is theoretically removed.

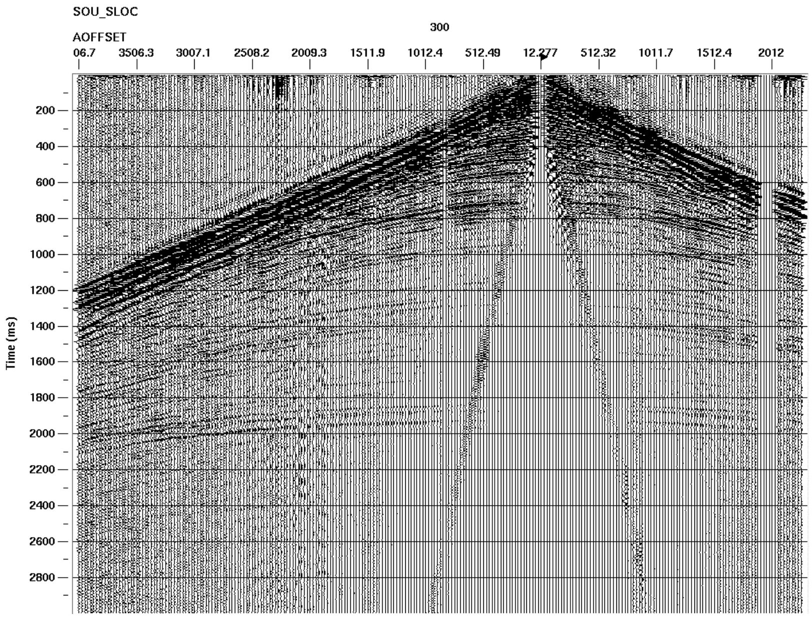

Figure 6.5: Shot gather after minimum-phase surface-consistent deconvolution.

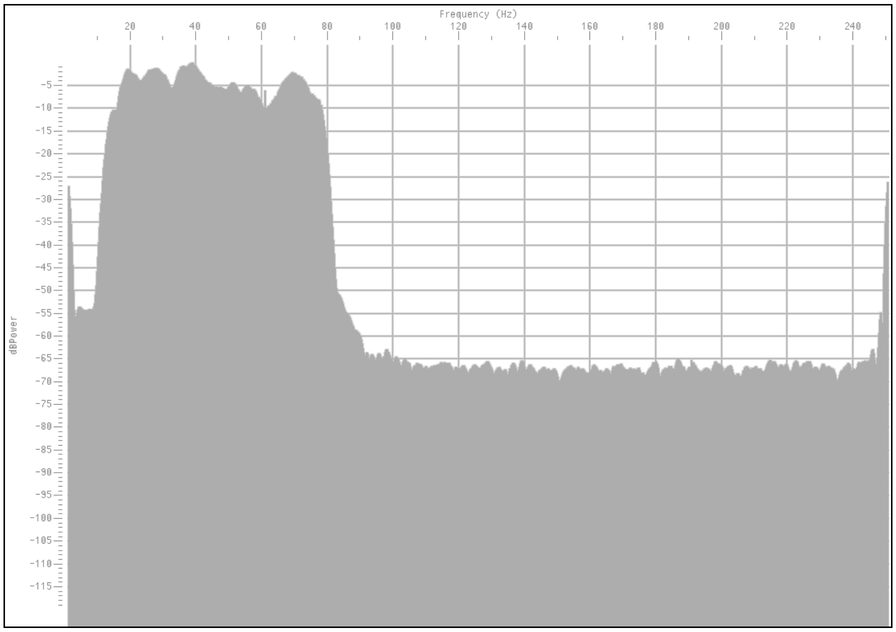

Figure 6.6: Amplitude spectrum of the crosscorrelation sweep deconvolution for 25FX. The spectrum has been whitened increasing the resolution of the data

The final processing step is to stack the data and apply residual statics (Figure 6.7). The residual statics are applied to remove any remaining irregularities that are a result of variations in the near surface. The stacking of the data increases the fold to 52 from CDP

498 to 666. The high fold number is a combination of individual trace summing from multi-sweep source locations and CDP stacking.

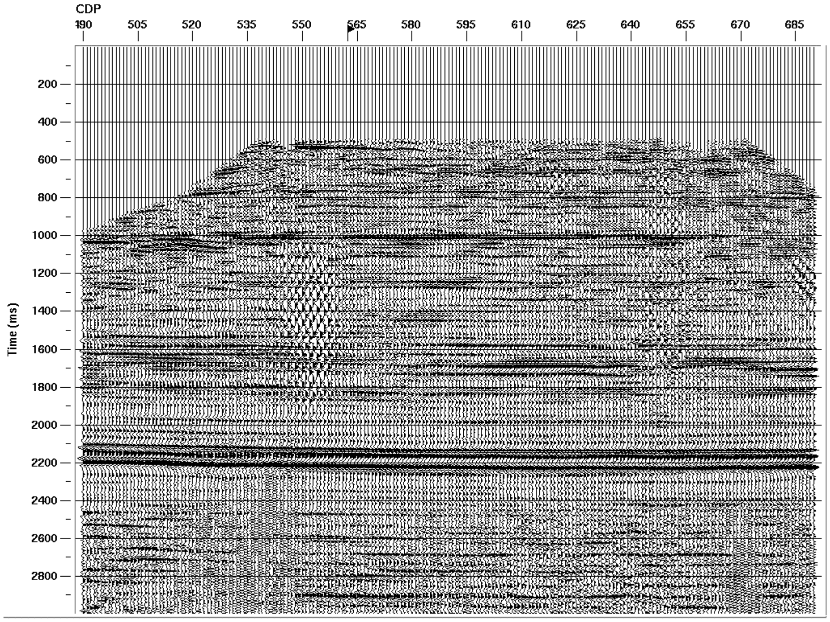

Figure 6.7: Final stack for line 25FX including residual statics with crosscorrelation used to deconvolve the embedded vibroseis sweep.

6.1.2 Frequency-domain sweep deconvolution

The first two figures (6.8 and 6.9) shown in this section are the shot gather and the associated average amplitude spectrum for shot 300 after the sweep has been removed by FDSD. There is more noise visible in the FDSD section that the comparable one processed with crosscorrelation. The noise is a result of the bandpass filter applied to the data. The bandpass filters have the same parameters for both vibroseis deconvolution methods. A more aggressive bandpass filter would remove the noise; however the remaining noise will be eliminated during stacking.

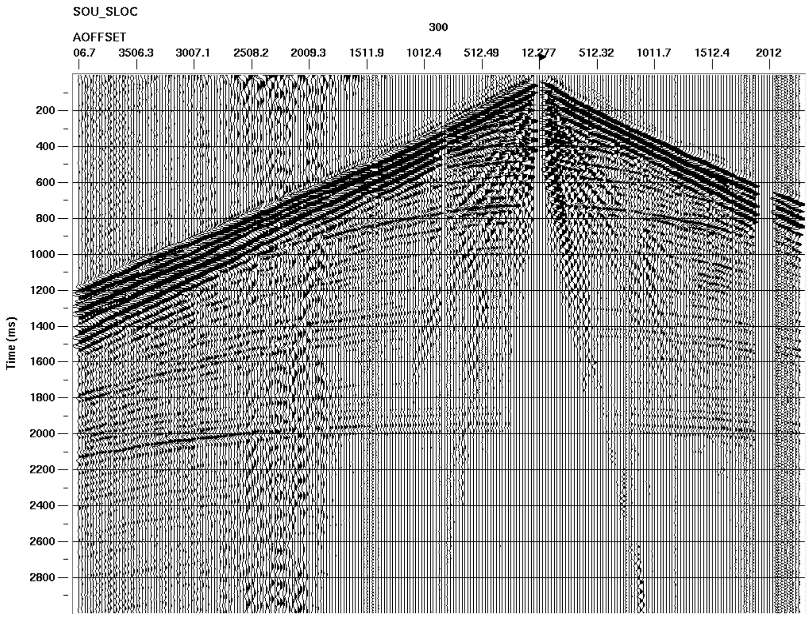

Figure 6.8: Shot gather 300 after the sweep is removed with FDSD.

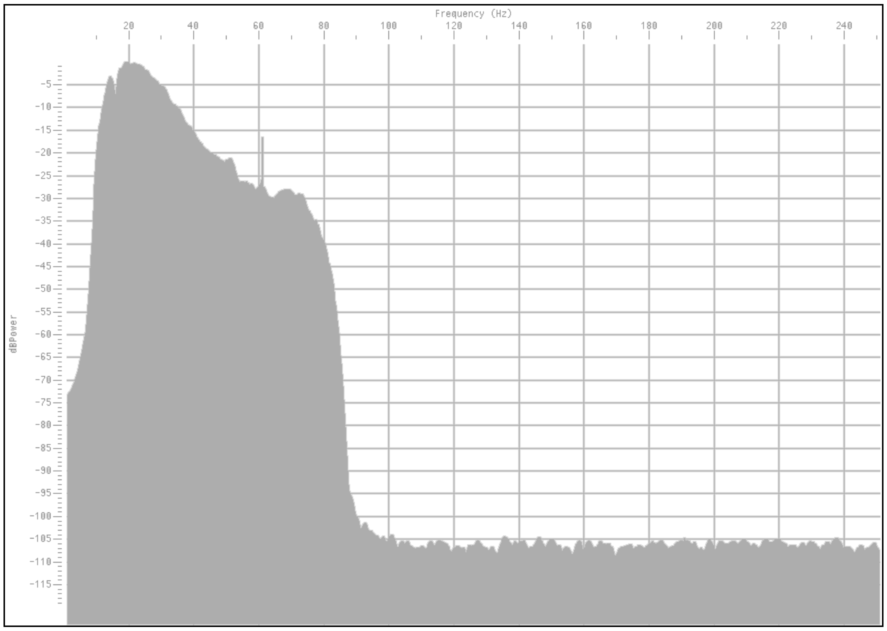

Figure 6.9: Average amplitude spectrum for shot 300 after FDSD.

To remove the noise excluded from the bandwidth of the sweep a 1% stability factor was added to the sweep, eliminating any possible division by zeros. A bandpass filter was also applied to the data, removing any remaining data in the frequencies other than those included in the sweep (Figure 6.10 and 6.11).

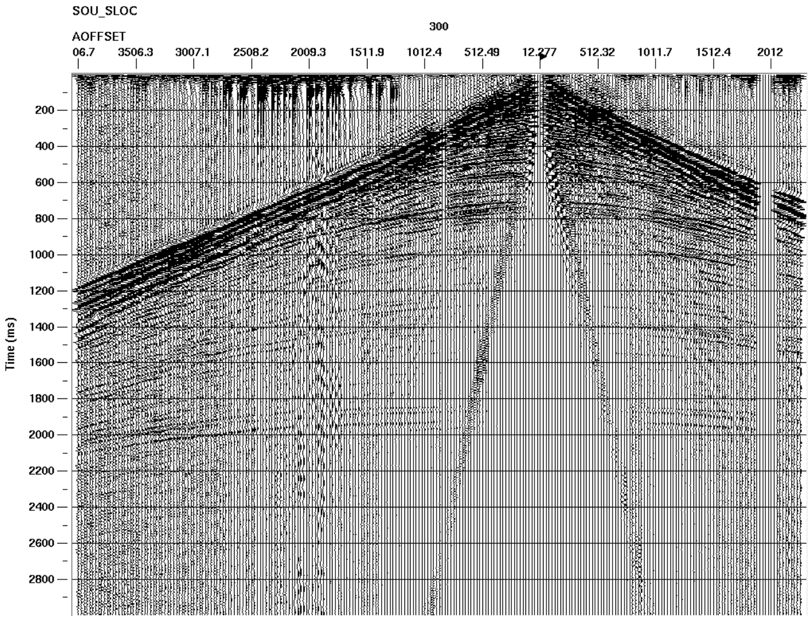

Figure 6.10: Shot gather 300 after FDSD and minimum-phase surface- consistent deconvolution.

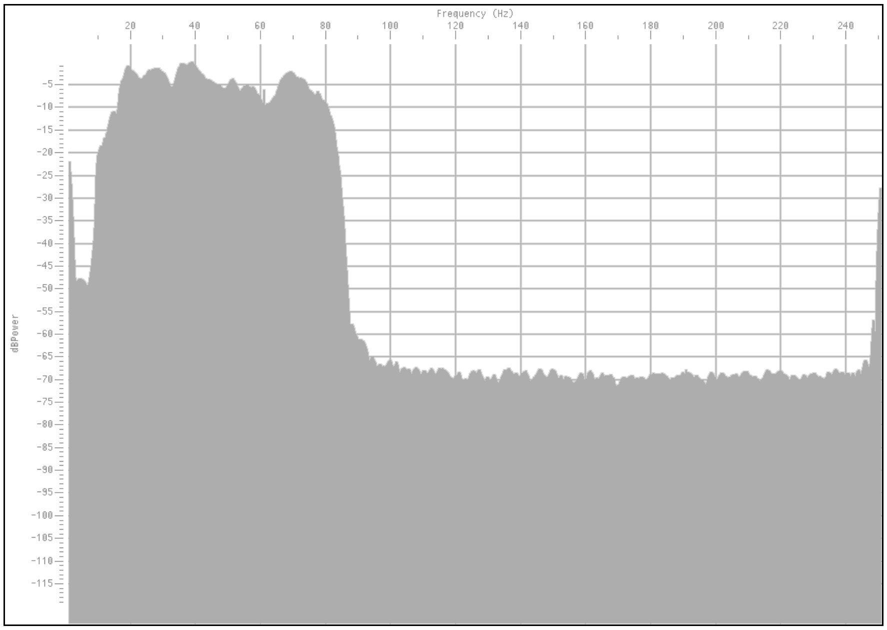

Figure 6.11: Average amplitude spectrum after FDSD and minimum-phase surface-consistent deconvolution

After minimum-phase surface-consistent deconvolution the spectrum has been whitened increasing the resolution of the data (Figure 6.12). The second effect of the deconvolution is the removal of the minimum-phase wavelet embedded in the data.

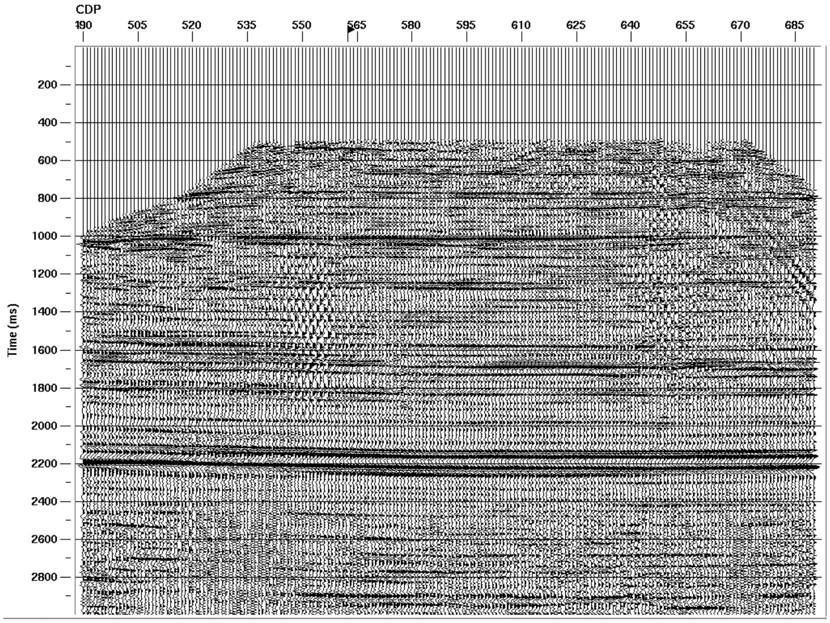

Figure 6.12: Stack with residual statics for line 25FX with the sweep removed by FDSD.

6.1.3 Comparison of results

A comparison of crosscorrelation and frequency-domain deconvolution for line 25FX can be done at the three different steps: after sweep deconvolution, after minimum-phase deconvolution and after the data have been stacked.

A match filter is derived to compare the results of FDSD and crosscorrelation at shot 300 immediately after the sweep is removed and the initial bandpass filter is applied. The match filter indicates that there is no distinguishable phase difference between the two sweep-removal methods. This can also be shown by visually examining the corresponding traces from both methods (Figure 6.13). Since the events are aligned for the traces deconvolved with crosscorrelation and FDSD this indicates that there is no phase distinguishable difference between the two sweep deconvolution methods.

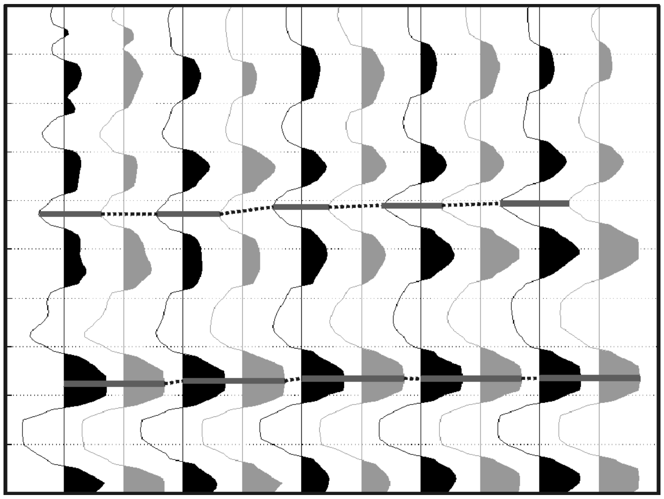

Figure 6.13: Comparison of a series of traces from shot 300. The black traces involve the use of crosscorrelation to deconvolve the sweep. The corresponding trace with FDSD as the sweep deconvolution method is on the immediate right. The peaks and troughs of the corresponding traces are aligned.

If a match filter is derived from the comparison of crosscorrelation and FDSD after minimum-phase surface-consistent deconvolution the phase difference varies for each trace. The average phase difference for source 300 is 16.5 degrees. The differences in the phases for crosscorrelation and FDSD can be seen in the visual comparison of the traces (Figure 6.14). The troughs and peaks of the events for the corresponding traces do not align, indicating a phase difference between the crosscorrelation and FDSD results.

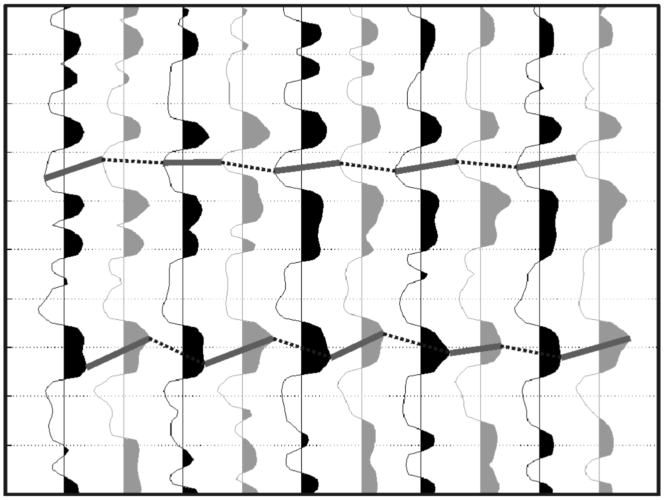

Figure 6.14: Comparison of a series of traces from shot 300 after minimum-phase deconvolution. The black traces involve the use of crosscorrelation to deconvolve the sweep. The corresponding trace with FDSD as the sweep deconvolution method is on the immediate right. The peaks and troughs of the identical traces are no longer aligned.

An identical comparison can be performed for the stacked data. The average match filter indicates that there is a phase difference of approximately 35 degrees between the crosscorrelation and FDSD results. This comparison can be further examined visually with a plot of the traces (Figure 6.15).

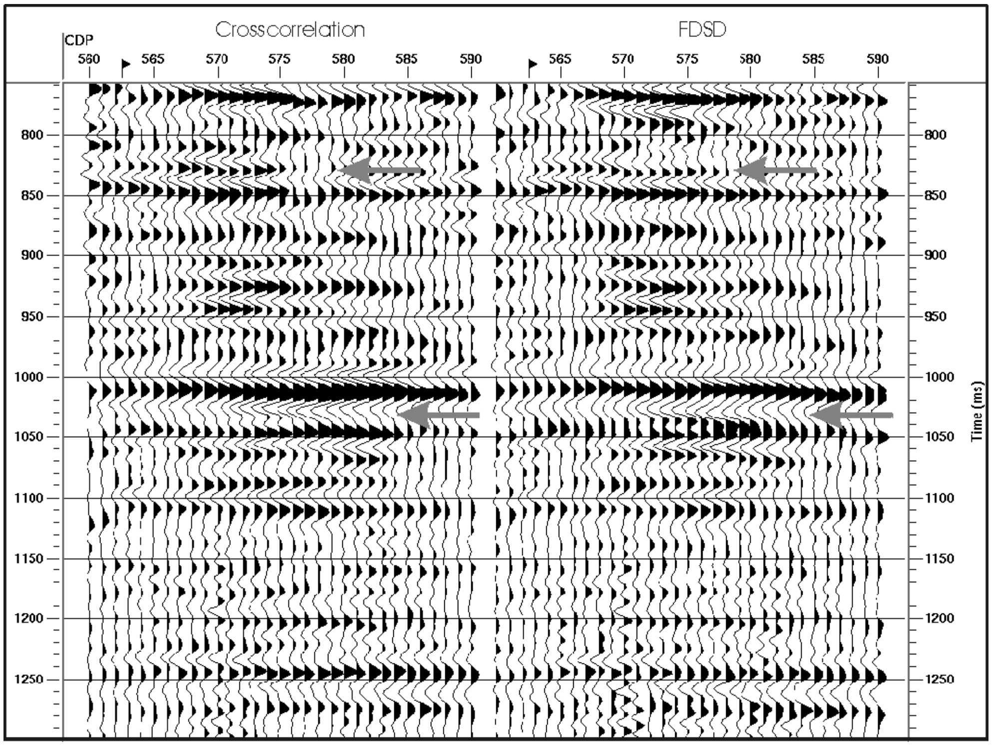

Figure 6.15: Plot of the stacked data after residual statics. There are slight phase differences visible between the crosscorrelation and FDSD data. The arrows indicate two visible differences in the data.

6.2 PETRO-CANADA LINE 31CX

The second seismic line processed as part of this thesis was acquired by Petro-Canada in 1999 in Alberta, Canada. The data were acquired with a linear 10-80 Hz sweep at a sample rate of 2 ms and a sweep length of 16 s (Figure 6.16). The data processed are a partial section of the line acquired.

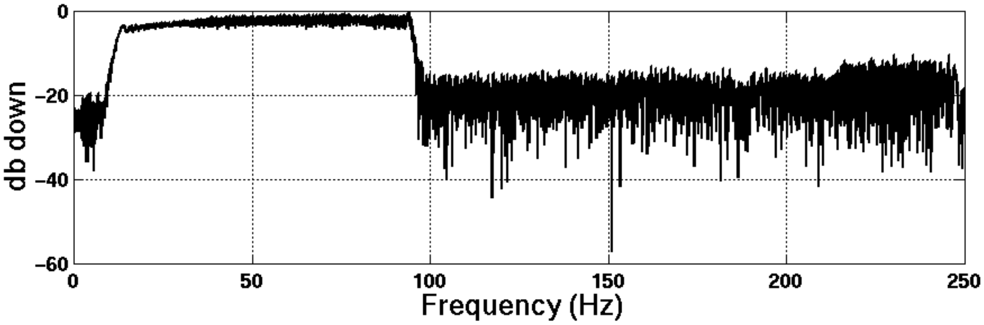

Figure 6.16: Amplitude spectrum of the sweep used for the seismic acquisition for line 31CX.

The sweep is slightly different from that of line 25FX although the sweep has identical parameters with a 300-ms taper. The shot point interval is 25m and the geophone interval is 5m.

The data were processed twice, with the sweep removal as crosscorrelation and FDSD. The preservation of identical processing flows allows a direct comparison between crosscorrelation and FDSD. The processing flow used for this line is identical to line 25FX and is shown in Figure 6.2.

A comparison of the data are made at three different points in the processing flow. The first is directly after the trace kill, the second after the surface-consistent deconvolution and a final comparison is made with the stacked sections.

6.2.1 Crosscorrelation

This data were processed with Landmark's *ProMAX 2D*, including the vibroseis crosscorrelation module. For comparative purposes source 293 on line 31CX are shown for the source gathers in all of the figures.

The first two figures (6.17 and 6.18) are the source gather and the corresponding amplitude spectrum with the sweep removed by crosscorrelation and the application of an 8-12-70-85 bandpass filter.

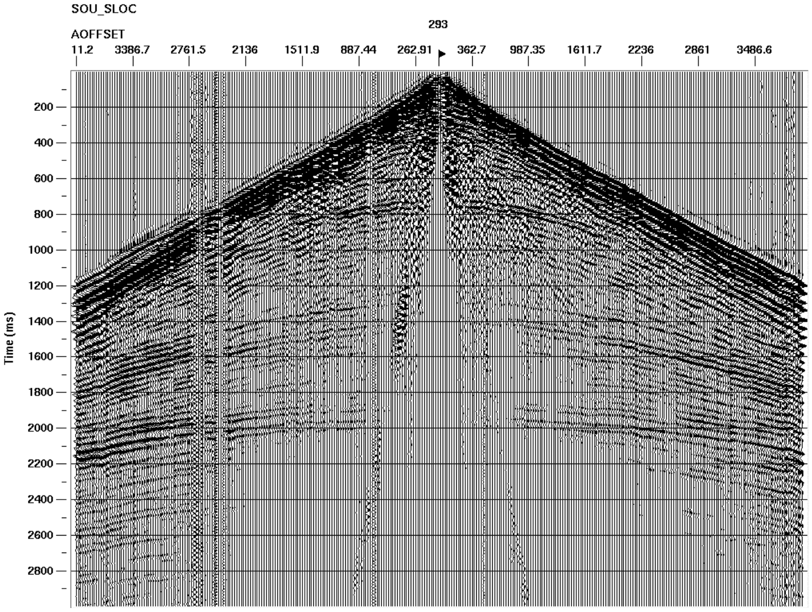

Figure 6.17: Source 293 from line 31CX with sweep removal by crosscorrelation.

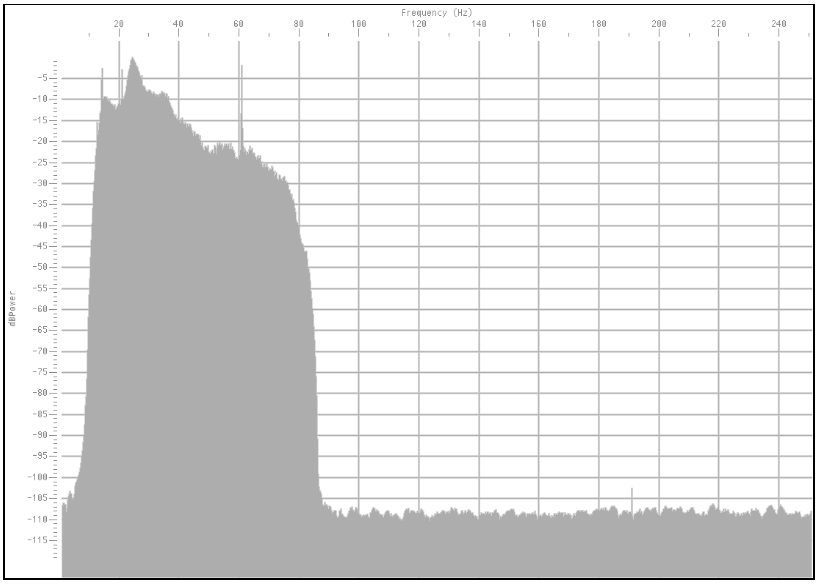

Figure 6.18: Amplitude spectrum after crosscorrelation and a bandpass filter for line 31CX.

After the initial sweep removal and the bandpass filter, the data were processed to include minimum-phase surface-consistent deconvolution and the source gathers reexamined (Figures 6.19 and 6.20).

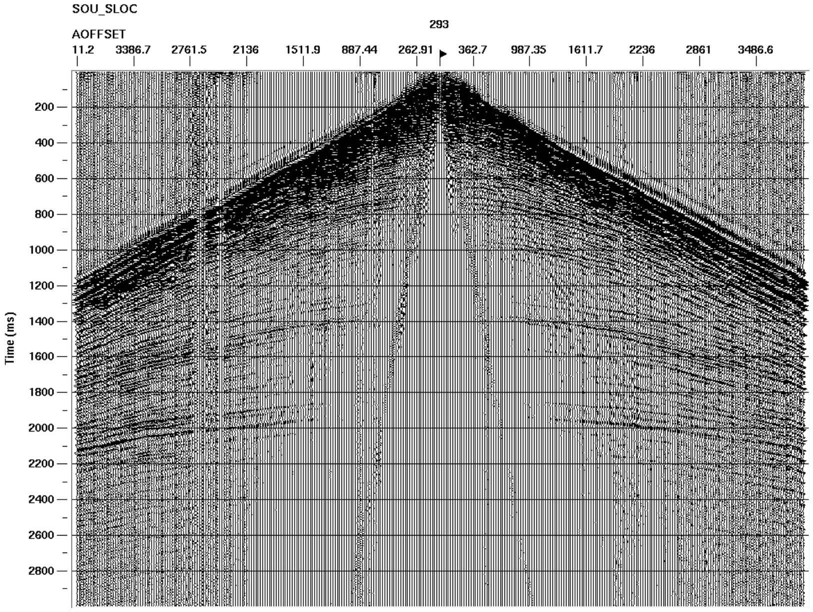

Figure 6.19: Source 293 from line 31CX after minimum-phase surface-consistent deconvolution

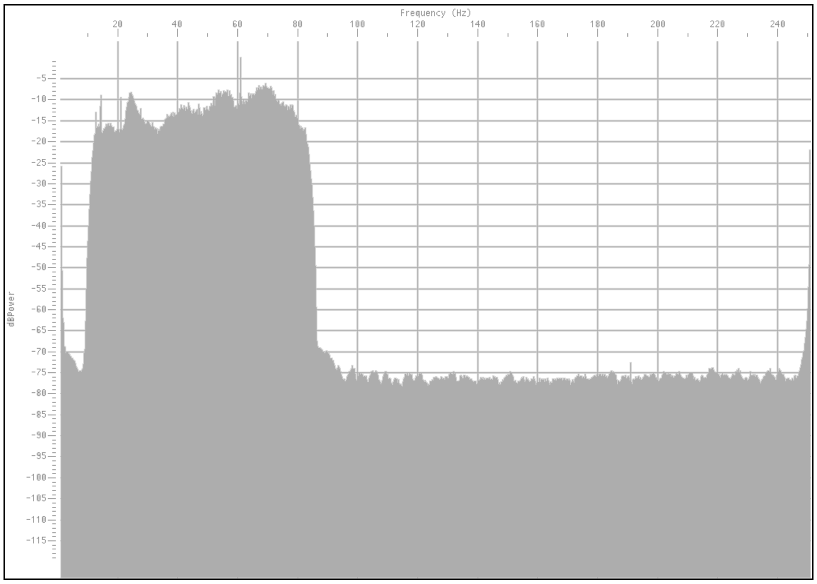

Figure 6.20: Amplitude spectrum after surface-consistent deconvolution. The spectrum has been whitened and an attempt to remove the minimum-phase earth filtering completed.

The minimum-phase deconvolution whitens the spectrum and attempts to remove the earth filter leaving only an embedded zero-phase wavelet.

The final processing step is the residual statics and the CDP stack. Residual statics are applied to remove any remaining near-surface irregularities (Figure 6.21). The stacking of the data increases the fold for the data to 22 from CDP 491 to 736. The fold number is a combination of the individual trace summing from multi-sweep source locations and CDP stacking.

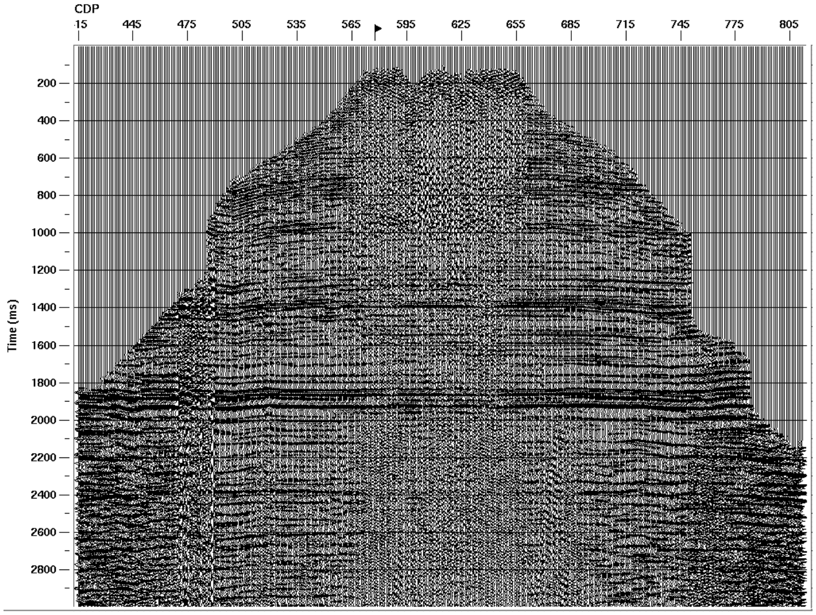

Figure 6.21: Brute stack with residual for line 31CX with crosscorrelation being used as the method to remove the embedded sweep.

6.2.2 Frequency-domain sweep deconvolution

Using the identical processing flow the previous section, the data are processed with the sweep deconvolved by frequency-domain sweep deconvolution. To reduce the noise associated with the frequencies excluded from the sweep bandwidth, a 1% stability factor was added to the sweep during the division in the frequency-domain. This eliminates any possibility of division by zero. A bandpass filter was also applied to the data to remove the high frequency noise.

The first two figures (6.22 and 6.23) are the shot gather and the associated amplitude spectrum after the sweep removal.

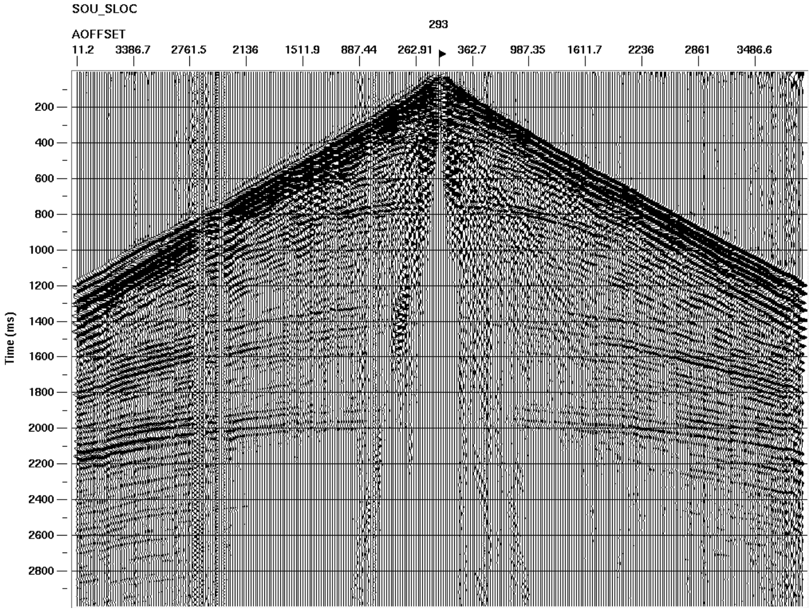

Figure 6.22: Source gather 293 after the sweep is removed with FDSD

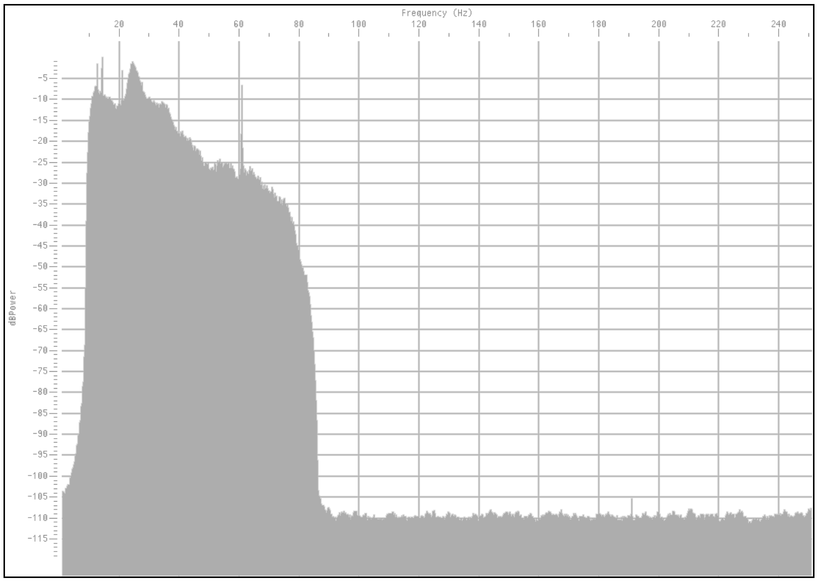

Figure 6.23: Average amplitude spectrum for source 293 after FDSD.

In order to improve the resolution of the data and attempt to remove the minimum-phase earth filter, minimum-phase surface-consistent deconvolution was applied. The results (Figure 6.24 and 6.25) show increases in the higher amplitudes that were attenuated as the waves propagated through the earth.

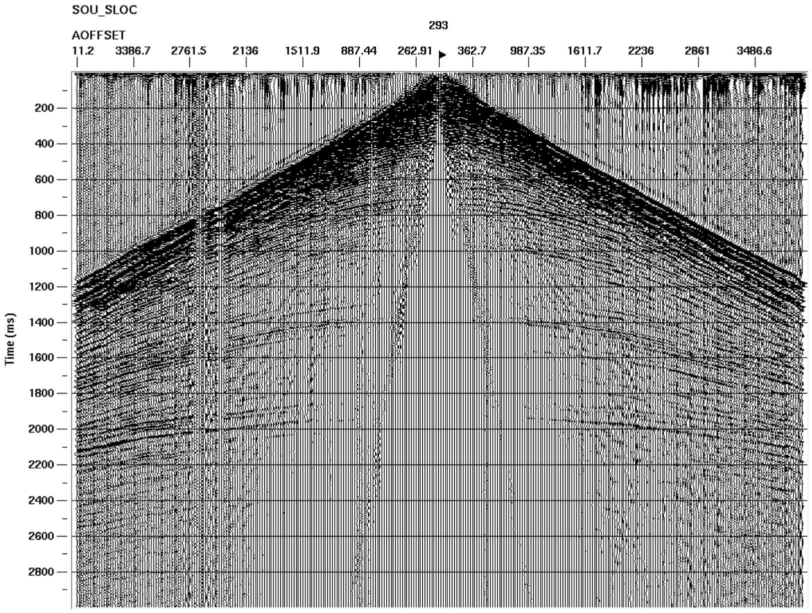

Figure 6.24: Average amplitude spectrum after FDSD and minimum-phase surface-consistent deconvolution.

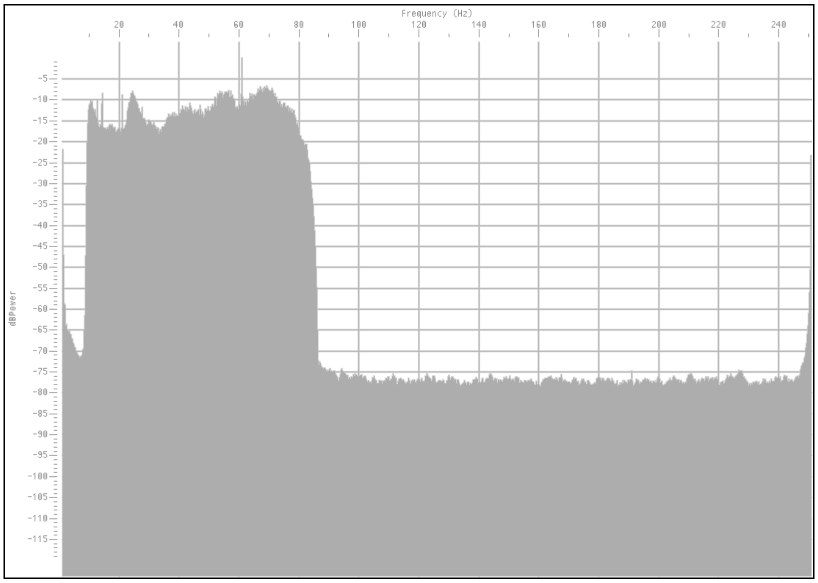

Figure 6.25: Average amplitude spectrum after FDSD and minimum-phase surface-consistent deconvolution.

The final figure (6.26) related to the processing of line 31CX with FDSD is the stack section with residual statics. The trace summing and CDP stack increases the fold to 22 at the centre of the line. There is a significant amount of shallow noise shown on the stacked section that could not be removed with the basic processing steps applied.

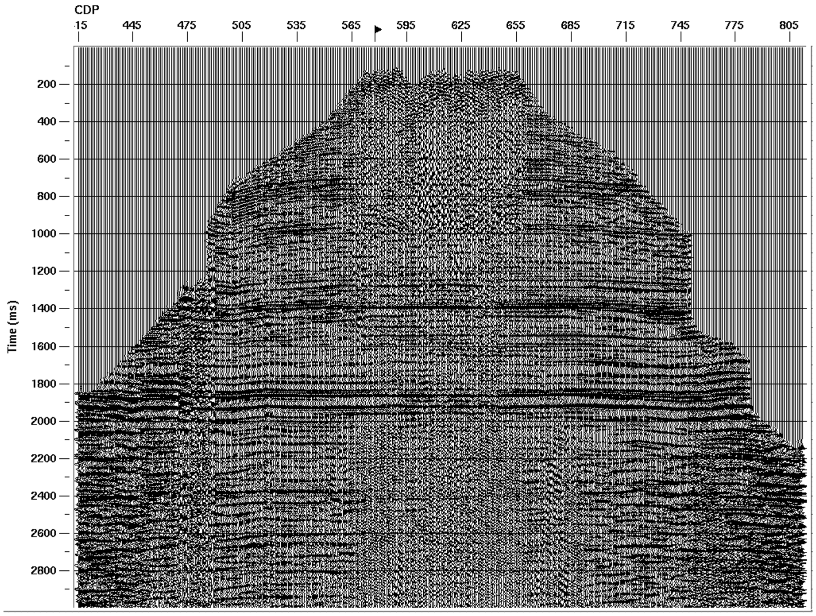

Figure 6.26: Stack for line 31CX with residual statics.

6.2.3 Comparison of results

A comparison of the two methods can be performed for line 31CX. The results are similar to those from the analysis of line 25FX. There are no discernible phase differences between crosscorrelation and FDSD before minimum-phase deconvolution. This is shown in Figure 6.27 as the peaks and troughs of the corresponding traces (identical source and offset values) from the crosscorrelation and FDSD processing are aligned.

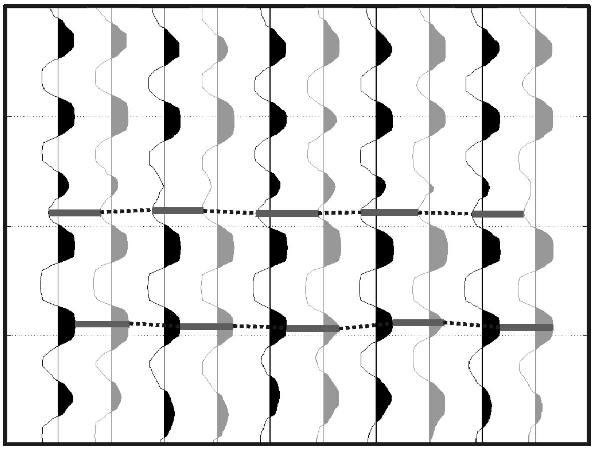

Figure 6.27:Comparison of a series of traces from shot 293. The black traces involve the use of crosscorrelation to deconvolve the sweep. The corresponding trace with FDSD as the sweep deconvolution method is on the immediate right. The peaks and troughs of the corresponding traces are aligned.

An identical comparison for the data can be made after minimum-phase surface-consistent deconvolution. The average phase difference for source 293, comparing crosscorrelation and FDSD, was calculated as 12 degrees with a match filter, with the value varying for each trace. A phase difference can be identified when the traces are visually examined (Figure 6.28).

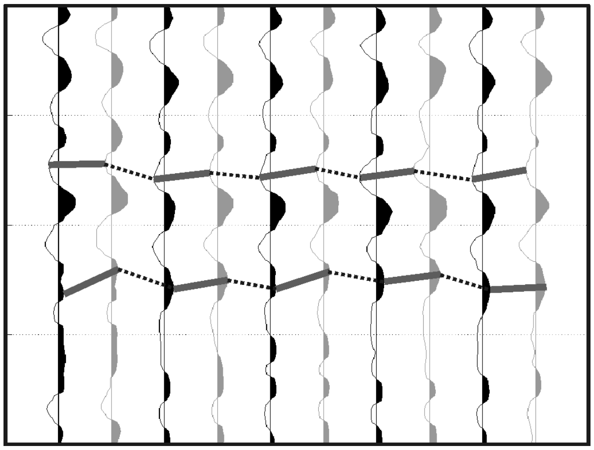

Figure 6.28: Comparison of a series of traces from shot 293 after minimum-phase deconvolution. The black traces involve the use of crosscorrelation to deconvolve the sweep. The corresponding trace with FDSD as the sweep deconvolution method is on the immediate right. The peaks and troughs of the corresponding traces are not aligned indicating a phase difference between the two sweep deconvolution processes.

A comparison can also be made for the data after CDP stacking. The average phase difference is calculated as 30 degrees with a match filter. The phase rotation can be identified when the data from both sweep deconvolution methods are plotted (Figure 6.29). At the lower time sections, the phase-difference is larger than the shallow sections with difference of approximately 120 degrees.

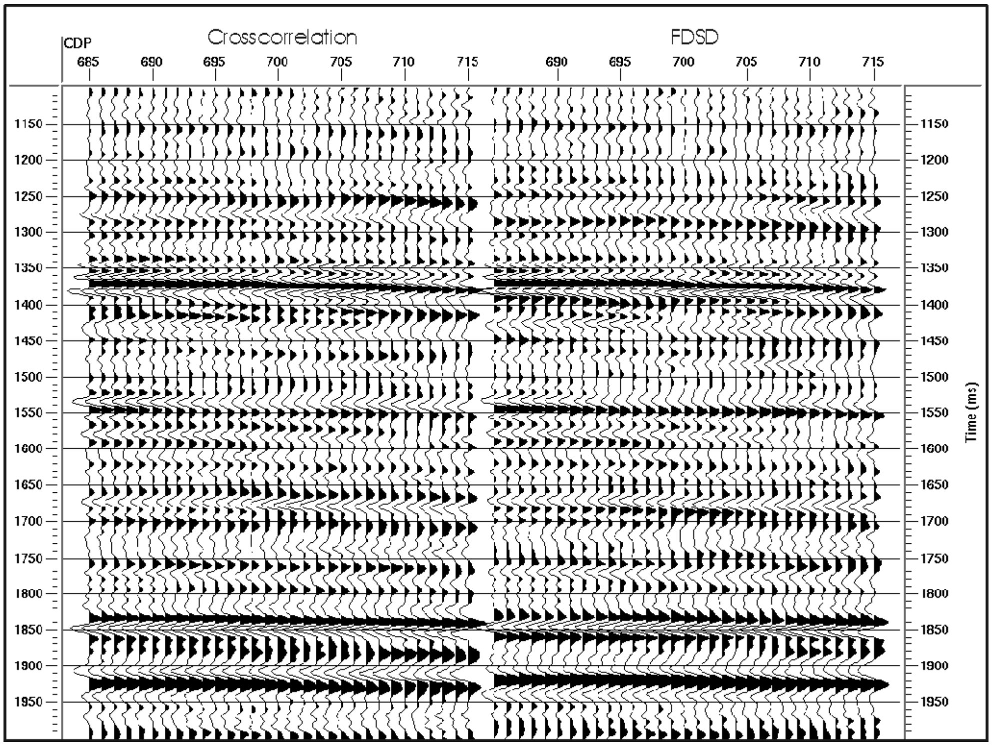

Figure 6.29: Plot of the stacked data after residual statics. There are phase differences visible between the crosscorrelation and FDSD data.

The best comparison for crosscorrelation and frequency-domain sweep deconvolution is with the earth's reflectivity. A comparison of the sweep deconvolution results can be made with the reflectivity calculated from sonic and density logs. The well is located off of the line; however, an excellent tie was performed between the seismic and the synthetic. The synthetic was created with a 10-80 Hz Klauder wavelet to replicate the ideal result of the field data. The tie was made at the clastic/carbonate interface, the most significant change in velocity (Figure 6.30). There is some stretch associated with the seismic data, which is not unexpected due to the location of the well relative to the line.

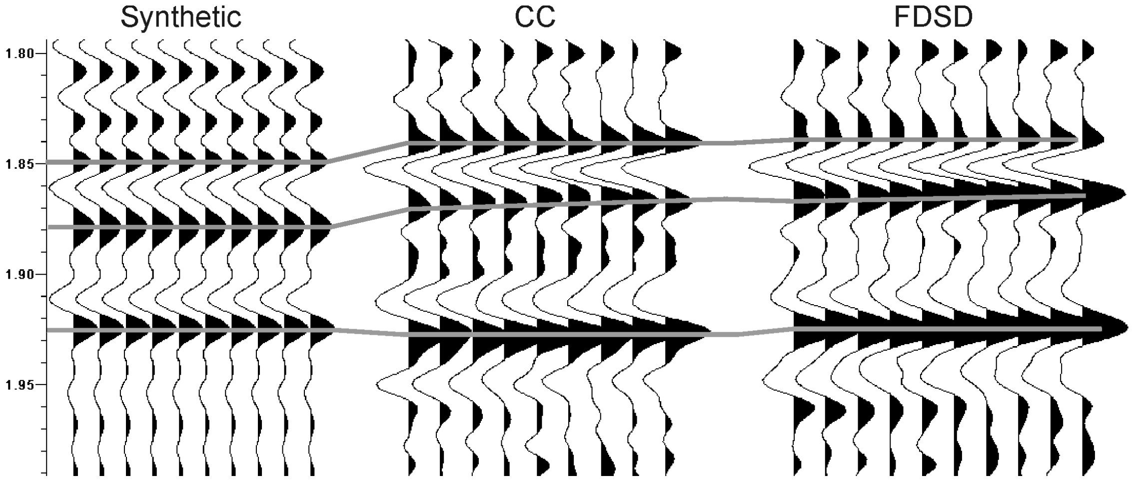

Figure 6.30: Comparison of the sweep deconvolutions with the synthetic calculated from a local well-log (10-80 Klauder wavelet).

Both the methods of crosscorrelation and FDSD show slight dissimilarities compared to the synthetic data obtained from the geophysical well-logs. The most significant difference between crosscorrelation and FDSD is at 1.90 seconds. At this time crosscorrelation shows small doublets that are not visible on the synthetic, where they show up as an increase in amplitude but do not become peaks. With a slight phase rotation these peaks can be recreated. Another significant difference is the wavelet shape for the lowest picked event. The crosscorrelation wavelet is slightly wider with a non-symmetrical shape compared to the synthetic data. This irregularity can be modelled if a 20-degree phase rotation is applied to the synthetic. A third comparison can be made at the top pick, where the result of FDSD is closer to the synthetic than is crosscorrelation.

6.3 PIKES PEAK ARRAY DATA

A 2D vibroseis line was acquired in March 2000 at Pikes Peak, Saskatchewan through the partnership of the University of Calgary's AOSTRA funding and Husky Energy Inc. Two vibrators swept four times at each source point with a nonlinear 16-second sweep, two-millisecond sample rate from 8 to 150 Hz (Figure 6.31). Each source point included four repeats of the sweep that were summed during the processing.

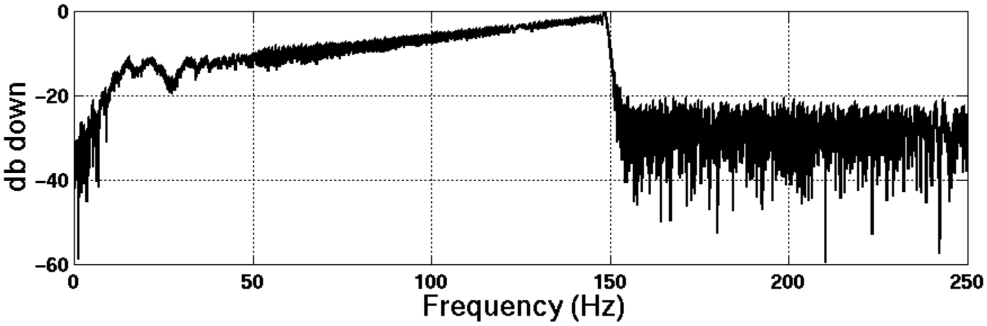

Figure 6.31: Sweep used to acquire the data at Pikes Peak in March 2000.

The processing flow is similar to that used for the Petro-Canada data analysed in the previous sections of this chapter. For the Husky data, refraction statics were applied in an attempt to remove any further near-surface irregularities that were still visible in the data after the application of both elevation and residual statics. The near-surface velocity inversion was carried out with Hampson-Russell *Gli3d*. The processing flow for the Pikes Peak data are shown in Figure 6.32.

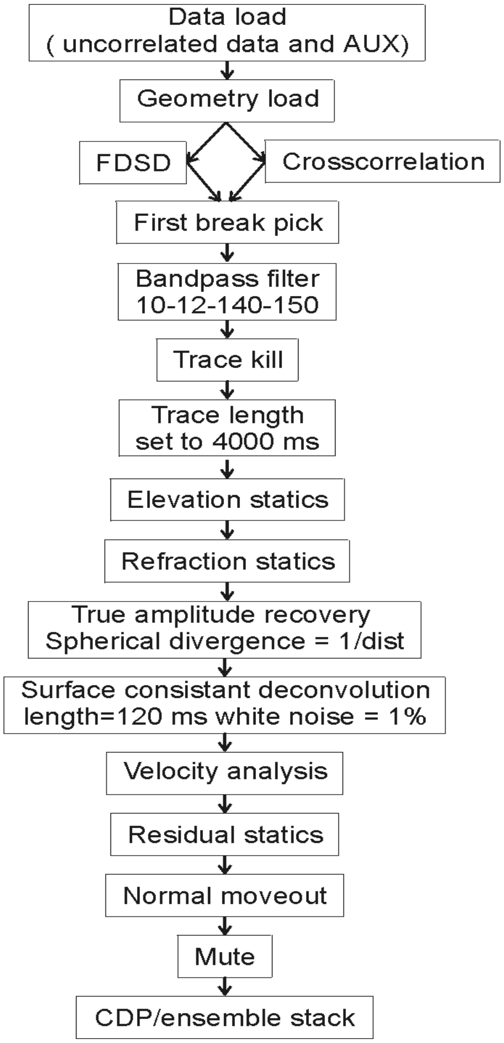

Figure 6.32: Processing flow for the data acquired at Pikes Peak, Saskatchewan

6.3.1 Crosscorrelation

The data from Pike Peak was recorded unsummed and uncorrelated with the sweeps recorded as auxiliary traces. The sweep embedded in each trace was deconvolved with crosscorrelation and then the data were summed for the multiple traces with equivalent geometry. For comparative purposes source 291 was chosen, as it is located at the centre of the line. The first step shown is for the source gather after crosscorrelation, trace summing and a 10-15-140-150 bandpass filter (Figure 6.33 and 6.34). The spectrum of the data are not white due to earth filtering and the filtering effect of the Klauder wavelet that is created by the sweep deconvolution.

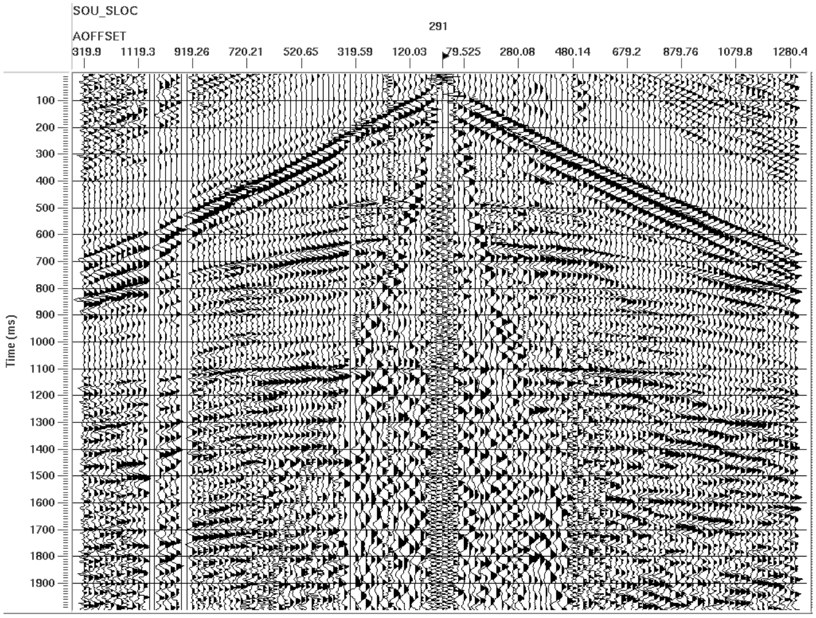

Figure 6.33: Source 291 from the Pikes Peak data after crosscorrelation and a bandpass filter.

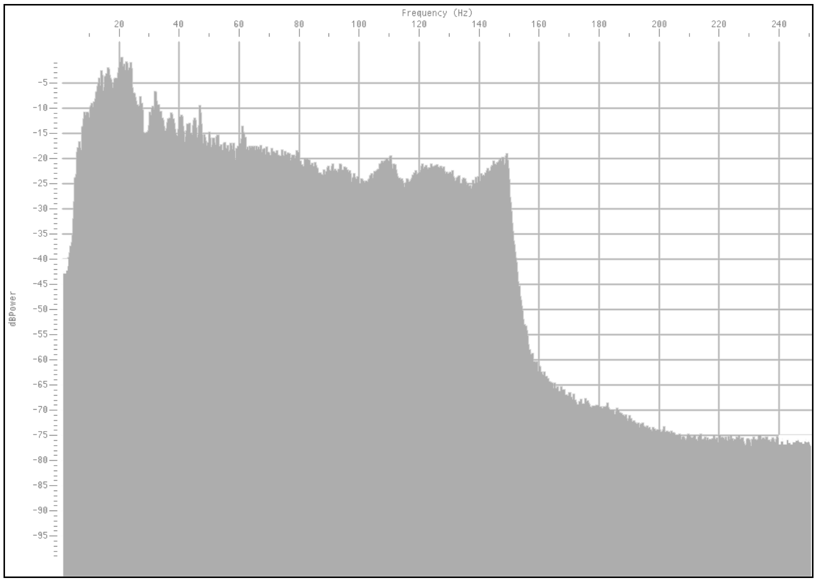

Figure 6.34: Average amplitude spectrum from source 291 after crosscorrelation.

To remove the earth effects, minimum-phase surface-consistent deconvolution is applied to the data. This whitens the spectrum of the individual traces in the gathers and improves the resolution of the data (Figures 6.35 and 6.36). The process also attempts to remove the minimum-phase wavelet embedded in the data to create a zero-phase section.

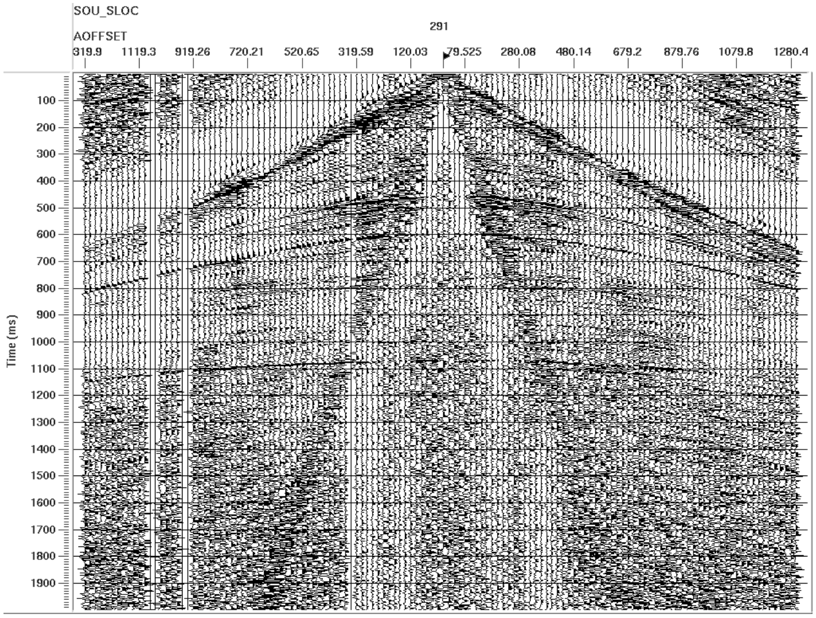

Figure 6.35: Source gather 291 after minimum-phase deconvolution

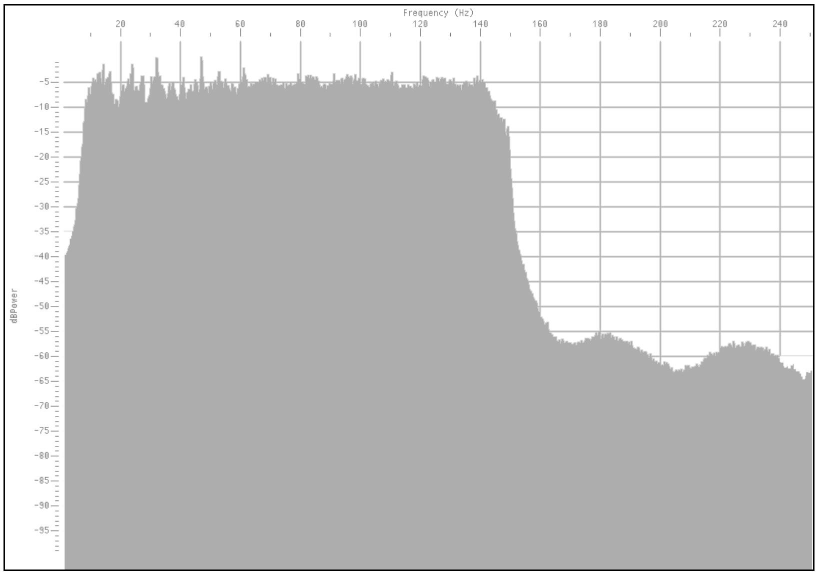

Figure 6.36: Average amplitude spectrum of source 291 after crosscorrelation and minimum-phase deconvolution.

The significant component of the processing is the final stack (Figure 6.37). The exploration target for this data are located at approximately 500-ms and shows excellent resolution.

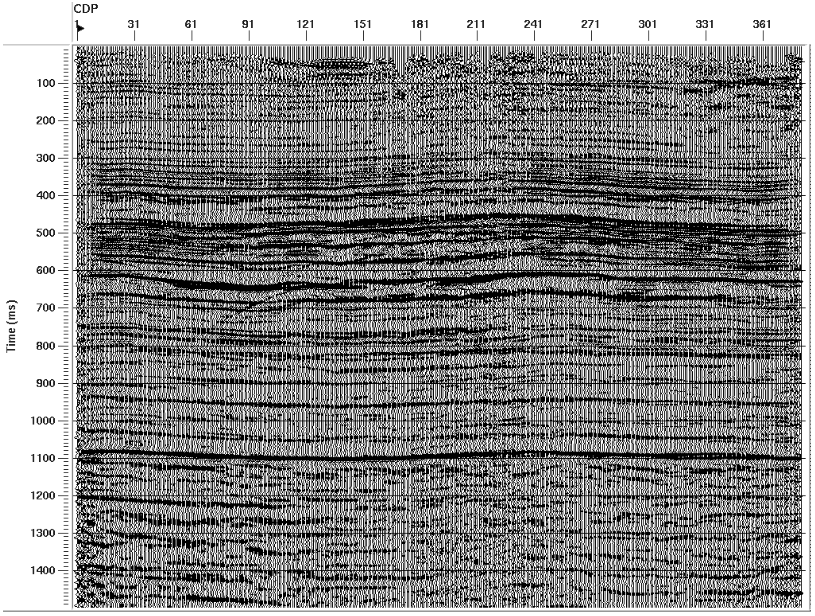

Figure 6.37: Stack of Pikes Peak line including refraction statics. The exploration target is located at 500-ms.

The final stack includes refraction statics that were used in an attempt to remove the near surface velocity variations. There are still some errors at the edges of the seismic section, which could not be removed with a simple processing flow.

6.3.2 Frequency-domain sweep deconvolution

An identical processing flow was employed for the Pikes Peak data with the exception of the sweep removal, which was completed by frequency-domain sweep deconvolution. A 1% stability factor was applied to the sweep to eliminate any divisions by zero during the sweep removal. This removed the amplification of noise outside of the sweep's frequency bandwidth. Figures 6.38 and 6.39 are the source gather and average amplitude spectrum of source 291. For the frequencies that contain data there is a significant decrease in amplitude with increasing frequencies, a result of the earth-attenuation.

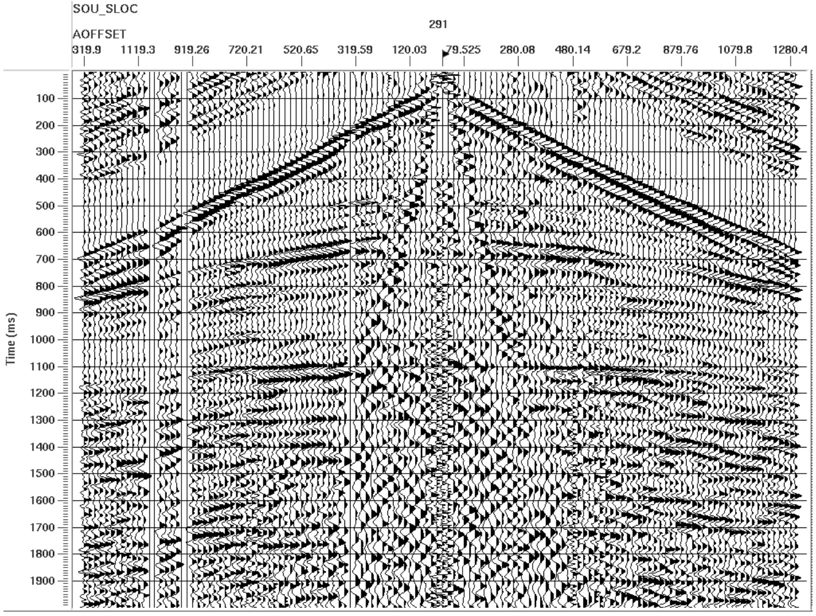

Figure 6.38: Source 291 from the Pikes Peak data after FDSD and a 10-12-140-150 bandpass filter.

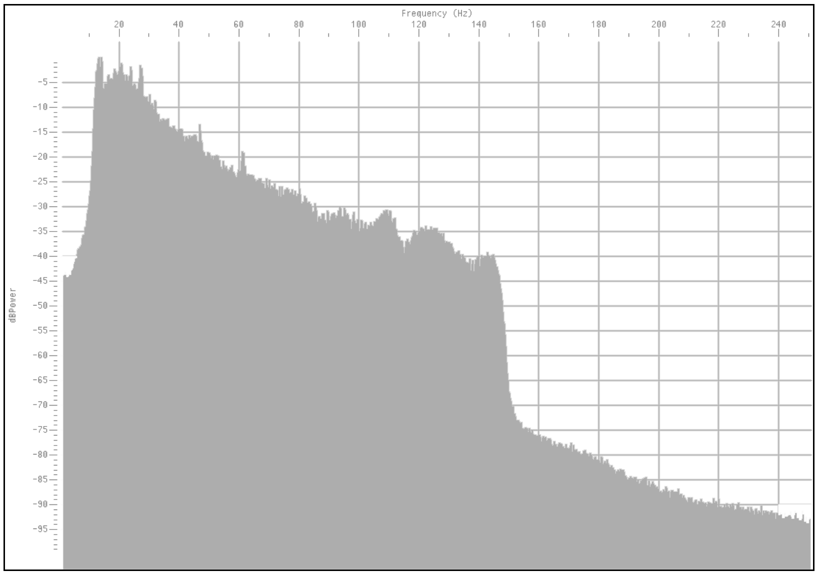

Figure 6.39: Average amplitude spectrum of source 291 after FDSD.

The next analysis is performed for the data after minimum-phase surface-consistent deconvolution, which whitens the data and increases the resolution (Figures 6.40 and

6.41). The increase in the amplitude spectrum should only include the effects of the earth-attenuation and not any filtering effects of the sweep deconvolution. The deconvolution will accurately estimate the spectrum of the minimum-phase earth filter wavelet embedded in the data for the frequencies of the sweep. It is not possible to estimate the minimum-phase wavelet for the frequencies excluded from the sweep.

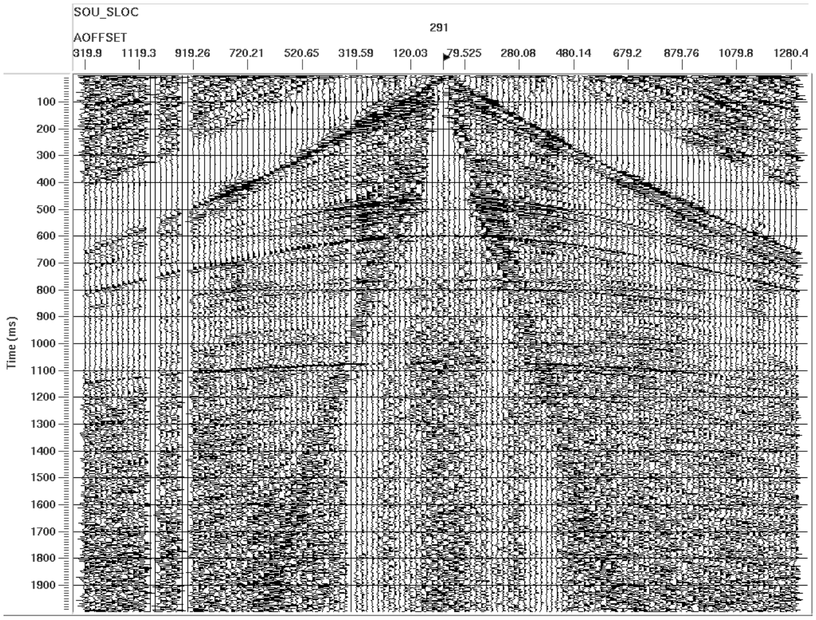

Figure 6.40: Source 291 of Pikes Peak data after minimum-phase deconvolution

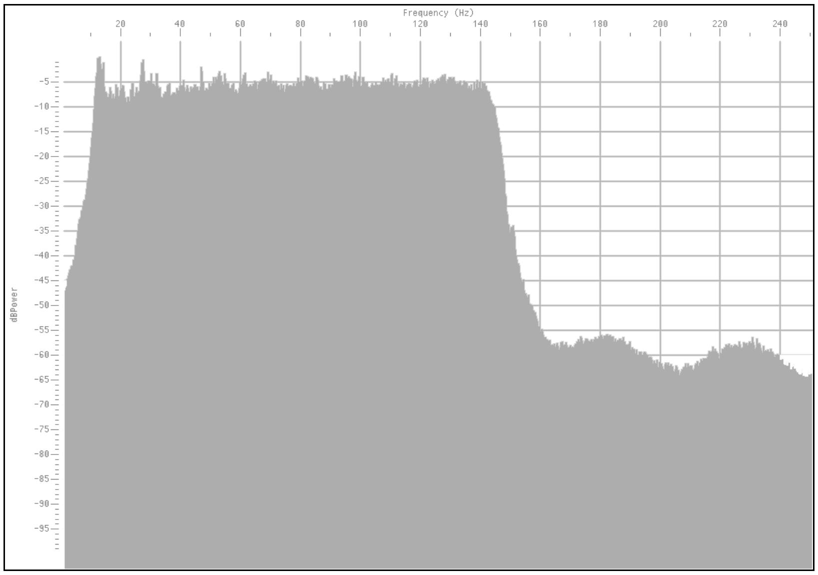

Figure 6.41: Average amplitude spectrum of source 291 after minimum-phase deconvolution.

Figure 6.42 is the final stack with basic processing including refraction statics. The reservoir zone is the Waseca sand located at approximately 500-ms with the data showing excellent resolution quality.

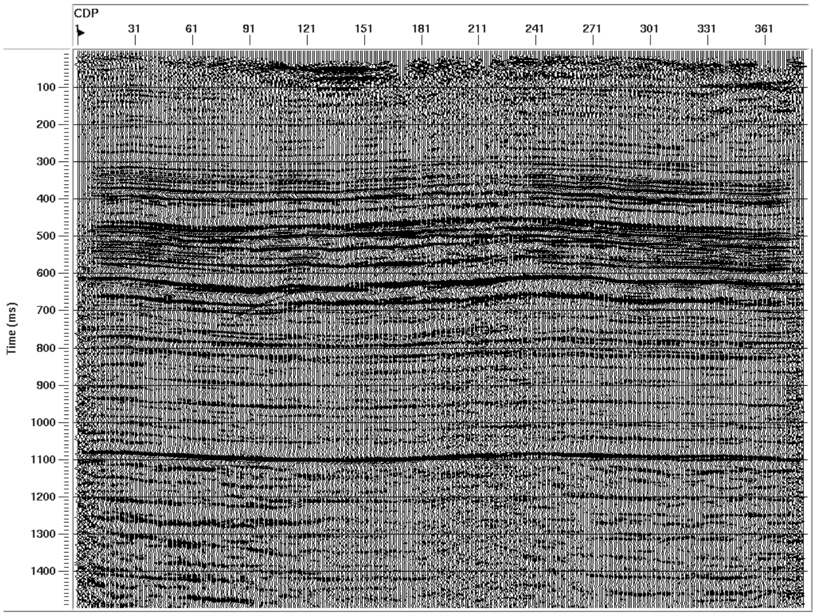

Figure 6.42: Stack of the Pikes Peak data with FDSD used to deconvolve the sweep.

6.3.3 Comparison of results

The Pikes Peak data can be compared with several different methods including a comparison between crosscorrelation and FDSD at the various processing steps. Both crosscorrelation and FDSD can be individually compared to a synthetic determined from a well-log and the VSP.

A comparison of the processing methods with a match filter, after the initial processing step of sweep deconvolution indicates no discernible phase difference (Figure 6.43). There are slight disparities related to different amplitude spectra, a result of the embedded Klauder wavelet in the crosscorrelation data.

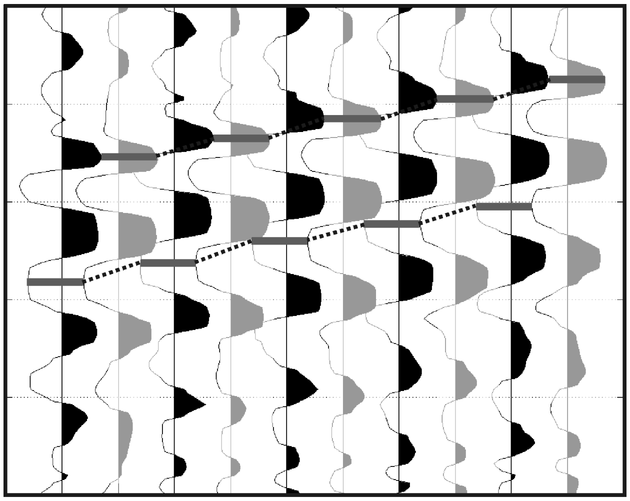

Figure 6.43:Comparison of a series of traces from shot 291. The black traces involve the use of crosscorrelation to deconvolve the sweep. The corresponding trace with FDSD as the sweep deconvolution method is on the immediate right. The peaks and troughs of the corresponding traces are aligned.

A comparison of the Pikes Peak data after minimum-phase surface-consistent deconvolution indicates an average phase difference of 37 degrees. The phase difference was calculated with an average match filter. The phase difference changes from trace to trace over the source gather. This phase difference can also be visually identified when the traces are displayed (Figure 6.44).

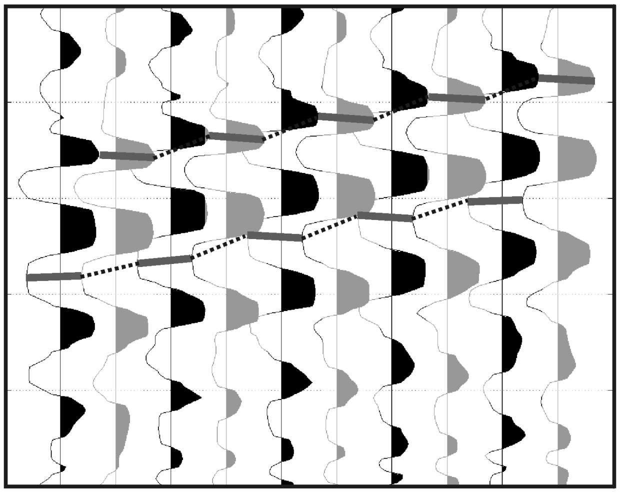

Figure 6.44: Comparison of a series of traces from shot 291 after minimum-phase deconvolution. The black traces involve the use of crosscorrelation to deconvolve the sweep. The corresponding trace with FDSD as the sweep deconvolution method is on the immediate right. The peaks and troughs of the corresponding traces are not aligned indicating a phase difference between the two sweep deconvolution processes.

A final comparison can be performed for the stacked data sets with the match filter indicating an average phase difference of 7 degrees over the section. The phase difference can also be seen in reservoir zone in Figure 6.45, a comparison of the two stacked sections. The phase difference for this line is extremely small in comparison to the two previous lines examined. This is a result of the larger sweep bandwidth and subsequently the more accurate minimum-phase wavelet estimation. The FDSD result contains more noise than the crosscorrelation result, which could be removed further with a more severe bandpass filter.

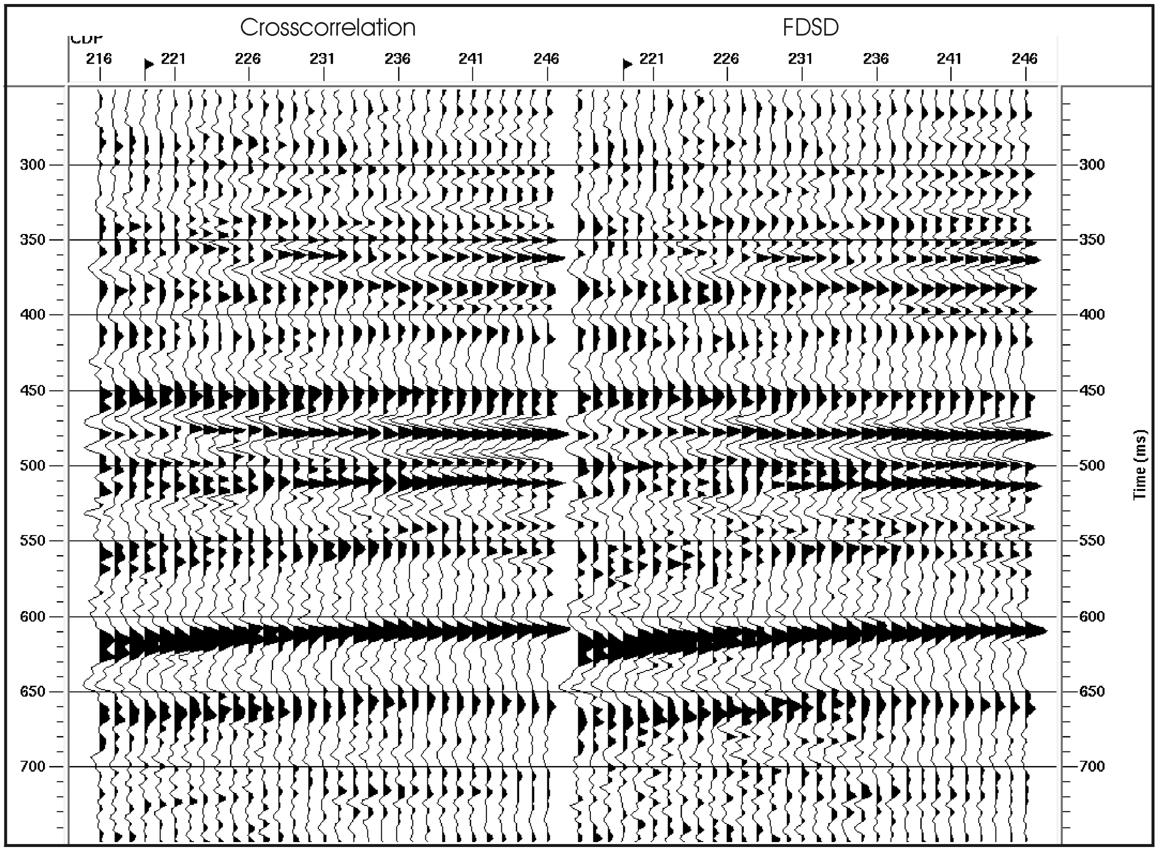

Figure 6.45: Plot of the stacked data after residual statics. There are slight phase differences visible between the crosscorrelation and FDSD data.

A comparison can also be made with the synthetic traces obtained from the well-log information of 111/15-06-050-23W3/00 located at CDP 231 on the seismic data. The well-log unfortunately does not include data down to the Devonian. A composite log with additional data to the Devonian was created and a 10-15-140-150 Ormsby wavelet used to generate the synthetic. The tie indicated that a significant amount of stretch is required; however, it is possible to compare the individual wavelets. While the phase rotation between crosscorrelation and FDSD was previously calculated to be extremely small at 7 degrees there are some small variations that can be accurately compared with the synthetic. The trough between the Colorado and Waseca on the synthetic ties more accurately to the FDSD result that that of crosscorrelation (Figure 6.46).

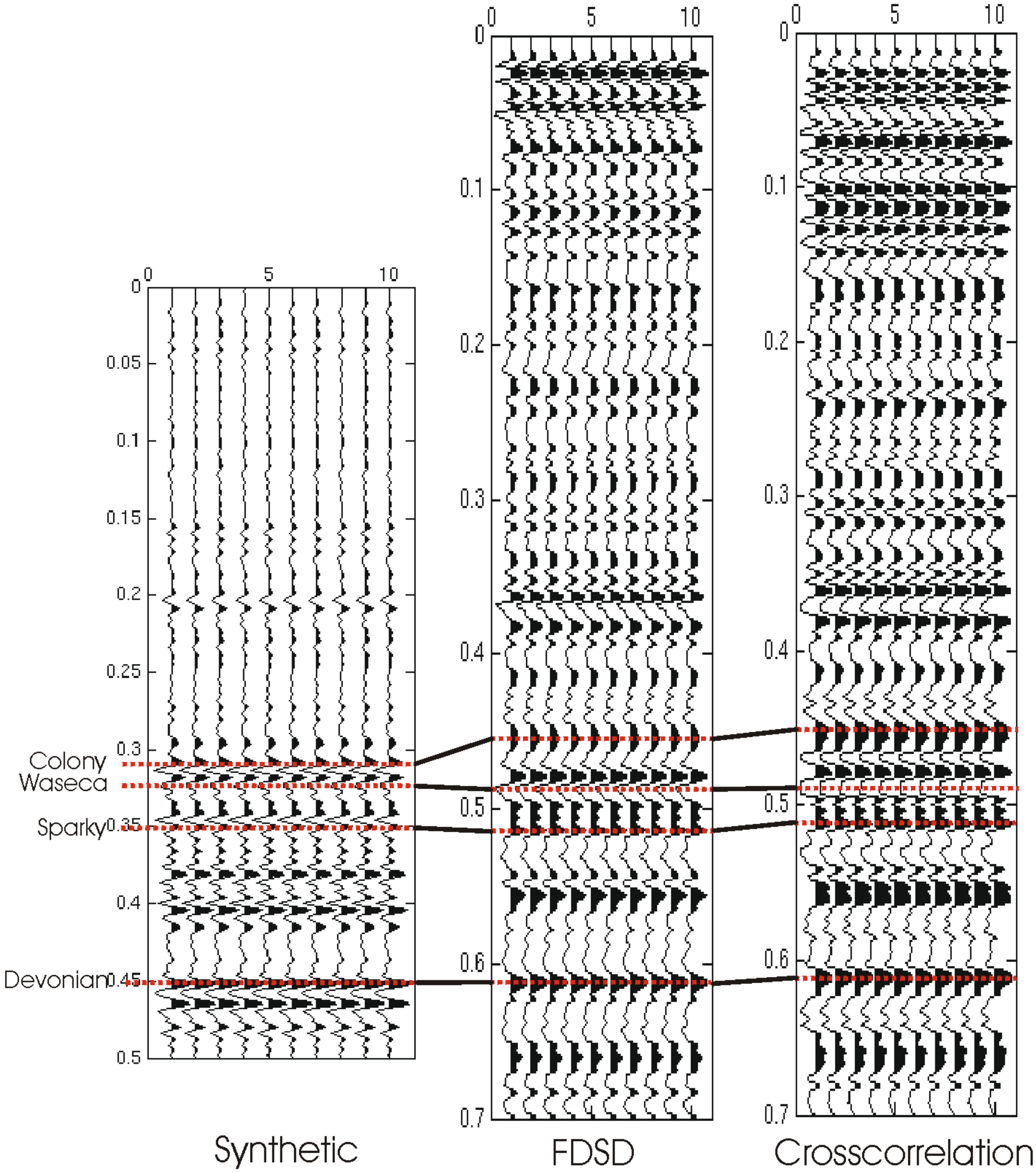

Figure 6.46: Tie between well-log synthetic, crosscorrelation and frequency-domain sweep deconvolution.

A variation can also be identified above the Sparky, in the reservoir zone. It is extremely significant to get the best possible representation of the data in this zone for any future reservoir interpretation and processing. Both FDSD and crosscorrelation provide a different estimation of the reflections in the zone directly above the Sparky compared to the well-log synthetic. Unfortunately, a well-log synthetic may not provide an accurate estimation of the reflectivity. The results from FDSD are closer to the synthetic than crosscorrelation indicating a more accurate result (Figure 6.47).

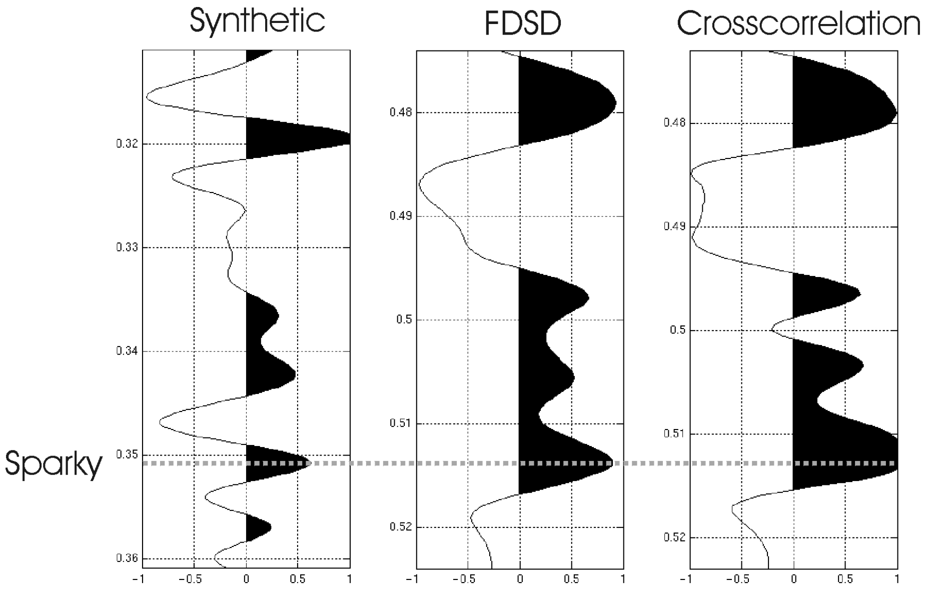

Figure 6.47: Reservoir zone including the pick for the Sparky. Both deconvolution methods provide different results than the shown by the synthetic, although FDSD is more closely related to the synthetic.

The final comparison for the vibroseis deconvolution methods can be made with the VSP results. A comparison of the processed seismic data with both FDSD and crosscorrelation is performed with the VSP corridor stack, where the sweep was removed with both of the vibroseis deconvolution methods. Figure 6.48 displays the tie from the surface to a time of 1.5 seconds. The best tie is for the case in which the seismic data and the VSP were both processed with FDSD, with equivalent amplitudes throughout the entire section. The seismic data with the FDSD processing also shows an excellent tie to the crosscorrelation VSP corridor stack. The crosscorrelation seismic data are comparative to both the VSPs for the shallow data; however, with increasing depth there are significant amplitude variations and phase differences. The comparisons between the seismic sections and the VSP corridor stacks were done with both statistical and visual techniques.

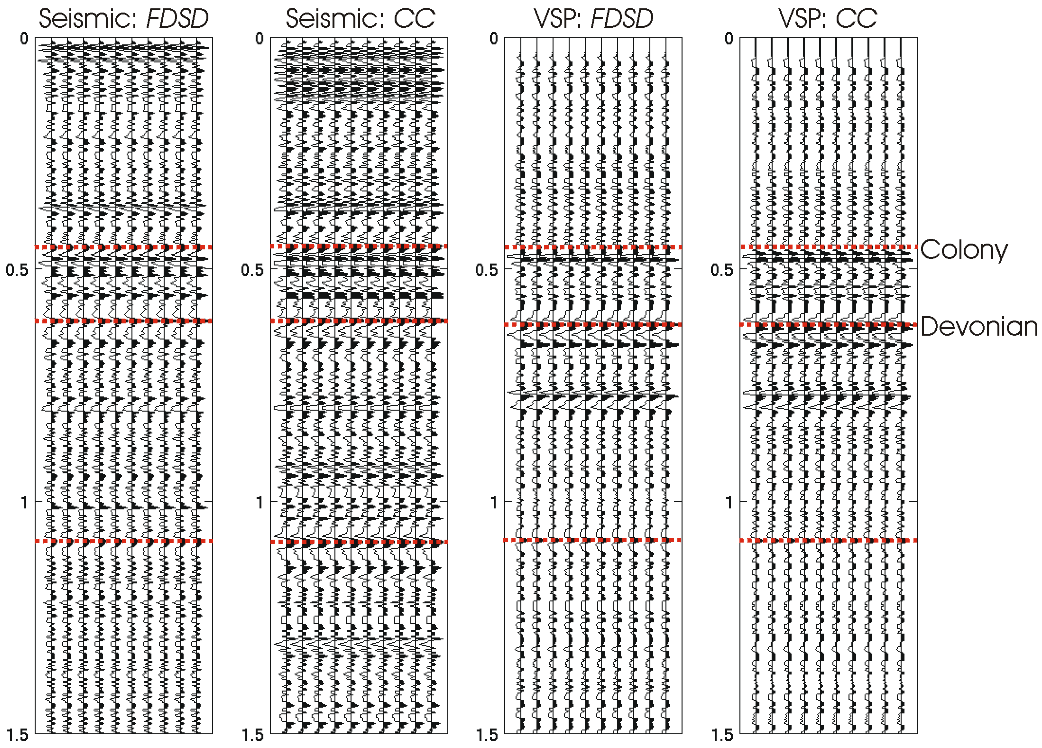

Figure 6.48: Comparison of the processed seismic data from Pike Peak with the VSP data obtained at the northern section of the line. The seismic data processed with FDSD tie surpasses that of crosscorrelation.

The same comparison between the VSPs and the seismic data for the reservoir zone provides identical conclusions (Figure 6.49). The seismic data processed with FDSD matches both VSP corridor stacks more accurately than the crosscorrelation seismic data.

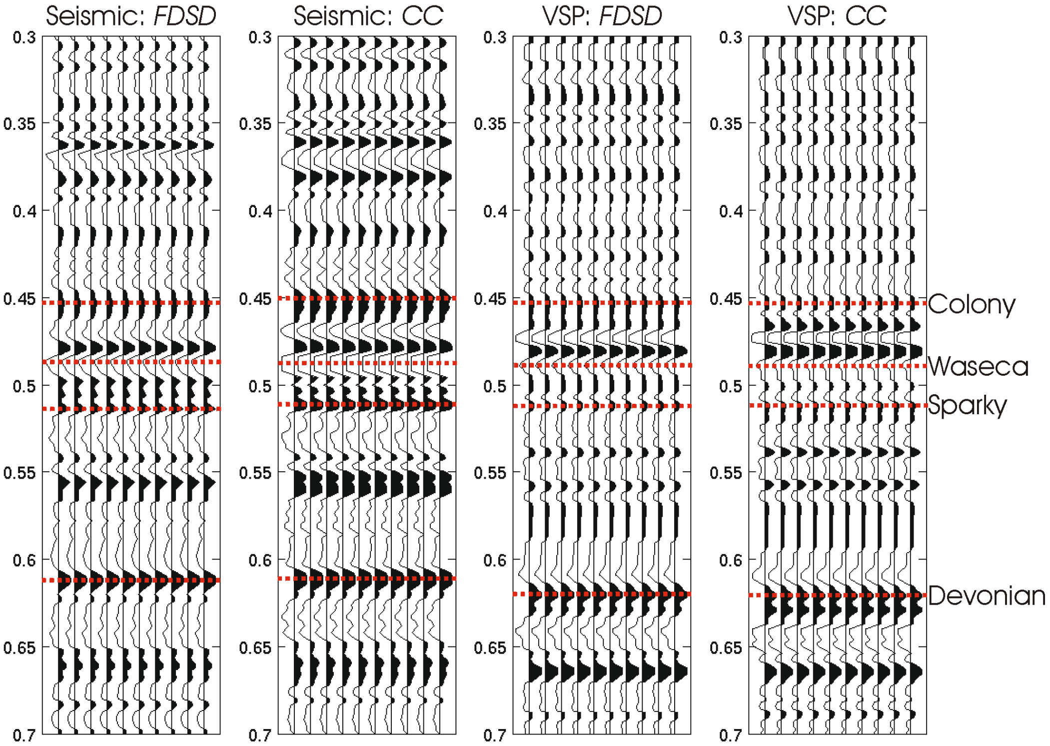

Figure 6.49: Comparison of the processed seismic data over the reservoir zone. The seismic data processed with FDSD tie surpass that of crosscorrelation.

The most accurate amplitude and phase values are important for future seismic analysis and interpretation. This is significant when examining time-lapse variations and AVO changes over a reservoir zone.

6.4 CHAPTER CONCLUSIONS

The comparison of the three data sets to the corresponding well-log synthetics and the VSP indicate that the method used to remove the vibroseis sweep from the trace has a significant impact on the quality of the final seismic section. The amplitude values change as a result of crosscorrelation, this is due to the filtering of the spectrum by the zero-phase Klauder wavelet. There are also phase changes after minimum-phase deconvolution is performed, which increase for nonlinear sweeps due to the incorrect assumption of an embedded minimum-phase wavelet as a result of earth-attenuation. The introduced vibroseis sweep deconvolution method of FDSD provided superior results over crosscorrelation for all three of the seismic lines. One disadvantage of the FDSD method is the large quantity of data that needs to be recorded in the field compared to crosscorrelation. It is possible to complete FDSD in the field, eliminating the extra storage space required. However, with increased computer memory, speed and disk storage size it is possible to record the large amount of data without any significant change in field acquisition time and subsequently cost.

CHAPTER 7

7 CONCLUSIONS

7.0 SUMMARY

In this thesis, frequency-domain sweep deconvolution (FDSD) is examined as an alternative vibroseis deconvolution method, replacing crosscorrelation. A comparison of FDSD to crosscorrelation is examined for both synthetic data and field data obtained from several areas. The synthetic vibroseis data involve analysis with the inclusion of random noise, a minimum-phase wavelet and minimum-phase earth-attenuation values obtained from a VSP in the Pikes Peak area.

A random reflectivity series was convolved with variable sweep types to examine the effects of both FDSD and crosscorrelation. The analyses include the addition of random noise and the convolution with a simple minimum-phase wavelet, simulating stationary minimum-phase attenuation. From the results the following observation are made:

(1) The results of crosscorrelation are dependent on both the bandwidth and the shape of the sweep. Crosscorrelation filters the data with the power spectrum of the sweep, varying the outcome. FDSD is only dependent on the bandwidth of the

sweep and not the shape, since the amplitude spectrum of the trace is divided by the amplitude spectrum of the sweep thereby removing the spectral effects of the sweep. FDSD limits the effect of the sweep design on the data.

(2) For the trace with additive random noise over the entire frequency spectrum, the data are filtered as a result of crosscorrelation, eliminating any substantial noise effect on the final result. For FDSD, the division of the frequencies outside of the sweep's bandwidth substantially amplifies the noise. This problem can easily be reduced with the inclusion of a small stability factor that is added to the sweep during the frequency division. Any further remaining noise can be eradicated with a bandpass filter.

(3) The inclusion of a stationary minimum-phase wavelet introduces a phase problem. For the crosscorrelated trace, the zero-phase Klauder wavelet is convolved with the stationary minimum-phase earth-attenuation wavelet, creating a mixed-phase wavelet. The traditional processes, including minimum-phase deconvolution cannot accurately remove the embedded wavelet due to the mixed-phase and the filtered spectrum, creating a phase rotation. The results of minimum-phase deconvolution after crosscorrelation are more accurate for linear sweeps than for the nonlinear ones. To avoid this problem, some have advocated the use of filters which convert mixed-phase wavelets to minimum-phase wavelets prior to minimum-phase deconvolution. For FDSD the results are independent of the sweep type, since the data are whitened for the sweep frequencies. After FDSD, minimum-phase deconvolution can then accurately estimate the embedded minimum-phase wavelet for the bandwidth of the sweep. It is not possible to

estimate the spectrum for data that does not exist, a result of the bandlimited nature of the vibroseis sweep. The wider the bandwidth of the sweep the more accurate the results obtained from minimum-phase deconvolution.

From the VSP obtained at Pikes Peak and a composite well-log, the non-stationary earth-attenuation was modelled to determine the effect of minimum-phase deconvolution and inverse *Q* filters for both crosscorrelation and FDSD. The following are observations from the analysis:

(1) The inclusion of the earth filter affects the data with the inclusion of a minimum-phase wavelet and the attenuation of the high frequency data. If the sweep is removed with crosscorrelation the data are not necessarily whitened for the effects of the sweep, causing problems when minimum-phase deconvolution is applied to remove the attenuation effects. The data shows a small phase rotation for the linear sweep and a larger phase rotation for the nonlinear sweep. If FDSD is used to remove the vibroseis sweep the results are independent of the sweep type. The results do not have an ideal tie to the data, however all the major reflections can be identified. There is a small amount of phase rotation, similar to that for the crosscorrelation with a linear sweep.

(2) The alternative method of applying an inverse *Q* filter is effective if the vibroseis deconvolution method is FDSD. If an accurate inverse *Q* filter can be designed for the data the result is a bandlimited version of the reflectivity, independent of the sweep type. An incorrect inverse *Q* filter estimation does not have a significant effect on the result of FDSD. After crosscorrelation the amplitude

spectrum is incorrect, a result of the filtering effect of the embedded Klauder wavelet. This causes significant problems when the inverse *Q* filter is applied. There is a substantial loss of amplitude for the shallow reflections as a result of the attenuation and a remaining phase rotation.

The final comparison was completed for the field data obtained from Petro-Canada and Husky Energy Inc. The conclusions are as follows:

(1) The field data results are extremely promising for FDSD with the random noise being controlled by the stability factor and the bandpass filter. There are no phase-differences between FDSD and crosscorrelation after the initial sweep removal; rather these are introduced through minimum-phase deconvolution. The phase-difference seen in the data varies on a trace-by-trace basis. Since the minimum-phase deconvolution is related to amplitude spectra and these differ for FDSD and crosscorrelation. A phase-variation between FDSD and crosscorrelation can be identified with a match filter and visually for the stacked data. The phase difference is related to both the sweep design and bandwidth of the sweep.

(2) Comparisons of the vibroseis deconvolution results with synthetic traces derived from well-logs indicate that FDSD provides a closer result to the ‘true’ reflectivity.

(3) A final comparison is completed with the seismic line and the processed corridor stacks from the Pikes Peak VSP. The data indicates that the seismic line processed with FDSD ties more accurately with the FDSD processed corridor

stack. The FDSD seismic line also ties more accurately than the crosscorrelated seismic line to the crosscorrelated corridor stack. The crosscorrelated seismic line does not tie satisfactorily with either corridor stack.

7.1 DISCUSSION

As shown in this thesis, the method of frequency-domain sweep deconvolution provides an accurate amplitude spectrum for the resulting seismic traces. This eliminates a significant amount of error associated with the removal of the minimum-phase wavelet embedded in the data, caused by the earth-attenuation. The result of FDSD is still limited by the bandwidth of the sweep, with a larger frequency range for the sweep providing better results. The error is associated with inability to estimate the spectrum for data that does not exist.

A problem associated with FDSD is the large volume of data that is recorded in the field. Traditionally, the data are summed and crosscorrelated in the field, reducing the data volume by orders of magnitude. FDSD could also be performed during the data acquisition, reducing the data volume to the equivalent of crosscorrelation. The advantage of recording the data unsummed and uncorrelated includes long-term processing control. For Pikes Peak, an area of steam zone monitoring, it is important to match the amplitudes and phases when examining the time-lapse surveys. If the data are crosscorrelated then the Klauder wavelet is embedded in the data and is difficult, if not impossible to remove. This can cause errors when matching the data sets, if the acquisition sweep is varied. If the sweep is removed by FDSD the only controlling factor is the bandwidth of the data, which can easily be matched for the two seismic lines.

Another advantage of FDSD is the preservation of the true amplitude, which is significant for any future amplitude dependent analysis, such as, amplitude variations with offsets (AVO).

7.2 FUTURE WORK

Additional work could extend research presented in this thesis, including the suggestions noted below.

(1) Research could be completed to examine any benefits obtained from time-lapse analysis with the vibroseis sweep removed by FDSD. This would require two seismic lines that are recorded uncorrelated from identical locations. Unfortunately, the initial dataset acquired at Pikes Peak in 1991 was correlated during acquisition. The advantages should include a better match between the datasets and a more accurate result.

(2) The use of FDSD for AVO analysis could be compared to the results when crosscorrelation is used as the vibroseis deconvolution method. The more accurate amplitudes obtained from the process should assist in obtaining more accurate analysis results. This would be even more significant for geographical areas where there are multiple seismic datasets being analysed.

(3) The development of field processing system based on FDSD could be designed in a manner similar to field crosscorrelation. This would reduce the volume of data that needs to be recorded in the field to the level of crosscorrelation.

REFERENCES

Aki, K. and Richards, P.G., 1980, Quantitative Seismology Theory and Methods: W.H. Freeman and Company.

Båth, M., 1974, Spectral analysis in geophysics, Development in solid earth geophysics: M. Båth (ed.), **7**, Elsevier Science Publishing Co.

Brittle, K.F., Lines, L.R. and Dey, A.K., 2001, Vibroseis deconvolution: A comparison of crosscorrelation and frequency-domain sweep deconvolution: submitted to Geophysical Prospecting.

Brittle, K.F. and Lines, L.R., 2001, Vibroseis Deconvolution: An example from Pikes Peak, Saskatchewan: CSEG recorder, **26**, no. 5, 28-34.

Cambois, G., 2000, Zero-phasing the zero-phase source: The Leading Edge, Society of Exploration Geophysicists, **19**, no. 01, 72-75.

Claerbout, J.F., 1976, Fundamentals of geophysical data processing with applications to petroleum prospecting: McGraw-Hill Book Co.

Claerbout, J.F., 1992, Earth Soundings Analysis: Processing versus Inversion: Blackwell Scientific.

Crawford, J. M., Doty, W. E. N. and Lee, M. R., 1960, Continuous signal seismograph: Geophysics, Society of Exploration Geophysicists, **25**, 95-105.

Futterman, W.I., 1962, Dispersive body waves: Journal of Geophysical Research, **69**, 5279-5291.

Geyer, R.L., 1989, Vibroseis, Vibroseis: Geophysical reprint series, Society of Exploration Geophysicists, 830.

Gibson, B. and Larner, K., 1984, Predictive deconvolution and the zero-phase source: Geophysics, Society of Exploration Geophysicists, **49**, no. 04, 379-397.

Goupillaud, P.L., 1976, Signal design in the "Vibroseis" Technique: Geophysics, Society of Exploration Geophysicists, **41**, no. 06, 1291-1304.

Hinds, R.C., Anderson, N.L. and Kuzmiski, R.D., 1996, VSP interpretive processing: Theory and Practice, Open Gfile Publications No. 3, Society of Exploration Geophysicists, 111.

Klauder, J.R., Price, A.C., Darlington, S. and Albersheim, W.J., 1960, The theory and design of chirp radars: Bell System Tech. Journ. **39**, 745-807.

Knopoff, L. and MacDonald, G.J.F., 1958, Attenuation of small amplitude stress waves in solids: Reviews of Modern Physics, **30**, 1178-1192.

Lines, L.R. and Clayton, R.W., 1977, A new approach to vibroseis deconvolution: Geophysical Prospecting, European Association of Geophysicists and Engineers, **25**, 417 –433.

Margrave, G. F., 1998, Theory of nonstationary linear filtering in the Fourier domain with application to time-variant filtering: Geophysics, Society of Exploration Geophysicists, **63**, 244-259.

Margrave, G.F., 1999, Methods of Seismic Data Processing, Geophysics 557/657 Course Lecture Notes: CREWES project, The University of Calgary.

Putnam, P.E., 1982, Fluvial channel sandstones within upper Mannville (Albian) of Lloydminster area, Canada: geometry, petrography, and paleogeographic implications. AAPG Bulletin, **66**, no. 4, 436-459

Robinson, E.A., 1999, Seismic inversion and deconvolution Part B: dual sensor technology, Pergamon, Amsterdam.

Sheppard, G.L., Wong, F.Y., and Love, D., 1998, Husky's success at the Pikes Peak Thermal Project : Unitar Conference, Beijing, China.

Sheriff, R.E., 1990, Encyclopedic dictionary of exploration geophysics: Society of Exploration Geophysicists.

Spencer, T.W., Sonnad, J.R. and Butler, T.M., 1982, Seismic-Q-stratigraphy or dissipation, Geophysics, Society of Exploration Geophysicists**, 47**, 16-24.

Tonn, R., 1991, The determination of the seismic quality factor from VSP data: a comparison of different computational methods: Geophysical Prospecting, European Association of Geoscientists and Engineers, **39**, 1-28.

Van Hulten, F.F.N., 1984, Petroleum geology of the Pikes Peak Heavy-oil field, Waseca formation, lower Cretaceous, Saskatchewan, In: The Mesozoic of middle North America. Memoir - Canadian Society of Petroleum Geologists, **9**, 441-454, Canadian Society of Petroleum Geologists.

Widess, M. B., 1973, How thin is a thin bed?: Geophysics, Society of Exploration Geophysicists, **38**, 1176-1254.

Yilmaz, O., 1987, Seismic data processing: Investigations in Geophysics Society of Exploration Geophysicists.